

Experimental Studies and Modelling of Surface Loss during Segregation

By

Shaun Cronjé

MSc

A thesis submitted in accordance with the requirements for the degree

Philosophiae Doctor

in the

**Department of Physics
Faculty of Natural and Agricultural Sciences**

at the

**University of the Free State
Republic of South Africa**

Supervisor: Prof W.D. Roos

Co-supervisor: Prof R.E. Kroon

Date: January 2015

Acknowledgements

The author wishes to thank the following individuals and institutions:

- Prof W.D. Roos, my supervisor for his advice, friendship and positive attitude. You truly were and remain to be a mentor to me.
- Prof R.E. Kroon, my co-supervisor for his advice, time and in particular for his help when mathematics become a bit “interesting”.
- Prof J.K.O. Asante for his assistance with the procuring and partial funding of the Inficon XTC/3s system via TUT.
- All the staff at the Instrumentation Unit at the University of the Free State. In particular Mr Kobus Kruger and Mr Johan Erasmus. Without your talents, this project would never have been completed.
- All the staff at the Electronics Unit at the University of the Free State. In particular Mr Innes Basson for assisting in solving equipment problems.
- Prof J.J. Terblans for useful discussions and for allowing the use of his source code for the Modified Darken software.
- Pat van Heerden for your kinship.
- My friend Dr Heinrich Joubert for useful discussions.
- The staff and students at the Department of Physics, University of the Free State. For all your support. In particular Ms Lizelke Klindt. You are a guiding star in dark times.
- Dr M.M. Duvenhage for all her assistance.

- Prof Pieter Meintjes for his interest in my life and his frequent words of encouragement.
- My family and friends for their unwavering support and patience. In particular my brothers Juan and Quinton.
- Lizelle for all her love and support which I do not deserve.
- My Here God.....dat alles altyd vir my uitwerk.

Abstract

Metallurgical products play an essential role in everyday life. The search for metals with better material properties such as strength, wear and corrosion resistance and for ways to reduce production costs and time continues to this day. The effect of impurities in metals is of particular interest. It is common to apply some sort of heat treatment during manufacturing of metallurgical products. At elevated temperatures, impurity atoms are invariably mobile and can diffuse to grain boundaries and other surfaces which can have a major influence on material properties. This redistribution of solute atoms between the surface and the bulk of the material is known as segregation.

Experimentally, the segregation of Sb from the bulk of a Cu(100) crystal doped with 0.05 at% Sb was measured. The Sb surface concentration was monitored using Auger Electron Spectroscopy during a linear temperature ramp. The segregation profile obtained was fitted with the Modified Darken model and the segregation parameters were determined to be $D_0 = 1.5 \times 10^{-5} \text{ m}^2 \cdot \text{s}^{-1}$, $E = 177.0 \text{ kJ} \cdot \text{mol}^{-1}$, $\Delta G = -89 \text{ kJ} \cdot \text{mol}^{-1}$ and $\Omega = -3 \text{ kJ} \cdot \text{mol}^{-1}$. This data is a valuable addition to previous measurements of segregation parameters made for Sb to Cu surfaces of different orientations.

In a number of binary alloy systems surface evaporation during segregation experiments has been reported. The effect of evaporation has however received very little attention in previous experimental studies. In particular, contemporary segregation models omit the influence of segregant evaporation. In this study a modified version of the Hertz-Knudsen equation was used to update the Modified Darken model, producing software that enables researchers to predict both kinetic and equilibrium segregation while including the effects of surface evaporation of the segregant. The effect of the proposed evaporation parameter introduced into the Hertz-Knudsen equation is discussed and shows how sensitive the segregation profile is to even very small segregant evaporation rates. It is clearly demonstrated that omitting evaporation from the simulations can generate inaccurate segregation parameters. Guidelines are given on correcting segregation parameters extracted from Modified Darken model fits

made with software before updating for the influence of evaporation. Interpreting segregation parameters in terms of evaporation is also discussed.

Modifications were made to an Auger Electron Spectroscopy system to measure evaporation by using an Inficon XTC/3s deposition controller. This modification and proposed procedures allows the surface of a sample used for evaporation studies, to be sputter-cleaned and analysed. Using this modified system the evaporation rate of pure Sb was measured. While there was qualitative agreement regarding the evaporation behaviour, it was found that the original Hertz-Knudsen equation highly over estimates the evaporation rate.

No evaporation of Sb from the surface of the Cu(100) sample could be measured as the evaporation flux was below the detection level of the equipment used. This is attributed to the very low evaporation rate of Sb, as observed in this study for pure Sb, compared to predictions from the Hertz-Knudsen equation. Nevertheless, comparison of the experimental segregation profile and simulations generated with the updated software suggest that evaporation of Sb does in fact take place from the Cu(100) surface during segregation.

This study has demonstrated the importance of taking evaporation into account during segregation studies and laid an important foundation for future studies of evaporation from the surfaces of metals during segregation by installing the necessary hardware into an Auger system, establishing experimental protocols and updating the existing Modified Darken software for simulating segregation profiles.

Opsomming

Metallurgiese produkte speel 'n onontbeerlike rol in die alledaagse lewe. Die soeke na metale met beter eienskappe soos sterkte, slytasie- en korrosieweerstand asook metodes om vervaardigingskoste en – tye te verminder duur steeds voort. Die invloed van onsuiverhede in metale is van besondere belang. Tydens die vervaardigingsproses van metallurgiese produkte is dit algemeen om een of ander hittebehandelingsproses te volg. By hoë temperature is die atome van onsuiverhede, sonder uitsondering, mobiel en kan dus na korrelgrense en ander oppervlakke diffundeer, wat weer 'n groot invloed op die eienskappe van die materiale het. Hierdie herverdeling van atome tussen die oppervlak en die bulk van die materiaal staan bekend as segregasie.

Die segregasie van Sb uit 'n Cu(100)-kristal, gedoteer met 0.05 at% Sb, is eksperimenteel gemeet. Tydens 'n liniêre temperatuurveeg, is die oppervlak-konsentrasie van Sb met behulp van Augerelektron-spektroskopie gemeet. Die segregasieprofiel is gepas met behulp van die Gemodifiseerde Darkenmodel en die volgende segregasieparameters is onttrek: $D_0 = 1.5 \times 10^{-5} \text{ m}^2 \cdot \text{s}^{-1}$, $E = 177.0 \text{ kJ} \cdot \text{mol}^{-1}$, $\Delta G = -89 \text{ kJ} \cdot \text{mol}^{-1}$ en $\Omega = -3 \text{ kJ} \cdot \text{mol}^{-1}$. Hierdie data is 'n waardevolle toevoeging tot vorige gemete segregasieparameters van Sb na Cu-oppervlakke met verskillende oriëntasies.

In 'n aantal binêre-legerings is die oppervlakverdamping tydens segregasie-eksperimente gerapporteer. Die invloed van verdamping tydens segregasiestudies het egter baie min aandag gekry. In besonder het onlangse segregasiemodelle die invloed van segregant-verdamping geïgnoreer. In hierdie studie is 'n gemodifiseerde weergawe van die Hertz-Knudsenvergelyking gebruik om die Gemodifiseerde Darkenmodel te verbeter. Hierdie rekenaarprogrammetuur stel navorsers in staat om beide die kinetika- en ewewigsegregasie, met inagneming van die oppervlakverdamping van die segregant, te voorspel. Die invloed van die verdampingsparameter wat in die Hertz-Knudsenvergelyking ingevoer is, word

bespreek en toon die sensitiviteit van die segregasieprofiel vir selfs baie klein verdampingstempos. Dit word duidelik getoon dat indien verdamping geïgnoreer word onakkurate segregasieparameters genereer kan word. Riglyne word gegee hoe om segregasieparameters, wat met behulp van die Gemodifiseerde Darkenmodel, sonder verdamping onttrek is, te korrigeer. Die interpretasie van die segregasieparameters, in terme van verdamping, word ook bespreek.

Veranderinge is aangebring aan 'n Augerelektron-spektroskopie-instrument om verdamping met behulp van 'n Inficon XTC/3s deponeringsbeheerder te meet. Hierdie veranderinge en voorgestelde eksperimentele prosedures, maak voorsiening vir die verstuiwing en analise van die oppervlak wat vir die verdampingsstudies gebruik word. Deur van hierdie sisteem gebruik te maak is die verdampingstempo van suiwer Sb gemeet. Alhoewel daar kwalitatiewe ooreenkomste rakende die verdampingsgedrag verkry is, is gevind dat die oorspronklike Hertz-Knudsenvergelyking die verdampingstempo ver oorskat.

Geen verdamping van Sb kon vanaf die gedoteerde Cu(100)-oppervlak gemeet word nie, aangesien die verdampingsvloed laer as die detekselimiet van die instrument was. Dit word toegeskryf aan die baie lae verdampingstempo van Sb, soos in hierdie studie vir suiwer Sb waargeneem is, indien vergelyk word met voorspellings deur die Hertz-Knudsenvergelyking.

Nogtans toon vergelykings tussen die eksperimentele segregasieprofiel en segregasieprofiel wat met behulp van die opgedateerde rekenaarprogram genereer is, dat Sb verdamping wel vanaf die Cu(100)-oppervlak tydens segregasie plaasvind.

Hierdie studie toon duidelik hoe belangrik dit is om verdamping tydens segregasiestudies in ag te neem. Die studie lê 'n belangrike fondament vir toekomstige verdampingstudies vanaf die oppervlakke van metale tydens segregasie, deur die nodige apparatuur in 'n Augersisteem te monteer, 'n eksperimentele protokol daar te stel en die opgradering van 'n rekenaarprogram van die bestaande Gemodifiseerde Darkenmodel om segregasieprofiel te simuleer.

Key Words

Antimony

Auger Electron Spectroscopy

Copper

Darken Model

Deposition Monitor

Evaporation

Segregation

Acronyms

AES	Auger Electron Spectroscopy
APPH	Auger Peak to Peak Height
CMA	Cylindrical Mirror Analyser
EBPVD	Electron Beam Physical Vapour Deposition
FCC	Face Centered Cubic
GDMS	Glow Discharge Mass Spectrometry
IGA	Interstitial Gas Analysis
ISS	Ion Scattering Spectroscopy
LEED	Low Energy Electron Diffraction
LTR	Linear Temperature Ramp
NLTR	Negative Linear Temperature Ramp
PVD	Physical Vapour Deposition
QCM	Quartz Crystal Monitor
SEM	Scanning Electron Microscope
SIMS	Secondary Ion Mass Spectrometry
XPS	X-Ray Photoelectron Spectroscopy

Contents

Chapter 1

Introduction

1.1	Overview.....	1
1.2	Research objectives.....	3
1.3	Thesis layout.....	4
1.4	References.....	5

Chapter 2

Diffusion Theory

2.1	Introduction.....	6
2.2	Diffusion equations.....	7
2.3	Diffusion mechanisms.....	8
	2.3.1 <i>Interstitial mechanism</i>	8
	2.3.2 <i>Ring mechanism</i>	9
	2.3.3 <i>Vacancy mechanism</i>	10
2.4	Temperature dependence of the diffusion coefficient.....	11
2.5	Summary.....	11
2.6	References.....	12

Chapter 3

Segregation Theory

3.1	Introduction.....	13
3.2	Segregation kinetics.....	14

3.3	Segregation equilibrium.....	17
3.4	The Darken model.....	23
	3.4.1 <i>The Modified Darken model</i>	24
	3.4.2 <i>The Modified Darken model with non-equilibrium vacancies</i>	29
3.5	Determining the segregation parameters.....	30
3.6	Summary.....	32
3.7	References.....	33

Chapter 4

Evaporation Theory

4.1	Introduction.....	34
4.2	Evaporation of pure metals.....	35
	4.2.1 <i>The vapour pressure of metals</i>	35
	4.2.2 <i>Evaporation flux and evaporation rate</i>	41
	4.2.3 <i>Further considerations</i>	48
4.3	Evaporation during segregation.....	49
	4.3.1 <i>A third flux of atoms</i>	49
	4.3.2 <i>Lea and Seah (1977)</i>	51
	4.3.3 <i>Stinespring and Lawson (1985)</i>	56
4.4	The Darken model with evaporation.....	60
4.5	Summary.....	63
4.6	References.....	64

Chapter 5

Experimental Setup and Procedures

5.1	Introduction.....	67
5.2	Sample preparation.....	68

5.2.1	<i>Evaporation of Sb</i>	70
5.2.2	<i>The evaporation system</i>	72
5.2.3	<i>Verification of deposited thickness by means of mass calculations</i>	76
5.2.4	<i>Annealing of Cu crystals</i>	77
5.2.5	<i>Determining the annealing time and temperature</i>	80
5.3	Equipment to measure evaporation/sublimation during segregation.....	84
5.3.1	<i>The AES system</i>	86
5.3.2	<i>The sample stage and manipulator</i>	89
5.3.3	<i>The resistance heater</i>	91
5.3.4	<i>The thickness monitor</i>	92
5.4	Some considerations when measuring evaporation.....	96
5.4.1	<i>Heat effects on the thickness monitor</i>	96
5.4.2	<i>Calibration of the QCM</i>	98
5.4.3	<i>Evaporation geometry</i>	99
5.4.3.1	<i>Point Source</i>	100
5.4.3.2	<i>An evaporating surface</i>	104
5.4.4	<i>Identification of evaporated species</i>	109
5.5	Experimental procedures.....	112
5.5.1	<i>Special considerations for sputter cleaning</i>	112
5.5.2	<i>Segregation measurements</i>	114
5.5.3	<i>Evaporation measurements</i>	115
5.5.3.1	<i>Pure Sb</i>	115
5.5.3.2	<i>Cu single crystal –linear heating method</i>	116
5.5.3.3	<i>Cu single crystal – equilibrium surface concentration method</i> ...	116
5.6	Summary.....	117
5.7	References.....	118

Chapter 6

Segregation Results and Discussion

6.1	Introduction.....	120
6.2	AES segregation data analysis procedure.....	122

6.3	Fit using Fick's Integral equation	123
6.4	The Bragg-Williams fit.....	125
6.5	The Modified Darken Fit.....	127
6.6	Summary.....	130
6.7	References.....	131

Chapter 7

Evaporation Results

7.1	Introduction.....	133
7.2	Evaporation of pure Sb.....	133
7.3	Evaporation of Sb from doped Cu(100) crystal.....	142
7.4	Summary.....	149
7.5	References.....	150

Chapter 8

Updated Modified Darken simulations including evaporation

8.1	Introduction.....	152
8.2	The Evaporation Parameter K	152
8.3	The influence of evaporation on segregation parameters.....	156
	8.3.1 The pre- exponential factor D_0	157
	8.3.2 The activation energy E	158
	8.3.3 The segregation energy ΔG	159
	8.3.4 The interaction parameter Ω	160
8.4	Summary.....	163
8.5	References.....	164

Chapter 9

Final Conclusions and Remarks

9.1	Introduction.....	165
9.2	Conclusions regarding segregation measurements.....	166
9.3	Conclusions regarding the modifications made to the AES and subsequent evaporation measurements.....	167
9.4	Conclusions regarding the adding of evaporation effects to the Modified Darken model.....	168
9.5	Suggestions for future work.....	168

Appendix A

Modified Darken Software with Evaporation.....	170
--	-----

Appendix B

Evaporation Geometry Software.....	173
------------------------------------	-----

Appendix C

Conference Contributions and Publications.....	176
--	-----

Chapter 1

Introduction

1.1 Overview

Metallurgical products play an important role in everyday life. The search for metals with better material properties such as strength, wear and corrosion resistance continues to this day. In addition to these desirable properties, the search for ways to reduce production costs and time has led to a large amount of research being conducted on the processes which determine the material properties of metals and alloys (Cronjé, 2007).

The effect of impurities in metals is of particular interest. Changing the chemical composition of surfaces in metals, whether grain boundaries or actual surfaces, can have a major influence on material properties like wear and corrosion resistance, as well as ductility (Joshi and Stein, 1973; Debarberis *et al.*, 2007). It is common to apply some sort of heat treatment during manufacturing of metallurgical products. At elevated temperatures, impurity atoms are invariably mobile and can subsequently diffuse to grain boundaries and other surfaces. This redistribution of solute atoms between the surface and the bulk of the material is known as segregation. This results in a solute surface concentration that is generally higher than the solute bulk concentration. The redistribution comes about so that the total energy of the crystal is minimized.

The start of surface segregation investigations over a century ago coincided with the appearance of surface analytical tools such as AES (Auger Electron Spectroscopy). Other surface sensitive techniques like XPS (X-ray Photoelectron Spectroscopy), SIMS (Secondary Ion Mass Spectrometry) and ISS (Ion Scattering Spectroscopy) have also been applied to study this phenomenon (Du Plessis, 1990). These surface sensitive techniques are performed under better than high vacuum conditions. In addition to the vacuum conditions which are used, samples may

be heated to high temperatures when temperature dependent parameters are measured. High vacuum coupled with the elevated temperatures employed during segregation studies are conducive to the evaporation of the segregating solute from the sample surface. As this process introduces an additional flux of atoms leaving the surface of the segregation system it is essential to factor in its influence when determining segregation parameters from experimental data obtained in these systems.

The effect of surface evaporation has however received relatively little attention in experimental segregation studies when compared to other nondiffusion processes like sputtering. Results for the evaporation of phosphorus from the surface of a FeSi sample have been obtained by Boudjema and Mosser (1988). Webber and Chadwick (1980) studied the Ni-Cu system which showed the effects of evaporation on the segregation process. The authors indicated that such evaporation leads to bulk depletion of the segregant and as a result true equilibrium cannot be obtained at the surface. According to Stinespring and Lawson (1985), the most widely accepted theoretical treatment of surface segregation inclusive of evaporation effects is that of Lea and Seah (1977). In their model however, the surface enrichment ratio, which is the key input parameter, must be determined experimentally and is subject to significant uncertainty if segregant evaporation occurs.

From the above it is clear that it is essential to consider surface evaporation during experimental segregation studies. In addition more research pertaining to the effects of evaporation on the segregation process is necessary in order to obtain a better understanding of segregation. From this it might be possible to construct models which can predict segregation behaviour more accurately than the current models which do not take into account evaporation such as the Modified Darken model (Terblans, 2001). In addition, without considering the influence of evaporation, current models might be able to predict segregation profiles, but will associate the segregation behaviour with inaccurate segregation parameters.

1.2 Research objectives

The aim of this project is to investigate surface evaporation during segregation. This is done in order to gain an understanding of the effect that surface evaporation has on the accuracy of contemporary segregation models. It is also hoped that the knowledge gained during this study can be extended to other experimental vacuum studies where surface evaporation might play a role.

The procedure will be to:

1. Dope Cu(100), Cu(110) and Cu(111) single crystals with the same homogeneous Sb concentration.
2. Measure and compare the segregation behaviour of Sb doped Cu crystals using the AES technique with the method of linear temperature ramp (LTR). Do simulations of the experimental data via the Modified Darken model and extract the segregation parameters of Sb in the low index Cu planes by fitting the modified Darken segregation model to the experimental results. The Modified Darken model is the most suitable model to use due to its ability to predict both kinetic and equilibrium segregation behaviour.
3. Modify an AES system to enable the user to measure evaporation from samples. Measure the evaporation both from pure Sb and from Sb doped Cu single crystals during LTR. Determine which parameters influences evaporation during segregation.
4. Use these results to incorporate the parameters which govern evaporation during segregation into the Modified Darken model.

5. Do simulations of the experimental results using the updated Modified Darken model which considers surface evaporation to extract the segregation parameters of Sb in the low index Cu planes.
6. Compare these segregation parameters to the parameters obtained with the standard Modified Darken model.

1.3 Thesis layout

Chapter 1 includes the introduction and aim of this study as well as the thesis layout. This is followed by *Chapter 2* and *Chapter 3*, in which diffusion and segregation theory is discussed respectively. Complementary to this, *Chapter 4* contains basic theory regarding the phenomenon of evaporation and also discusses past research done on the phenomenon of surface evaporation during segregation. This chapter also gives an in-depth discussion on the adaption of the Modified Darken model to include evaporation parameters. *Chapter 5* gives background information regarding the theory, and experimental use of the most important experimental techniques used during the course of this study including, but not limited to EBPVD (Electron Beam Physical Vapour Deposition) and AES. This chapter also includes a detailed description of the sample preparation as well as modifications made to the AES system in order to measure evaporation during segregation, and contains experimental results and tests performed using this modified AES system. *Chapter 6* contains segregation measurements and results for the Sb doped Cu(100) sample. *Chapter 7* contains evaporation measurements for pure Sb as well as the evaporation of Sb from the Cu(100) surface. In *Chapter 8* simulations done using the updated version of the Modified Darken model that includes the effects of surface evaporation are shown. These results are discussed. The conclusion as well as recommendation for future work is presented in *Chapter 9*. The modifications made to Modified Darken model software is shown in *Appendix A*. The development of Matlab software relating to evaporation geometry are discussed in *Appendix B*, and finally already announced results are shown in *Appendix C*.

1.4 References

Boudjema M.F. and Mosser A. [1988] *Journal of Less Common Metals* **145** p55.

Cronjé S. [2007] *TEM investigation of rapidly deformed Cu and Mo shaped charge liner material*, MSc dissertation, University of the Free State.

Debarberis L., Acosta B., Zeman A., Pirfo S., Moretto P., Chernobaeva A. and Nikolaev Y. [2007] *International Journal of Microstructure and Materials Properties*, **2(3/4)** p326.

Du Plessis J. [1990] *Solid State Phenomena, surface segregation* (11).

Joshi A. and Stein D.F. [1973] *Journal of Testing and Evaluation* **1(3)** p202.

Lea C. and Seah M.P. [1977] *Philosophical- Magazine* **35** p213.

Stinespring C.D. and Lawson W.F. [1985] *Surface Science* **150** p209.

Terblans J.J. [2001] *Modellering en eksperimentele ondersoek van Sb – oppervlak segregasie in Cu-enkelkristalle*, PhD thesis, University of the Free State.

Webber P.R. and Chadwick D [1980] *Surface Science* **94** pL151.

Chapter 2

Diffusion Theory

2.1 Introduction

Bulk diffusion in materials can be described as a random motion of atoms from a region of high concentration to a region of low concentration, with thermal energy as a driving force (see figure 2.1). This diffusion process takes place in order to reduce the total energy of the system to obtain a minimum value at equilibrium. This results in a homogeneous, uniform distribution of atoms in the bulk (Askeland, 1998).

Bulk diffusion plays an essential role in the manufacturing of materials for industrial use by changing the properties of bulk materials used through heat treatment. By understanding how mass is transferred by diffusion, new and cost-effective materials processing techniques for industrial use can be designed. Some examples of such industrial applications of diffusion include the hardening of steel by means of added carbon (Guy, 1972) and the manufacturing of semiconductor alloys for electrical components (Askeland, 1998).

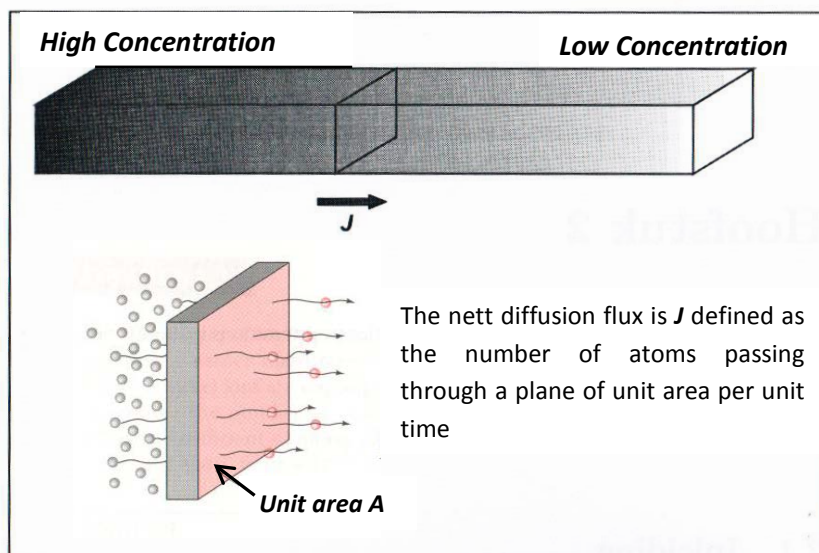


Figure 2.1: Diffusion is the movement of atoms along a concentration gradient. (Adapted from Terblans (2001) and Askeland (1998))

2.2 Diffusion equations

Changes in atomic concentration in a solid can only be achieved through diffusion. This relationship between atomic motion and concentration is described by a property known as the diffusion coefficient D . The diffusion coefficient is described by Fick's laws.

The diffusion flux J_x of atoms moving from a high concentration to a low concentration is given by Fick's first law (Omar, 1975)

$$J_x = -D \frac{\partial C}{\partial x} \quad (2.1)$$

where the concentration gradient is given by $\frac{\partial C}{\partial x}$ and can be considered the driving force behind diffusion. The negative sign indicates that the movement is from a high concentration to a low concentration and ensures that D has a positive value.

Equation 2.1 is not in a generally useable form since, during most practical situations, steady state conditions are not established and require that the concentration be described in terms of time. By combining Fick's first law with the continuity equation

$$\frac{\partial C}{\partial t} + \frac{\partial J_x}{\partial x} = 0 \quad (2.2)$$

Fick's second law can be obtained, namely

$$\frac{\partial C}{\partial t} = D \frac{\partial^2 C}{\partial x^2} \quad (2.3)$$

where C is the concentration, t is the time and x is the position in the crystal. The diffusion coefficient thus relates the diffusion distance and time. Fick's second law is a differential

equation and a number of solutions are possible depending on the boundary conditions. A complete derivation of Fick's laws is given by Joubert (2004).

2.3 Diffusion mechanisms

The most important diffusion mechanisms that are found in metals include the interstitial mechanism, the ring mechanism and the vacancy mechanism. In crystalline solids, it is possible to describe these diffusion mechanisms in simple terms because the crystal lattice restricts the positions and the migration paths of atoms which allow a simple description of each atom's displacement during diffusion (Mehrer, 2007).

The diffusion coefficient, in general, is determined by both the jump frequency and the jump distance. These are determined by the type of mechanism that an atom uses to move through the crystal, as well as by factors like the size difference between the diffusing atom and the atoms which constitute the matrix and whether the diffusion is dependent on the presence of defects or not.

2.3.1 Interstitial mechanism

Solute atoms that are significantly smaller than the matrix atoms can be incorporated in the interstitial sites of the matrix lattice. An interstitial solid solution is thus formed. The movement of these interstitial impurity atoms from one interstitial site to another interstitial site is called interstitial diffusion and is shown in figure 2.2. This mechanism is of importance for the diffusion of small impurity atoms such as H, C, N and O in metals and other materials. Small atoms fit in interstitial sites and subsequently do not significantly displace the matrix atoms from their lattice sites when moving to the interstitial position (Mehrer, 2007).

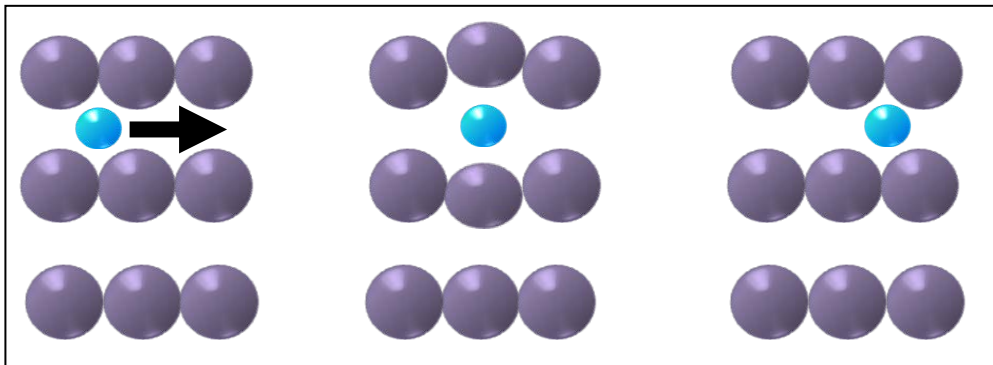


Figure 2.2: Graphical representation of interstitial diffusion.

2.3.2 Ring mechanism

When the solute and matrix atoms are similar in size, a direct exchange rather than interstitial movement takes place and this is called ring diffusion. In the early days of diffusion studies it was suggested that self-diffusion in metals occurs by a direct exchange of neighboring atoms, in which two atoms move simultaneously (Glicksman, 2000). In a close packed lattice this mechanism requires a large deformation of the crystal lattice. This entails a high activation barrier and makes this process energetically unfavourable. This led to the conclusion that direct exchange in close packed structures, was unlikely. The ring mechanism was proposed for crystalline solids, which corresponds to a rotation of three or more atoms as a group by one atom distance (see figure 2.3). The required lattice deformation is not as great as in direct exchanges and subsequently ring versions of atomic exchanges have lower activation energies (Mehrer, 2007). The probability of three or more atoms moving simultaneously is however remote, which makes this mechanism unlikely for crystalline solids (Tuck, 1974).

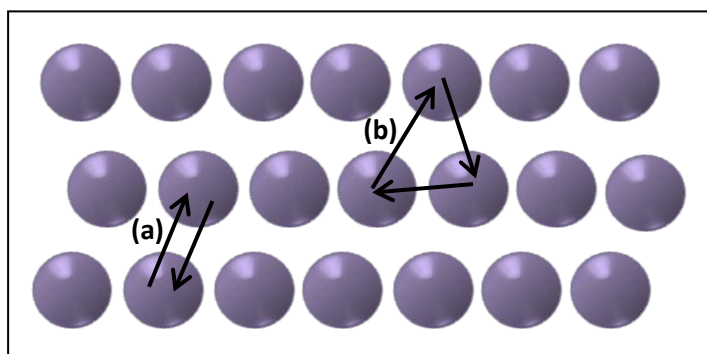


Figure 2.3: Graphical representation of (a) direct exchange diffusion and (b) ring diffusion.

2.3.3 Vacancy mechanism

According to Mehrer, 2007, vacancies have come to be accepted as the most important form of thermally induced atomic defects in metals. It has also been recognized that the vacancy mechanism is the dominant mechanism for the diffusion of matrix atoms and of substitutional solutes in metals. An atom is said to diffuse by this mechanism, when it jumps into a neighbouring vacancy which from time to time are in its vicinity. The energy barrier as shown in figure 2.4, which inhibits motion of an adjacent atom into a vacancy in a close-packed crystal lattice, is small compared to the energy barrier present during the direct exchange or ring exchange.

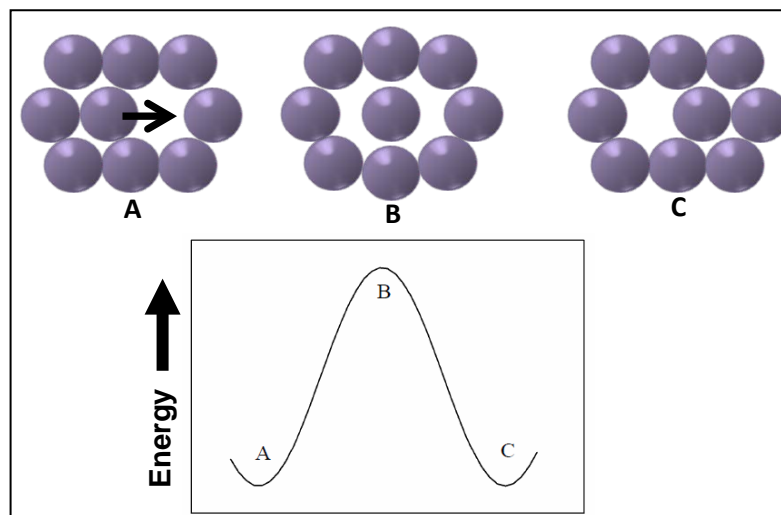


Figure 2.4: Graphical representation of vacancy diffusion.

This diffusion type depends on the availability of vacancies in the crystal lattice. The number of vacancies in a monoatomic crystal, at a temperature T , can be determined by

$$N_v = N_0 \exp\left(\frac{-E_v}{RT}\right) \quad (2.4)$$

where N_0 is the number of lattice sites, E_v the vacancy formation energy and R the universal gas constant (Omar, 1975).

2.4 Temperature dependence of the diffusion coefficient

From diffusion experiments it is clear that the diffusion coefficient is highly dependent on temperature. An empirical equation which describes the temperature dependence of the diffusion coefficient is given by (Omar, 1975).

$$D = D_0 \exp\left(\frac{-E}{RT}\right) \quad (2.5)$$

where D_0 is the pre-exponential factor and $\frac{-E}{RT}$ is the exponential factor, with E known as the activation energy for diffusion. It has also been shown that the diffusion coefficient is dependent on the surface orientation (Terblans, 2001).

2.5 Summary

Bulk diffusion plays an essential role in the manufacturing of materials for industrial use by changing the properties of bulk materials through heat treatment. The process of bulk diffusion can be described as a random motion of atoms from a region of high concentration to a region of low concentration, with thermal energy as a driving force. The relationship between this atomic motion and the resultant changes in concentration that diffusion causes is described by a property known as the diffusion coefficient D which is temperature dependent. The diffusion coefficient D can be predicted by using Fick's equations. Although a number of diffusion mechanisms have been proposed, it has generally been accepted that the vacancy mechanism is the dominant mechanism for the diffusion of matrix atoms and of substitutional solutes in metals.

2.6 References

Askeland D.R. [1998] *The Science and Engineering of Materials*, Stanley Thornes Ltd.

Glicksman M.E. [2000] *Diffusion in Solids*, Wiley.

Guy A.G. [1972] *Introduction to materials science*, McGraw-Hill Book Co.

Joubert H.D. [2004] *A Monte Carlo program for simulating segregation and diffusion utilizing chemical potential calculations*, MSc dissertation, University of the Free State.

Mehrer H. [2007] *Diffusion in Solids: Fundamentals, Methods, Materials, Diffusion-Controlled Processes*, Springer.

Omar M.A. [1975] *Elementary solid state physics: principles and applications*, Addison-Wesley Pub. Co.

Terblans J.J. [2001] *Modellering en eksperimentele ondersoek van Sb – oppervlak segregasie in Cu-enkelkristalle*, PhD thesis, University of the Free State.

Tuck B. [1974] *Introduction to diffusion in semiconductors*, Peter Peregrinus Ltd.

Chapter 3

Segregation Theory

3.1 Introduction

Knowledge of segregation theory is essential if the effects of surface evaporation during segregation are to be understood. Surface segregation is the enrichment at the surface or surface region of one component of an alloy as a result of diffusion of that element from the bulk to the surface region. This takes place so that the total energy of the crystal is lowered. The driving force behind segregation is thus the reduction of the crystal's total energy (Hofmann and Erlewein, 1978). This movement of atoms is contrary to Fick's diffusion model (see section 2.2) where the concentration gradient is given as the driving force behind diffusion. Under certain circumstances and with certain assumptions diffusion theory can still be used to give a physical description of segregation (see section 3.2). Throughout this chapter it will be assumed that a binary system is used with only two components as in the case of this study.

A typical segregation profile can be divided into two regions, namely the kinetic region and the equilibrium region (figure 3.1). During the kinetic phase of segregation the surface concentration increases with temperature and time until such point where an equilibrium surface concentration is reached.

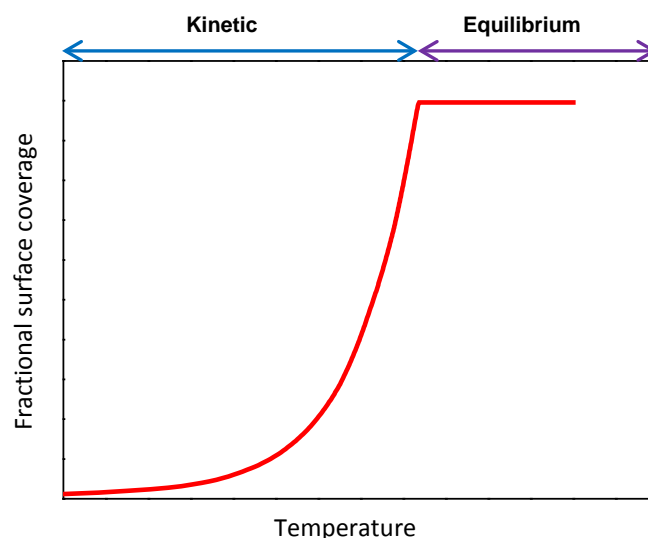


Figure 3.1: Kinetic and equilibrium regions of a typical segregation profile.

In the next sections of this chapter the mathematical modelling of these regions will be discussed.

3.2 Segregation kinetics

Segregation kinetics can be defined as the rate at which impurity atoms diffuse from the bulk to the surface of a crystal and can be described by Fick's semi-infinite model.

It is assumed that the segregating impurity atoms have no interaction with each other. This condition can be implemented mathematically by considering that the segregating atoms reaching the surface are immediately removed from the surface, and that the concentration on the surface is always equal to zero. Now let $C(x, t)$ represent the concentration at x after a time, t . This means that at the surface

$$C(0, t) = 0 \quad \text{for } t \geq 0.$$

It is also assumed that the distribution of impurity atoms in the bulk is initially uniform and homogeneous, thus

$$C(x, 0) = C^B \quad \text{for } x > 0$$

where C^B is the initial bulk concentration. These boundary conditions are shown in figure 3.2.

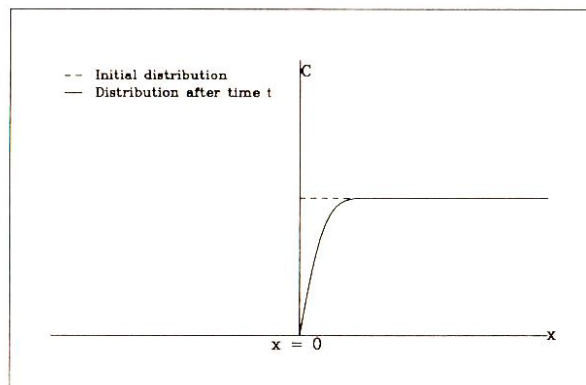


Figure 3.2: Initial and boundary conditions for the semi-infinite solid. (Du Plessis, 1990)

These boundary conditions can be used to solve Fick's second law

$$\frac{\partial C}{\partial t} = D \frac{\partial^2 C}{\partial x^2} \quad (3.1)$$

using Laplace transformations as described in detail in Crank (1975). The solution which describes the bulk concentration is then given by

$$C(x, t) = C^B \operatorname{erf}\left(\frac{x}{2\sqrt{Dt}}\right). \quad (3.2)$$

Equation 3.2 and Fick's first law (equation 2.1) can be used to derive the flux of atoms at the surface ($x = 0$).

$$J_{x=0} = \left(-D \frac{\partial C}{\partial x}\right)_{x=0} = -C^B \sqrt{\frac{D}{\pi t}}. \quad (3.3)$$

By integrating the flux, the total number of atoms $\Delta N(t)$ which moves through the surface A at $x = 0$ up to time t can be calculated as

$$\Delta N(t) = A \int_0^t |J_{x=0}| dt = 2AC^B \sqrt{\frac{Dt}{\pi}}. \quad (3.4)$$

If it is assumed that the atoms that move through area A subsequently form part of the surface layer instead of being removed, the change in concentration of segregated atoms in the

surface layer ΔC_s can be calculated by dividing the total number of additional atoms in the surface layer by the volume of the surface layer, giving

$$\Delta C^s = \left[2AC^B \sqrt{\frac{Dt}{\pi}} \right] / Ad = \frac{2C^B}{d} \sqrt{\frac{Dt}{\pi}} \quad (3.5)$$

with d the interplanar spacing.

Considering that at $t = 0$ the surface concentration C^s was the same as that of the bulk, $C^s = C^B + \Delta C^s$ and so

$$C^s = C^B \left[1 + \frac{2}{d} \sqrt{\frac{Dt}{\pi}} \right]. \quad (3.6)$$

This well known equation is often used to determine the surface concentration during segregation (Viljoen, 1995), (Terblans, 1997). A typical example of its use for comparison to experimental data is shown in figure 3.3.

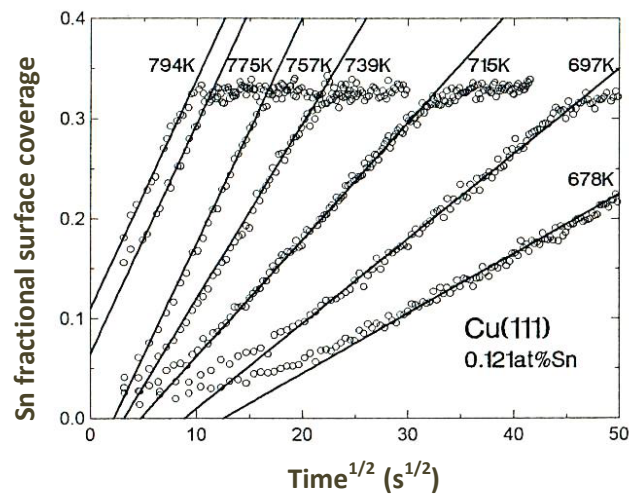


Figure 3.3: Practical use of equation 3.6 to fit kinetic segregation data. (Adapted from Viljoen, 1995)

Unfortunately this equation cannot predict the surface concentration when equilibrium has been reached. One can see this in figure 3.3 where the experimental data reaches a plateau at a surface fractional coverage of one third.

3.3 Segregation equilibrium

For the following derivations regarding segregation equilibrium the following assumptions are made (Terblans, 2001):

1. The crystal is regarded as a closed system consisting of the two phases, surface s and bulk B which are both open systems.
2. The surface region is finite consisting of a finite number of atoms n^s .
3. The bulk is infinite in size consisting of an infinite number of atoms $n^B = \infty$.
4. Atoms may be exchanged between the two phases until the energy of the crystal is minimized.

Equilibrium for such a closed system with p phases can be described in terms of the change in total energy of the system as described by Lupis (1983)

$$(\delta E)_{S,V,n_i} = \sum_{v=1}^p \delta E^v \geq 0 \quad (3.7)$$

i.e. the total energy E of the crystal is a minimum. Each term may be expanded

$$\delta E^v = T^v \delta S^v - P^v \delta V^v + \delta G^v \quad (3.8)$$

with T^v the temperature, S^v the entropy, P^v the pressure and V^v the volume of the phase v and n_i the number of atoms of species i . The change in the Gibbs free energy of phase v is given by δG^v .

If the temperature and pressure of all phases are equal equation 3.7 becomes

$$(\delta E)_{n_i} = (\delta G)_{n_i} \geq 0. \quad (3.9)$$

In such a case of constant temperature and pressure, the change in Gibbs free energy can thus be used to describe the equilibrium state (minimum energy state) of a system instead of using the total energy E . The advantage of this is that the Gibbs free energy may be written in terms of the chemical potential of the various constituents and that the equilibrium condition may be expressed as a function of the chemical potential μ

$$G^v = \sum_{i=1}^m n_i^v \mu_i^v \quad (3.10)$$

where n_i^v is the number of moles of species i in phase v and μ_i^v is the chemical potential of species i in phase v .

The total Gibbs free energy of the systems which consists of p phases can then be expressed as

$$G = \sum_{v=1}^p G^v = \sum_{v=1}^p \sum_{i=1}^m n_i^v \mu_i^v. \quad (3.11)$$

Using equation 3.11 the change in Gibbs free energy can be written as

$$\delta G = \sum_{v=1}^p \left[\sum_{i=1}^m (\delta n_i^v \mu_i^v) + \sum_{i=1}^m (n_i^v \delta \mu_i^v) \right]. \quad (3.12)$$

The equilibrium state can thus be expressed as

$$\sum_{v=1}^p \left[\sum_{i=1}^m (\delta n_i^v \mu_i^v) + \sum_{i=1}^m (n_i^v \delta \mu_i^v) \right] \geq 0. \quad (3.13)$$

From equation 3.11 it follows that for a system with two phases s and B the total Gibbs free energy of the system can be written as

$$G = G^s + G^B. \quad (3.14)$$

The variation in Gibbs free energy can then be written according to equation 3.12 as

$$\delta G = \left[\sum_{i=1}^m (\delta n_i^s \mu_i^s) + \sum_{i=1}^m (\delta n_i^B \mu_i^B) \right] + \left[\sum_{i=1}^m (n_i^s \delta \mu_i^s) + \sum_{i=1}^m (n_i^B \delta \mu_i^B) \right] \quad (3.15)$$

with n_i^s the number of moles of species i in the surface, μ_i^s is the chemical potential of species i on the surface, n_i^B is the number of moles of species i in the bulk, μ_i^B is the chemical potential of species i in the bulk.

The expression in the second square brackets in equation 3.15 is known as the Gibbs-Duhem relation and reduces to zero (Du Plessis, 1990). Equation 3.15 thus reduces to

$$\delta G = \left[\sum_{i=1}^m (\delta n_i^S \mu_i^S) + \sum_{i=1}^m (\delta n_i^B \mu_i^B) \right]. \quad (3.16)$$

It is assumed that the surface region is finite, consisting of a fixed number of atoms. This means that for every atom that moves out of the surface, an atom will move into the surface. The total change in the number of atoms in the surface can thus be expressed as

$$\delta n_1^S + \delta n_2^S + \dots + \delta n_m^S = 0. \quad (3.17)$$

By making the m^{th} term the subject of equation 3.17

$$-\delta n_m^S = \delta n_1^S + \delta n_2^S + \dots + \delta n_{m-1}^S \quad (3.18)$$

and using equation 3.16 the change in the Gibbs free energy of a crystal can be written as

$$\sum_{i=1}^{m-1} (\mu_i^S - \mu_i^B - \mu_m^S + \mu_m^B) \delta n_i^S \geq 0 \quad (3.19)$$

The $(m - 1)$ terms are now independent of δn_i^S and subsequently equation 3.19 can be satisfied only if

$$\mu_i^S - \mu_i^B - \mu_m^S + \mu_m^B = 0. \quad (3.20)$$

Equation 3.20 is the boundary condition for atoms segregating from the bulk B to a surface s , with which it is in contact, in terms of the chemical potential. It is also important to note that equation 3.20 does not imply that $\mu_i^s = \mu_i^B$ (Du Plessis, 1990).

In the case of a binary alloy, the equilibrium conditions in equation 3.20 becomes

$$\mu_1^s - \mu_1^B - \mu_2^s + \mu_2^B = 0. \quad (3.21)$$

The chemical potential terms must now be expanded in terms of the surface and bulk concentrations respectively in order to derive an analytical expression for the segregation equation. This can be done by means of a regular solution model (Lupis, 1983)

$$\mu_1^v = \mu_1^{0v} + \Omega_{12}(X_2^v)^2 + RT \ln X_1^v \quad (3.22)$$

$$\mu_2^v = \mu_2^{0v} + \Omega_{12}(X_1^v)^2 + RT \ln X_2^v \quad (3.23)$$

where μ_1^v is the chemical potential of species 1 in phase v , μ_2^v is the chemical potential of species 2 in phase v , μ_1^{0v} is the standard chemical potential of species 1 in phase v , μ_2^{0v} is the standard chemical potential of species 2 in phase v , and Ω_{12} is the chemical interaction parameter between species 1 and 2. X_1^v and X_2^v are the fractional concentrations of species 1 and 2 in phase v respectively.

Substituting equations 3.22 and 3.23 into equations 3.21 yields the well-known Bragg-Williams equation (Blackely, 1973)

$$\frac{X_1^s}{1 - X_1^s} = \frac{X_1^B}{1 - X_1^B} \exp \left[\frac{\Delta G + 2\Omega_{12}(X_1^s - X_1^B)}{RT} \right] \quad (3.24)$$

where $\Delta G = \mu_1^{0B} - \mu_1^{0s} - \mu_2^{0B} + \mu_2^{0s}$ is the segregation energy.

If the interaction parameter Ω_{12} is equal to zero, equation 3.24 reduces to the well-known Langmuir-McClean expression (Tauber *et al.*, 1978)

$$\frac{X_1^s}{1 - X_1^s} = \frac{X_1^B}{1 - X_1^B} \exp \left[\frac{\Delta G}{RT} \right]. \quad (3.25)$$

A typical example of the Langmuir-McClean expression compared to experimental data for two crystal orientations is shown in figure 3.4.

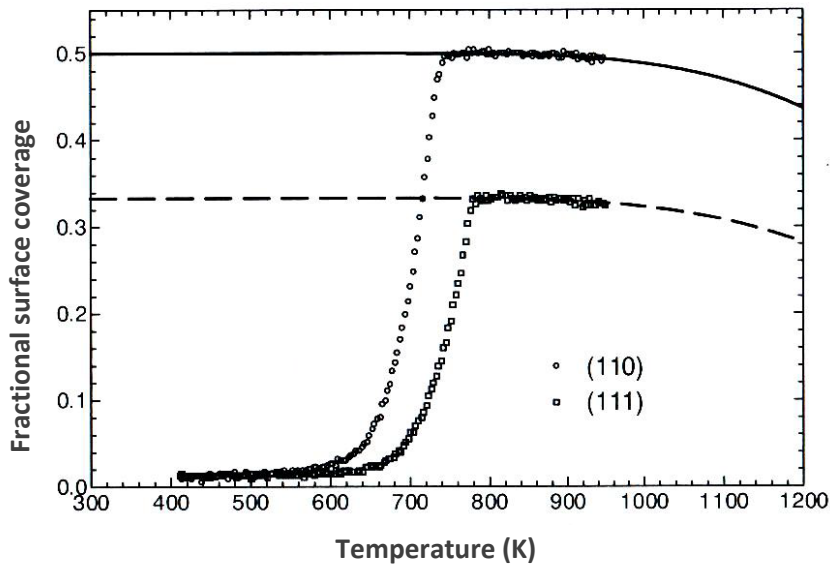


Figure 3.4: Practical use of equation 3.25 to fit equilibrium segregation data. (Adapted from Terblans, 2001)

Unfortunately this equation can only predict the surface concentration in the equilibrium region.

3.4 The Darken model

As mentioned in section 3.1 the driving force behind segregation is the reduction of the crystal's total energy. This movement of atoms is contrary to Fick's diffusion model where the concentration gradient is given as the driving force behind diffusion. The fundamental problem with trying to force a segregation application of the Fick equation is that a model which describes downhill diffusion as far as the concentration profile is concerned is applied to a situation where the diffusion is in fact uphill. Such attempts are mathematical manipulations in order to arrive at the right sort of answer. The mathematical manipulations may be accepted if their specific form can be justified by physical arguments.

The problem of uphill diffusion in terms of the concentration gradient was addressed by Darken (1948). It should be noted that Darken himself referred to these equations as "phenomological" equations. The Darken description is a macroscopic description which chooses as macroscopic entity the energy at x rather than the concentration C , which makes sense based on the assumption that surface segregation is the redistribution of atoms in order to minimize the total energy. The model considers the difference in the chemical potential energy between the multi layers of atoms as the driving force for segregation. The segregating atoms will diffuse from the bulk which has a high chemical potential to the surface which has a low chemical potential.

The major advantage of the Darken equations is that the Darken model describes both the kinetic - and equilibrium segregation simultaneously.

In this model the flux of species i through a plane at $x = b$ can be expressed in terms of the chemical potential as:

$$J_i = -M_i C_i^b \left(\frac{\partial \mu_i}{\partial x} \right)_{x=b} \quad (3.26)$$

where C_i^b is the concentration of the species i in the plane, μ_i is the chemical potential of species i and M_i is the mobility of the species i . M_i plays a role equivalent to D in Fick's law. In fact M_i can be expressed in terms of D . Darken defined the mobility (Du Plessis, 1990) as

$$M_i = \frac{D}{RT}. \quad (3.27)$$

This holds only for a dilute ideal solution.

3.4.1 The Modified Darken model

In order to obtain a physically more correct model, the Darken model was modified by Du Plessis (1990). In this modification the crystal is divided in $(N + 1)$ discrete layers which are parallel to the surface. The thickness d of the layers are the same as the interplanar distance of the planes parallel to the surface.

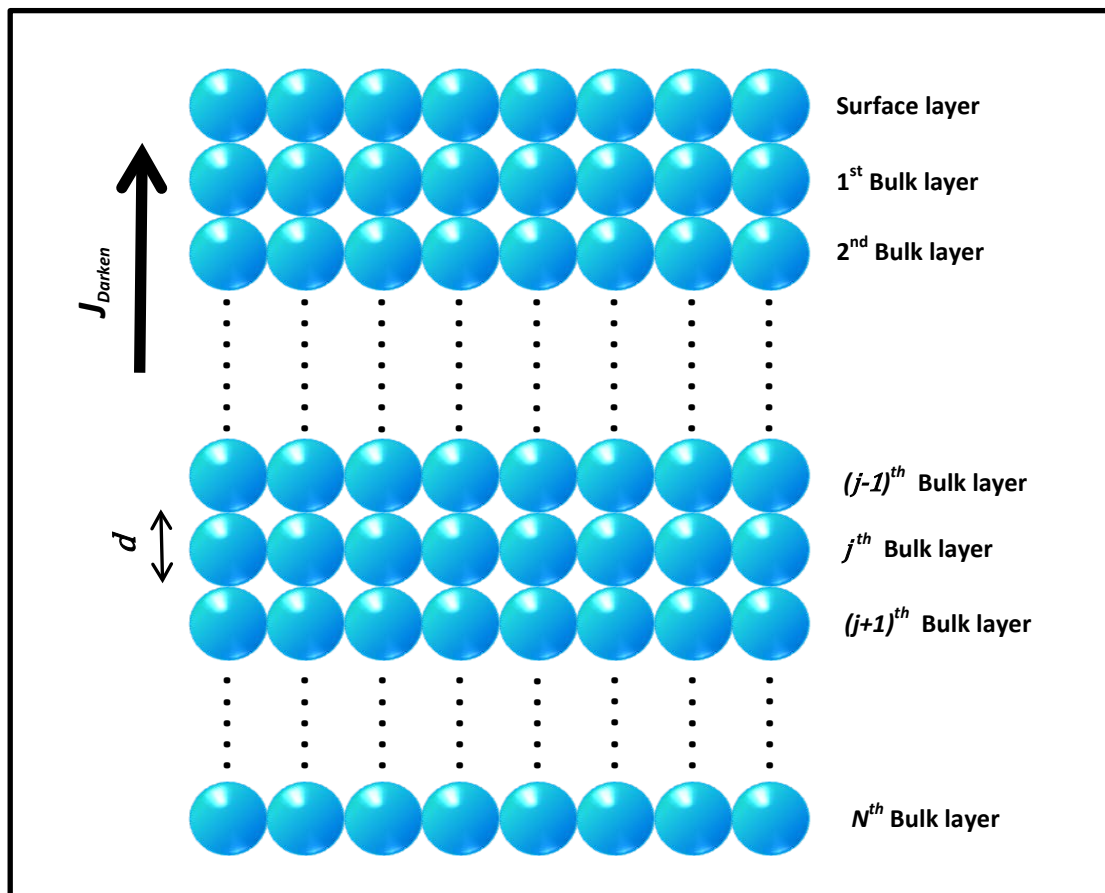


Figure 3.5: Schematic diagram of a crystal divided in $(N + 1)$ discrete layers.

The second modification made by Du Plessis (1990) was using the discrete form of $\left(\frac{\partial\mu_i}{\partial x}\right)$, namely

$$-\left(\frac{\partial\mu_i}{\partial x}\right) = \frac{\Delta\mu_i^{(j+1 \rightarrow j)}}{d}. \quad (3.28)$$

It was also shown that the change in chemical potential can be written as

$$\Delta\mu_i^{(j+1 \rightarrow j)} = \left(\mu_i^{(j+1)} - \mu_i^j\right) - \left(\mu_m^{(j+1)} - \mu_m^j\right) \quad (3.29)$$

with $\mu_i^{(j+1)}$ the chemical potential of the species i in the layer $(j + 1)$, μ_i^j the chemical potential of the species i in the layer j , $\mu_m^{(j+1)}$ the chemical potential of the species m in the layer $(j + 1)$ and μ_m^j the chemical potential of the species m in the layer j .

Lastly, Du Plessis (1990) changed the concentration C_i^b which according the Darken model was defined as the concentration of species i at $x = b$ which is at a plane between two layers j and $(j + 1)$. This has no physical meaning in a layer by layer description. It was argued that the concentration of the atomic layer out of which the diffusion takes place determines the flux out of that layer. If diffusion takes place from the $(j + 1)^{\text{th}}$ layer to the j^{th} layer in the direction of the surface then the $(j + 1)^{\text{th}}$ layer is the source and subsequently the flux of diffusing atoms can be written as

$$J_i^{(j+1 \rightarrow j)} = M_i C_i^{(j+1)} \frac{\Delta\mu_i^{(j+1 \rightarrow j)}}{d}. \quad (3.30)$$

If the flux is in the opposite direction away from the surface, then the j^{th} layer is now the diffusion source and it follows that

$$J_i^{(j \rightarrow j+1)} = M_i C_i^j \frac{\Delta\mu_i^{(j+1 \rightarrow j)}}{d}. \quad (3.31)$$

The flux between two adjacent layers is thus described by two equations, with only one of the equations being valid at any specific time.

If $\Delta\mu_i^{(j+1 \rightarrow j)} > 0$, then the Gibbs free energy decreases as atoms of species i move from the $(j + 1)^{\text{th}}$ layer to the j^{th} layer with $C_i^{(j+1)}$ being the supply. If $\Delta\mu_i^{(j+1 \rightarrow j)} < 0$, then the Gibbs free energy decreases when atoms of species i moves from the j^{th} layer to the $(j + 1)^{\text{th}}$ layer with C_i^j being the supply.

Explicitly this can be written as

$$J_i^{(j+1 \rightarrow j)} = M_i C_i^{(j+1)} \left| \frac{\Delta\mu_i^{(j+1 \rightarrow j)}}{d} \right| \quad \text{if } \Delta\mu_i^{(j+1 \rightarrow j)} > 0, \quad (3.32)$$

$$J_i^{(j \rightarrow j+1)} = M_i C_i^j \left| \frac{\Delta\mu_i^{(j \rightarrow j+1)}}{d} \right| \quad \text{if } \Delta\mu_i^{(j \rightarrow j+1)} < 0. \quad (3.33)$$

These equations can be used to calculate the rate at which the concentration of species i in the j^{th} layer changes. The rate of increase in the number N_i^j of atoms of species in the j^{th} layer is given by

$$\frac{\partial N_i^j}{\partial t} = d^2 (J_i^{(j+1 \rightarrow j)} - J_i^{(j \rightarrow j-1)}) \quad (3.34)$$

Dividing on both sides of equation 3.34 by d^3 yields the rate at which the concentration of species i in the j^{th} layer changes

$$\frac{\partial C_i^j}{\partial t} = \frac{J_i^{(j+1 \rightarrow j)} - J_i^{(j \rightarrow j-1)}}{d} \quad (3.35)$$

where C_i^j is the concentration of species i in layer j .

This equation can be expanded to a set of $(m - 1)(N + 1)$ equations by considering the flux as described in equation 3.31 and rewriting equation 3.35 with $C_i^j = \frac{X_i^j}{d^3}$. This yields

$$\frac{\partial X_i^j}{\partial t} = \left(\frac{M_i X_i^{(j+1)}}{d^2} \Delta\mu_i^{(j+1 \rightarrow j)} - \frac{M_i X_i^j}{d^2} \Delta\mu_i^{(j \rightarrow j-1)} \right). \quad (3.36)$$

With this set of equations the rate of species i change in concentration in the j^{th} layer can be calculated:

$$\begin{aligned} \frac{\partial X_i^s}{\partial t} &= \left(\frac{M_i^{(B_1 \rightarrow s)} X_i^{B_1}}{d^2} \Delta\mu_i^{(B_1 \rightarrow s)} \right) \\ \\ \frac{\partial X_i^{B_1}}{\partial t} &= \left(\frac{M_i^B X_i^{B_2}}{d^2} \Delta\mu_i^{(B_2 \rightarrow B_1)} - \frac{M_i^{(B_1 \rightarrow s)} X_i^{B_1}}{d^2} \Delta\mu_i^{(B_1 \rightarrow s)} \right) \\ &\quad \vdots \\ \frac{\partial X_i^j}{\partial t} &= \left(\frac{M_i^B X_i^{(j+1)}}{d^2} \Delta\mu_i^{(j+1 \rightarrow j)} - \frac{M_i^B X_i^j}{d^2} \Delta\mu_i^{(j \rightarrow j-1)} \right) \\ &\quad \vdots \end{aligned} \quad (3.37)$$

for $i = 1, 2, 3 \dots, m - 1$ and $M_i^{B \rightarrow s}$ the mobility of species i moving from the bulk B to the surface s . $X_i^{B_1}$ is the concentration of the first subsurface layer and the mobility in the bulk is given by M_i^B . These rate equations are applicable for the specific case of the flux being in the direction of the surface and can be solved numerically. The solution makes it possible to calculate the concentration of species i in any layer as a function of time.

Equations 3.20 - 3.23 can thus be used to rewrite the set of rate equations in order to describe a specific binary system.

$$\begin{aligned}
\frac{\partial X_1^s}{\partial t} &= \left(\frac{M_1^{(B_1 \rightarrow s)} X_1^{B_1}}{d^2} \right) \left[\Delta G + RT \ln \left(\frac{X_1^{B_1} X_2^s}{X_1^s X_2^{B_1}} \right) \right] \\
\frac{\partial X_1^{B_1}}{\partial t} &= \left(\frac{M_1^B X_1^{B_1}}{d^2} \right) \left[RT \ln \left(\frac{X_1^{B_2} X_2^{B_1}}{X_1^{B_1} X_2^{B_2}} \right) - RT \ln \left(\frac{X_1^{B_1} X_2^s}{X_1^s X_2^{B_1}} \right) \right] \\
&\vdots \\
\frac{\partial X_1^{B_j}}{\partial t} &= \left(\frac{M_1^B X_1^{(B_{j+1})}}{d^2} \right) \left[RT \ln \left(\frac{X_1^{(B_{j+1})} X_2^{B_j}}{X_1^{B_j} X_2^{(B_{j+1})}} \right) - RT \ln \left(\frac{X_1^{B_j} X_2^{(B_{j-1})}}{X_1^{(B_{j-1})} X_2^{B_j}} \right) \right] \\
&\vdots
\end{aligned} \tag{3.38}$$

This set of rate equations were derived for a binary system without interactions. This binary system is assumed to be an ideal solution and thus

$$X_1^j + X_2^j = 1 \tag{3.39}$$

where X_i^j is the fractional concentration of species i in the j^{th} layer with $i = 1$ or 2 . This set of rate equations makes it possible to describe the equilibrium segregation as well as segregation kinetics.

3.4.2 The Modified Darken model with non-equilibrium vacancies

In chapter 2 the vacancy mechanism of diffusion was described as the dominant mechanism for the diffusion of matrix atoms and of substitutional solutes in metals. It is thus only logical that the migration of vacancies should play an important role in any model which attempts to describe the segregation process. A change to the Modified Darken model to include non-equilibrium vacancies was proposed by Terblans (2001).

Terblans (2001) proposed that a new mobility m_i be defined as

$$m_i = \frac{D_0 \exp\left(-\frac{E_m}{RT}\right)}{RT} \quad (3.40)$$

and

$$M_i = m_i X_v \quad (3.41)$$

with E_m the migration energy of a vacancy (or atom) and X_v the equilibrium concentration of vacancies. The flux of atoms between two adjacent layers can then be expressed as

$$J_i^{(j+1 \rightarrow j)} = m_i X_v^j C_i^{(j+1)} \left(\frac{\Delta \mu_i^{(j+1 \rightarrow j)}}{d} \right). \quad (3.42)$$

This modification gives a better description of segregation when the temperature of the crystal changes. Terblans (2001) also showed that the effects of vacancies on the segregation profile could be reduced if the sample was slowly cooled after annealing and before a segregation measurement was done, and that surface orientation influences the bulk diffusion coefficient under the surface. This shifts the segregation curves due to the different applicable activation energies. The use of the Modified Darken model is shown in figure 3.6 for two different crystal orientations.

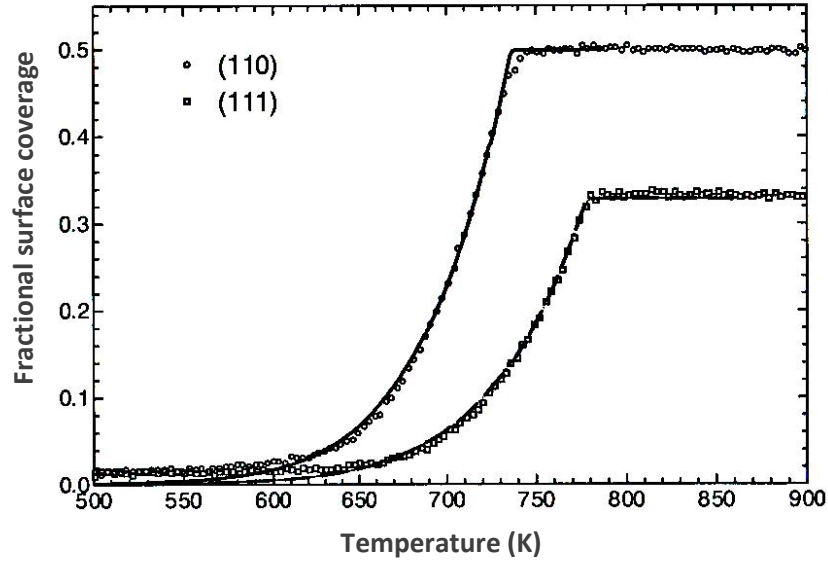


Figure 3.6: Practical use of the Modified Darken model to fit segregation data. (Adapted from Terblans, 2001)

3.5 Determining the segregation parameters

The following segregation parameters are of importance in this study:

1. D the diffusion coefficient with unit m^2s^{-1} .
2. D_0 the pre exponential factor with unit m^2s^{-1} .
3. E the activation energy with unit $\text{kJ}\cdot\text{mol}^{-1}$.
4. ΔG the segregation energy with unit $\text{kJ}\cdot\text{mol}^{-1}$.
5. Ω the interaction parameter with unit $\text{kJ}\cdot\text{mol}^{-1}$.

The segregation parameters can be determined by solving the Arrhenius equation which is an empirical equation relating the relationship between the diffusion coefficient and temperature

$$D = D_0 \exp\left(\frac{-E}{RT}\right). \quad (3.43)$$

If D_0 and E are known for a specific system, then the diffusion coefficient D can be calculated for any temperature and subsequently the segregation behavior of the system can be simulated for any temperature. To achieve this equation 3.43 can be rewritten in the form

$$\ln(D) = \left(\frac{-E}{R}\right)\left(\frac{1}{T}\right) + \ln(D_0) \quad (3.44)$$

By plotting a graph of $\ln(D)$ vs. $\frac{1}{T}$ a straight line is obtained with $\left(\frac{-E}{R}\right)$ the slope of the line and $\ln(D_0)$ the vertical-axis intercept. This plot known as the Arrhenius plot can be obtained if a number of diffusion coefficients for different temperatures are known. This can be done by measuring the surface concentration of the segregant as a function of time, at a constant temperature. By fitting the Fick - or Modified Darken model to the measured data, the diffusion coefficients can be determined. If the modified Darken model is used, ΔG can also be determined. The drawback of this constant temperature method is that a number of segregation curves for different temperatures must be measured.

Linear heating is a method which allows the segregation parameters to be determined with a single segregation curve. In this method the sample is heated at a constant heating rate and a segregation curve in terms of temperature is obtained. Once again the various segregation models can be fitted to the experimental segregation curve and the segregation parameters ($D_0, E, \Delta G, \Omega$) can be determined (Viljoen, 1995).

It is clear from the preceding section that segregation theory has constantly evolved during the last century. Currently the Modified Darken model is widely accepted and used to fit segregation curves to experimental results from which the segregation parameters are then extracted. Software to accomplish this has also been developed in house at the Department of Physics at the University of the Free State (figure 3.7). The quest for more accurate segregation and diffusion models continues to this day. One aspect which has received relatively little attention is the phenomena of surface loss due to evaporation during segregation. In the following chapter the theory of this phenomenon will be discussed, and how it can be taken into consideration in an attempt to improve on the existing segregation models.

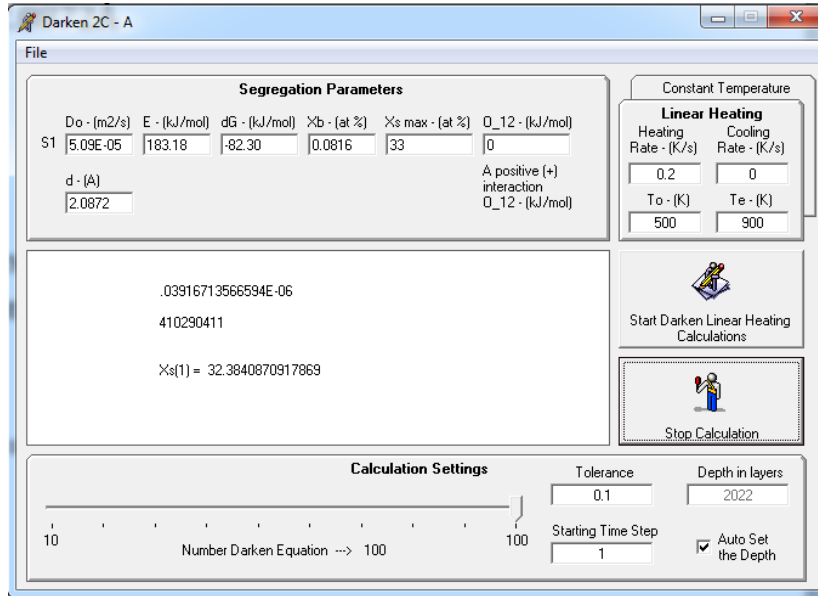


Figure 3.7: Software implementing the Modified Darken segregation model.

3.6 Summary

Surface segregation is the enrichment at the surface or surface region of one component of an alloy as a result of diffusion of that element from the bulk to the surface region. This takes place so that the total energy of the crystal is lowered. A typical segregation profile can be divided into two regions, namely the kinetic region and the equilibrium region. During the kinetic phase of segregation the surface concentration increases with temperature and time until such point where an equilibrium surface concentration is reached. A number of models have been proposed to predict surface segregation. From these models the various segregation parameters (D_0 , E , ΔG , Ω) can be obtained. Most of these models however, have the drawback of only being able to predict segregation behavior in either the kinetic region or the equilibrium region of segregation. One notable exception is the Modified Darken model which can predict both kinetic and equilibrium segregation behaviour. While efforts continue to refine the Modified Darken model, no effort has been made to include the effects of surface evaporation in this model.

3.7 References

Crank J. [1975] *The Mathematics of diffusion*, 2nd edition, Elsevier.

Du Plessis J. [1990] *Solid State Phenomena, surface segregation* (11).

Hofmann S. and Erlewein J. [1978] *Surface Science* **77**, p591.

Lupis C.H.P. [1983] *Chemical Thermodynamics of Materials*, Elsevier Science Ltd.

Tauber G. and Grabke H.J. [1978] *Berichte der Bunsengesellschaft für physikalische Chemie*. **82**, p298.

Terblans J.J. [2001] *Modelling en eksperimentele ondersoek van Sb – oppervlak segregasie in Cu-enkelkristalle*, PhD thesis, University of the Free State.

Viljoen E. [1995] *Lineêre verhittingstudies van oppervlaksegregasie in binêre allooie*, PhD thesis, University of the Orange Free State.

Chapter 4

Evaporation Theory

4.1 Introduction

Volatilization of elements is a well known phenomenon. A number of metals have been found to exhibit evidence of volatility at temperatures significantly below their melting points. As early as 1872, Merget showed that frozen mercury volatilised in air in the course of time (Kaye and Ewen, 1913). In 1882, Demarcay conducted similar experiments in vacuum and found that cadmium evaporated at as low a temperature as 160°C, zinc at 184°C and lead and tin at 360°C (Kaye and Ewen, 1913). A familiar illustration of metallic volatilisation is furnished by the blackening of tungsten filament lamps. Deposits of a definite outline can occasionally be detected on the bulbs of the lamps, a fact which seems to point to the projection of particles in definite directions from the filament (Kaye and Ewen, 1913).

The kinetics of materials evaporation is important in many areas such as vacuum metallurgy, welding, electron beam processing and thin film technology and is the fundamental technique used in Physical Vapour Deposition (PVD) processes (Das, 2003; Herman *et al.*, 2004). The distillation of metals for eliminating impurities, for example, is an area in materials science where these kinetics play a crucial role. Developing the fundamental knowledge of evaporation kinetics is thus of crucial importance, not only with regards to this study, but also in general (Safarian and Engh, 2013).

The evaporation process from a metal is governed by four distinct regimes: mass transport of atoms from the interior of the metal bulk to the surface, phase change to gaseous state at the surface and the resultant escape of these atoms from the surface, mass transport in the gas phase above the metal surface and finally condensation (Das, 2001). In this chapter the fundamentals of

evaporation theory will be discussed along with previous research from literature conducted on evaporation during the segregation process. Particular emphasis will be placed on the evaporation flux from the surface as this is the regime which plays the most important role in this study.

4.2 Evaporation of pure metals

4.2.1 The vapour pressure of metals

Vapour pressure or equilibrium vapour pressure is defined as the pressure exerted by a vapour in thermodynamic equilibrium with its condensed phases (solid or liquid) at a given temperature in a closed system. The equilibrium vapour pressure of a material is an indication of the materials potential evaporation rate in terms of a particles tendency to escape from the solid or liquid. While knowledge of the vapour pressure curve of any material is of theoretical significance in understanding its basic physical properties, it is of practical importance when the material is used in high temperature vacuum applications. Vapour pressure values may be calculated from thermodynamic data, but can be complicated in the case of solids for a number of reasons, one being that the magnitude of vapour pressure for solids at low temperature can be considerably below practical measurements (Arblaster, 2007).

The vapour pressure of any substance increases non-linearly with temperature according to the Clapeyron relation where the variation of vapour pressure p with temperature T can be represented by

$$\frac{dp}{dT} = \frac{\Delta H}{T\Delta V} \quad (4.1)$$

where ΔV is the change of volume during the transition from condensed phase to gas, ΔH is the latent heat of sublimation or vaporisation depending on whether the temperature is below or

above the melting point respectively. Since the volume change is very large, the value for the condensed phase can be neglected and using the ideal gas law equation 4.1 becomes

$$\frac{dp}{dT} = \frac{p\Delta H}{RT^2} \quad (4.2)$$

and therefore

$$\frac{d \log p}{dT} = \frac{\Delta H}{RT^2} \cdot \quad (4.3)$$

Integrating the above equation gives the Clausius-Clapeyron equation

$$\log p = \frac{A}{T} + B \quad (4.4)$$

where B is an integration constant and $A = \frac{\Delta H_T}{R}$ where ΔH_T is the average enthalpy centered on the mid-range temperature. It has been observed that equation 4.4 holds for most materials if the vapour pressures are less than 1 torr (Dushman, 1966). ΔH_T can only be taken as a constant over a relatively narrow temperature range. In order to cover a wider temperature range ΔH_T can be expanded as

$$\Delta H_T = \Delta H_0 + aT + bT^2 + cT^3 \dots \quad (4.5)$$

with $\Delta H_0, a, b, c$ as constants. Substituting equation 4.5 into the Clapeyron equation 4.1 and following the same steps of reasoning gives

$$d \log p = \frac{\Delta H_0 dT}{RT^2} + \frac{adT}{RT} + \frac{bdT}{R} + \frac{cTdT}{R} . \quad (4.6)$$

Rearranging the coefficients and integrating gives

$$\log p = A - \frac{\Delta H_0}{RT} + \frac{a \log T}{R} + \frac{bT}{R} + \frac{cT^2}{2R} \quad (4.7)$$

where A is the integration constant. Substituting in the constants $B = \frac{-\Delta H_0}{R}$, $C = \frac{a}{R}$, $D = \frac{b}{R}$ and $E = \frac{c}{2R}$ gives an expression for vapour pressure in the form

$$\log p = A + \frac{B}{T} + C \log T + DT + ET^2 . \quad (4.8)$$

This equation can be used practically to fit experimental vapour pressure measurements with A , B , C , D and E as fitted constants. It should be noted that this equation can be altered in terms of the constants used depending on the units of p that are used or the base of the logarithmic function that is used. *CRC Handbook 89th edition 4-136* for instance uses the following equation for the vapour pressure curve of Cu

$$\log p = 2.881 + A + \frac{B}{T} + C \log T . \quad (4.9)$$

Dushman (1966) obtained a similar equation for correlating experimental observations on vapour pressure data by using a function known as free energy. Denoting this function ΔF , he derived the vapour pressure from values of ΔF (calories per gram-mole) by means of the relation

$$\log p = -\frac{\Delta F}{4.575T} \quad (4.10)$$

where the vapour pressure p is expressed in atmospheres. In terms of the unit torr this equation takes the form

$$\log p = 2.881 - \frac{\Delta F}{4.575T} \cdot \quad (4.11)$$

This means that vapour pressure can once again be expressed in terms of the following equation

$$\log p = A - \frac{B}{T} \quad (4.12)$$

where A and B are constants specific to this equation, which is different but has the same form as equation 4.4.

For most elements these constants and vapour pressure equations can be obtained in resources like the *CRC Handbook 89th edition 4-136*, Dushman (1966) or the *Handbook of Vapor Pressure* by Yaws, (1995). Alternatively the value of p for a certain temperature T can be obtained from vapour pressure curves, an example of which is shown in figure 4.1. It represents the vapour pressures of the elements over a wide range of temperatures using equation 4.8.

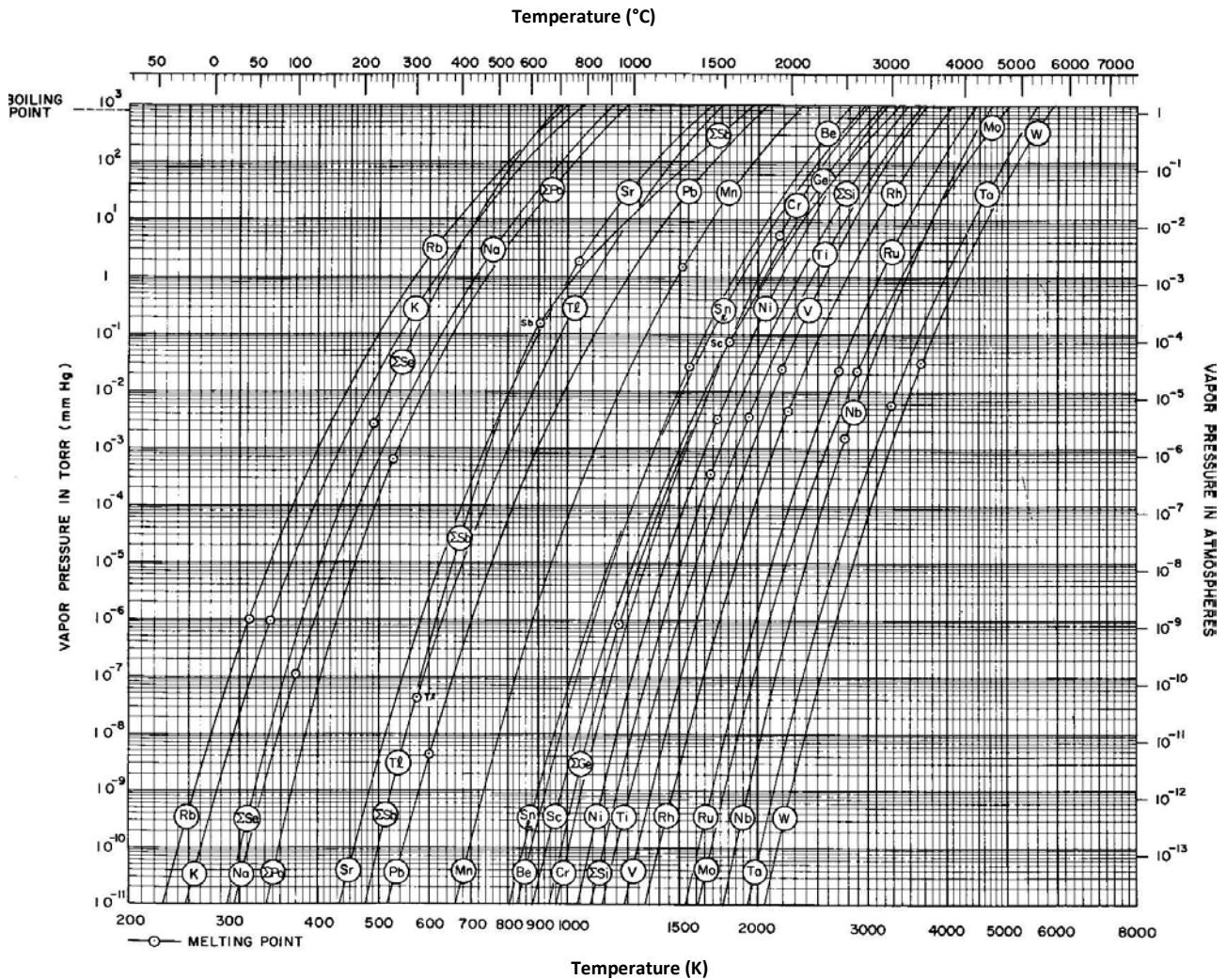


Figure 4.1: A graph showing vapour pressure curves of the elements. (Honig and Kramer, 1969).

Equations 4.8 and 4.9 were used together with constants obtained from the *Handbook of Vapor Pressure* by Yaws (1995) and the *CRC Handbook 89th edition 4-136* to construct vapour pressure curves for Sb and Cu used in this study. These curves are shown in figure 4.2 and figure 4.3. The constants used are shown in table 4.1. Experimental data obtained from Honig (1957) are also shown.

Table 4.1: Values used to represent the vapour pressure curves of Cu and Sb

Element	A	B	C	D	E	Temp Range (K)
Cu	9.123	-17748	-0.7317	-	-	298 - 1356
Sb	-14.9322	-1.3754x10 ⁴	15.738	-2.3835x10 ⁻²	5.1947x10 ⁻⁶	617 - 1898

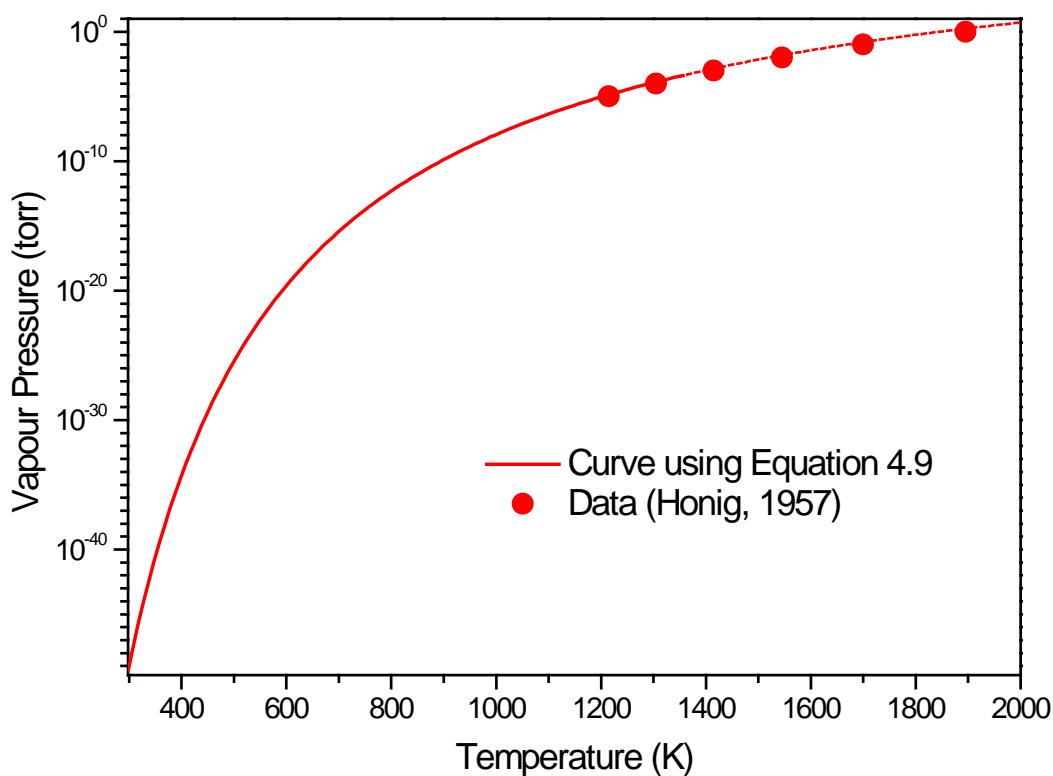


Figure 4.2: Vapour pressure curve for Cu.

The dashed line in figure 4.2 shows the curve above the melting point of Cu and outside the temperature range recommended by the *CRC Handbook 89th edition 4-136* for the use of the given constants. It does however still produce an excellent fit to the available data.

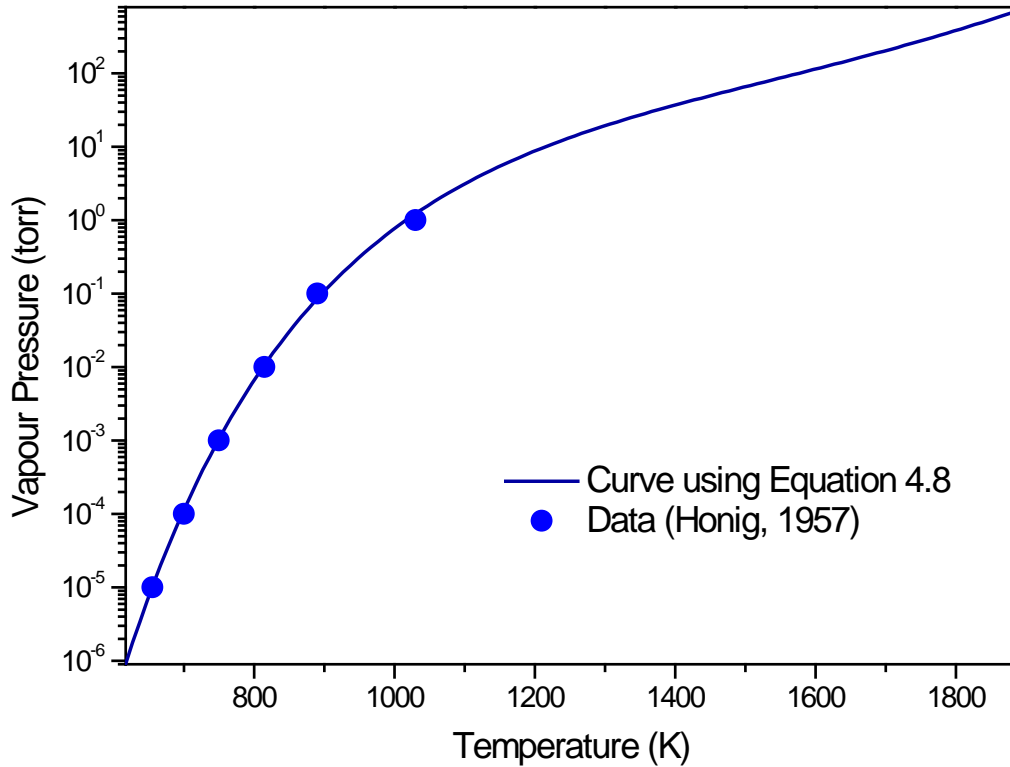


Figure 4.3: Vapour pressure curve for Sb.

It can be seen from figures 4.2 and 4.3 that at similar temperatures the vapour pressure of Cu is orders of magnitude less than that of Sb. As an example, at a temperature of 1000 K the vapour pressure of Sb is in the order of 1 torr while at the same temperature the vapour pressure of Cu is only in the order of 10^{-8} torr. It can thus be predicted that the evaporation rate of Cu will be insignificant compared to that of Sb.

4.2.2 Evaporation flux and evaporation rate

The fundamental physics of evaporation phenomena is connected mainly to the names of Hertz, Knudsen and Langmuir. The molecular (or atomic) rate of evaporation per unit area and time for a liquid in equilibrium with its vapour was derived first by Hertz and later modified by Knudsen. The first investigation of evaporation rates in a vacuum was conducted by Hertz in 1882. Hertz distilled mercury at reduced air pressure and observed the evaporation losses while

simultaneously measuring the hydrostatic pressure exerted on the evaporating surface by the surrounding gas (Herman *et al.*, 2004). It was shown that a liquid has a specific ability to evaporate and that a specific maximum evaporation rate at a given temperature cannot be exceeded even if the supply of heat is unlimited. In addition, it was observed that the theoretical maximum evaporation rate is obtained only if as many molecules evaporate from the surface as would be required to exert the equilibrium or vapour pressure p on the same surface and none of them return. This means that a hydrostatic pressure of $p_a = 0$ must be maintained (Herman *et al.*, 2004).

The evaporation rates as originally measured by Hertz were only about one tenth as high as the theoretical maximum rates as calculated from kinetic theory. In 1915, Knudsen and later others (Kennard, 1938) carried out investigations of the rate of evaporation for pure mercury. The results consistently indicated that the evaporation rate was less than the maximum rate predicted from classical kinetic theory (Rahimi and Ward, 2005). Knudsen argued that the molecules impinging on the evaporating surface may be reflected back into the gas rather than incorporated into the liquid. This means that there is a certain fraction $(1 - \alpha)$ of vapour molecules which contribute to the evaporant pressure, but not to the net molecular flux from the condensed phase into the vapour phase. Therefore Knudsen introduced the evaporation coefficient α , defined as the ratio of the observed evaporation rate in vacuum to the value predicted by classical theory (Herman *et al.*, 2004). These considerations led to the famous Hertz – Knudsen equation (Herman *et al.*, 2004)

$$\frac{\partial N_e}{A_e \partial t} = \frac{\alpha N_A (p - p_a)}{\sqrt{2\pi MRT}} \quad (4.13)$$

where the number of molecules evaporating from a surface area A_e during a time ∂t is given by ∂N_e . M is the molecular or atomic mass of the evaporating species, T is the temperature, p_a is the hydrostatic pressure of the evaporant gas phase, p is the vapour pressure R and N_A are the universal gas constant and Avogadro's number respectively.

It was shown by Langmuir in 1913 that the Hertz-Knudsen equation also applies to evaporation from solid surfaces (Herman *et al.*, 2004). He investigated the evaporation of tungsten from filaments in evacuated glass bulbs and assumed that the evaporation rate of a material at pressures below 1 torr is the same as if the surface were in equilibrium with its vapour. Since recondensation of evaporated species was thereby excluded, he obtained the maximum rate as stated in equation 4.14 for $p_a = 0$ and $\alpha = 1$

$$\frac{\partial N_e}{A_e \partial t} = \frac{N_A p}{\sqrt{2\pi MRT}} = J_N \quad (4.14)$$

where J_N is the molecular or atomic flux. Phase transitions of this type, which constitute evaporation from free surfaces, are commonly referred to as Langmuir or free evaporation. In addition, it was demonstrated that for pressures below 0.1 torr, the evaporation rate is independent of residual gas pressure due to the negligible resistance offered (Herman *et al.*, 2004). This implies that at pressures below 0.1 torr, the vacuum can be seen as perfect for the purposes of this study and subsequently $p_a = 0$.

The flux of evaporation or condensation from and to both liquid and solid surfaces in high vacuum as used in this study can thus be expressed as

$$J_N = 3.513 \times 10^{22} \frac{p}{\sqrt{MT}} \text{ (atoms. cm}^{-2}\text{. s}^{-1}\text{)}. \quad (4.15)$$

This can also be put into mass units by multiplying the flux by the atomic mass

$$J_m = 5.84 \times 10^{-2} p \sqrt{\frac{M}{T}} \text{ (g. cm}^{-2}\text{. s}^{-1}\text{)} \quad (4.16)$$

When perfect vacuum is not used the continuum should be taken into account. The Hertz-Knudsen equation is based on considering a certain distribution function of velocity for gas particles (full range Maxwellian), where there is no interaction between particles, and thus

particles move freely between collisions. Schrage (1953) introduced a simple correction for a non perfect vacuum scenario and argued that the Maxwellian due to the mass movement of the vapour must be shifted by the mean velocity of the gas. According to Schrage (1953) the equation becomes

$$J_N = \frac{p_{eq}}{\sqrt{2\pi MRT}} - \frac{\Gamma p}{\sqrt{2\pi MRT_g}} \quad (4.17)$$

where T_g is the vapour temperature far from the evaporation interface. Γ recognizes the effect of the vapour mass flow (Safarian and Engh, 2013). These conditions are however beyond the scope of this study as all evaporation experiments will be performed under high vacuum or better conditions.

In spite of extensive studies on evaporation of pure metals, the Hertz-Knudsen expression is still widely used due to its simple form (Safarian and Engh, 2013).

According to Dushman (1966) the rate of evaporation can be obtained as follows.

Let W be the rate of evaporation ($\text{g.cm}^{-2}.\text{s}^{-1}$) and M the molecular weight, then

$$\log W = 5.7660 + 0.5 \log M + \log p - 0.5 \log T = C - 0.5 \log T - \frac{B}{T} \quad (4.18)$$

where

$$C = A + 0.5 \log M + 5.7660 \quad (4.19)$$

When using equation 4.18 the vapour pressure p is expressed in millitorr.

Dushman (1966) provides a table for the evaporation rates of the various elements based on equation 4.18. These values are shown in tables 4.2 and 4.3. Figures 4.4 and 4.5 were plotted using this table showing the evaporation rate as a function of temperature for Sb and Cu respectively. It should be noted that according to Dushman (1966) it is known that Sb evaporates largely in the form of Sb_2 molecules. The values given in the table 4.2 for Sb were based on this consideration, that is, $M = 243.52 \text{ g. mol}^{-1}$.

Table 4.2: Evaporation rates for Sb_2 as given by Dushman (1966).

Temperature ($^{\circ}\text{C}$)	382	427	477	542	617	757
Evaporation rate ($\text{g.cm}^{-2}.\text{s}^{-1}$)	2.52×10^{-7}	2.43×10^{-6}	2.35×10^{-5}	2.26×10^{-4}	2.16×10^{-3}	2.01×10^{-2}

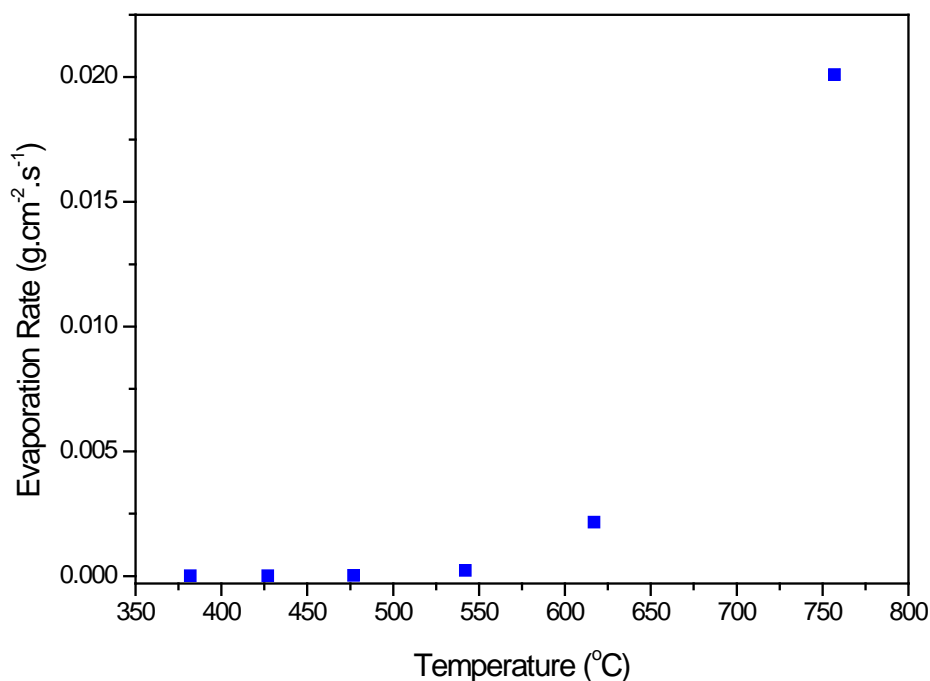


Figure 4.4: Evaporation rate graph for Sb_2 using data in table 4.2.

Table 4.3: Evaporation rates for Cu as given by Dushman (1966).

Temperature (°C)	942	1032	1142	1272	1427	1622
Evaporation rate (g.cm ⁻² .s ⁻¹)	1.33x10 ⁻⁷	1.29x10 ⁻⁶	1.24x10 ⁻⁵	1.18x10 ⁻⁴	1.13x10 ⁻³	1.07x10 ⁻²

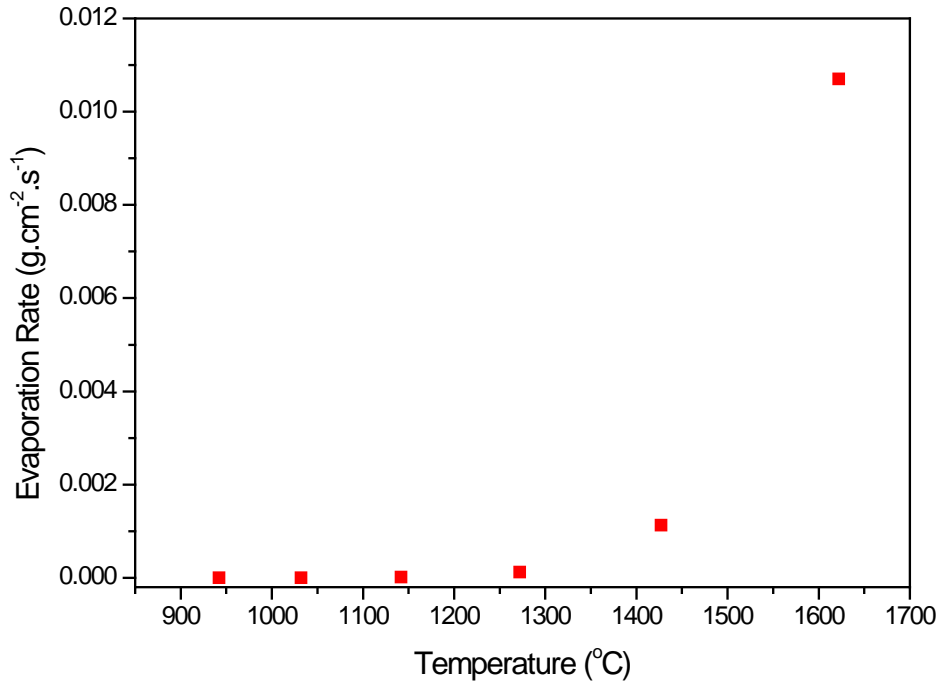


Figure 4.5: Evaporation rate graph for Cu using data in table 4.3.

At this point it should be apparent that an equation to describe the evaporation flux from a solid or liquid surface will have to include a term that describes the vapour pressure for the evaporating element or compound. This can be done as an example by combining the equation used to predict the vapour pressure of Sb as shown in equation 4.8 with the Hertz-Knudsen equation as shown in equation 4.16. By carefully ensuring that due regard are given to the use of the correct units, such a combination can be used to predict the evaporation flux. This is shown in figure 4.6 where the mass evaporation rate as a function of temperature were calculated for Sb₂ using different values of the evaporation coefficient α . These calculations are also shown

compared to the values given by Dushman (1966). The evaporation coefficient α in general appears to be poorly understood. It can however be stated that in the case of solids, α approaches unity if the solid is in polycrystalline form, but that the corresponding α for the single crystal form of the same solid is significantly lower than unity (Pound, 1972).

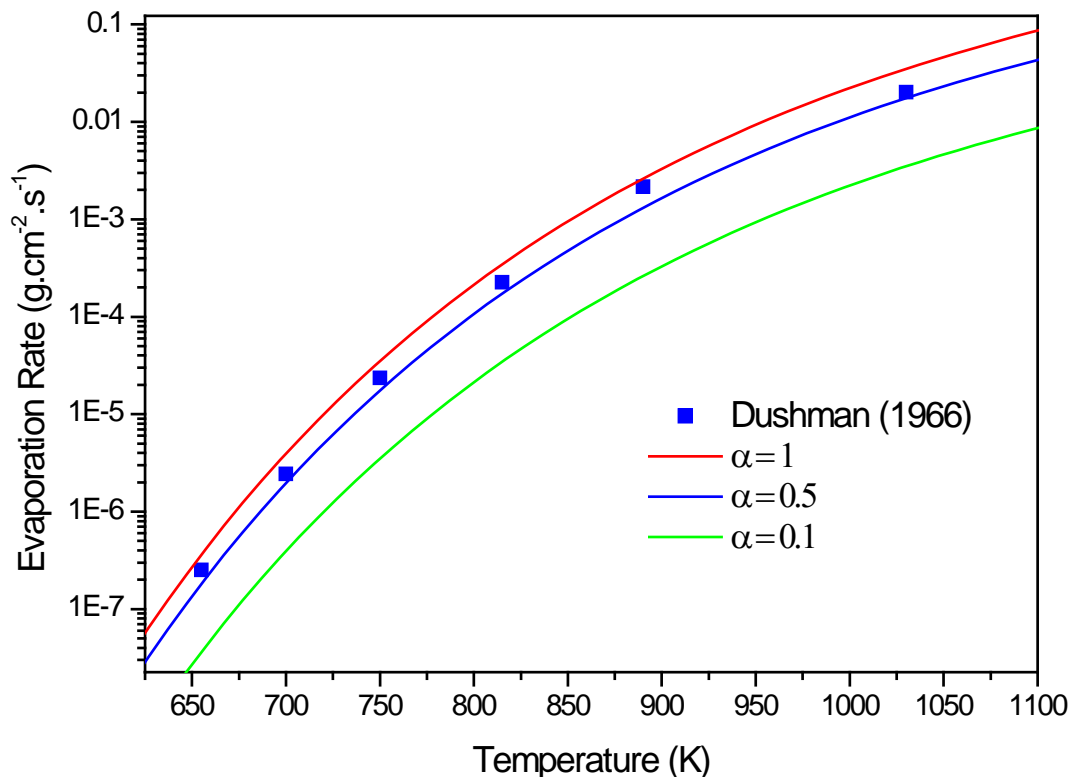


Figure 4.6: Calculated evaporation rates for Sb_2 .

As there are some dispute in literature regarding the molecular form in which antimony evaporates (Dushman, 1966; Goldberg, 1970) these calculation where repeated for Sb , Sb_2 and Sb_4 using $\alpha = 1$ and assuming that the vapour pressure for all three molecular forms of Sb are the same. These calculations are shown in figure 4.7.

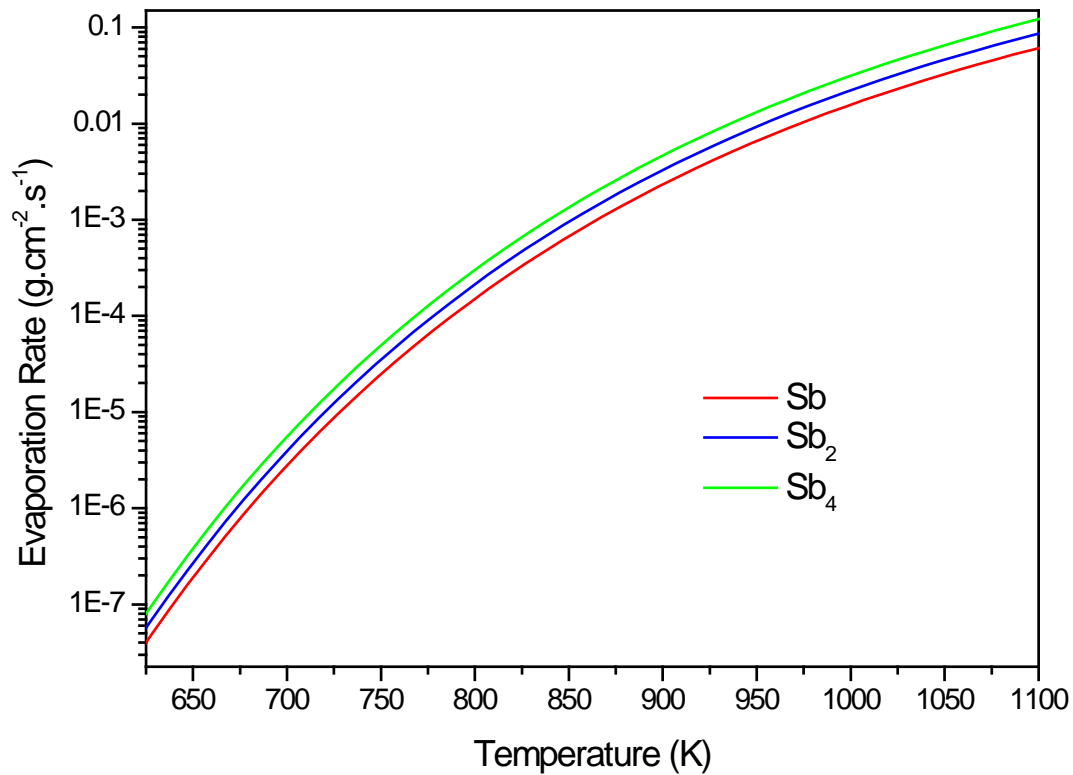


Figure 4.7: Calculated evaporation rates for Sb, Sb₂ and Sb₄ using $\alpha = 1$.

4.2.3 Further considerations

The following two observations are of importance. Knudsen found the evaporation coefficient to be strongly dependent on the condition of the surface, especially in relation to contaminants (Herman *et al.*, 2004). This fact that surface impurities might affect evaporation rates are especially made clear by Pound (1972). In addition it has been shown that the evaporation rate of a solid is affected by crystallographic faults and the surface atomic structure (Hirth and Pound, 1957).

4.3 Evaporation during segregation

4.3.1 A third flux of atoms

As discussed in chapter 1, experimental surface segregation studies may involve (a) high temperatures for the measurement of temperature dependent parameters which may result in the evaporation of the segregating solute and (b) cleaning of the sample surface by means of ion sputtering. Both these processes introduce an additional flux of atoms leaving the surface (see figure 4.8). Although different in a physical sense, these two problems are very similar in mathematical sense with the important distinction that the surface recedes into the bulk as atoms are sputtered from the surface (Du Plessis, 1990).

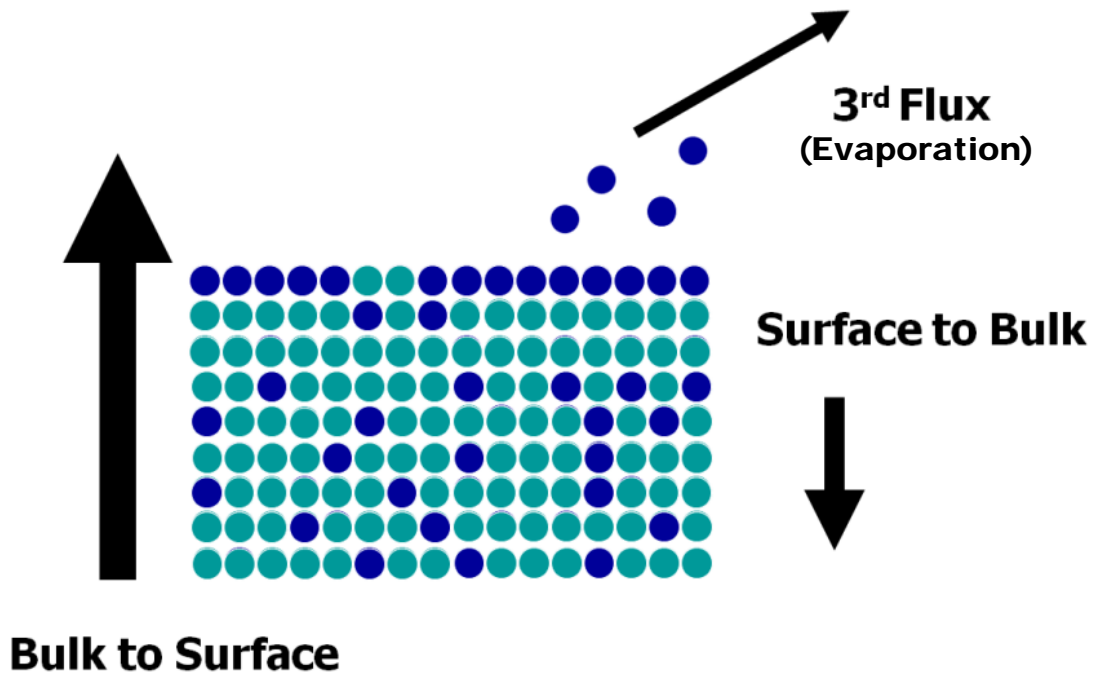


Figure 4.8: Evaporation constitutes a third flux of atoms in a segregation system.

In a number of binary alloy systems, surface evaporation during segregation experiments has been reported. Webber and Chadwick (1980) reported studies on the Ni-Cu system which show the effects of evaporation on the segregation process. For 5% Cu in Ni alloys, their results indicated that Cu evaporation occurs as low as 870 K and at 1000 K irreversible Cu depletion was observed. Tabe and Nakamura (1979) reported As evaporation from As doped Si during segregation measurements and Burton *et al.* (1976) discussed the effects of evaporation during segregation of Au to the surface of Ni.

Briant (1988) drew the conclusion that an evaporation phenomenon directly affects the kinetics of segregation and need to be included in complete treatments. Although some attempts have been made to develop segregations models that take surface evaporation into account, these models can only predict segregation in either the kinetic region or when equilibrium has been reached. In contrast to the effects of sputtering, the effect of evaporation has also received very little attention in previous experimental studies.

It should be noted at this stage that the key difference between the models used to describe 'normal' evaporation in section 4.2 and any model used to describe evaporation during segregation is that of a limited supply of solute atoms at the surface which can evaporate during segregation. In the case of 'normal' evaporation significant evaporation will start to take place at a specific temperature. The evaporation rate will then increase with temperature indefinitely given that the evaporation source is infinite. In the case of evaporation during segregation, significant evaporation can only take place when the surface enrichment of solute atoms becomes significant. The evaporation rate will then increase with temperature until a point is reached where the evaporation rate overtakes the rate of solute atoms segregating to the surface. The evaporation rate will thus start to decrease due to the depletion of segregated atoms on the surface. Throughout the process of evaporation the surface concentration of the evaporating species will decrease relative to a situation where the species does not evaporate.

The two most noteworthy attempts to develop a theoretical model for combined surface segregation and evaporation were done by Lea and Seah (1977) and Stinespring and Lawson (1985). These two models will now be discussed and compared.

4.3.2 Lea and Seah (1977)

Lea and Seah (1977) introduced the concept of evaporation into the grain boundary description as proposed by McLean (1957) and was expanded on in a further study by Lea and Molinari (1984). They accounted for the evaporation rate by taking the rate of accumulation in the surface layer as the difference between the rate of diffusion from the atom layer below the surface and the rate of evaporation:

$$d \frac{\partial C_s^t}{\partial t} = D \left. \frac{\partial C_x^t}{\partial x} \right|_{x \rightarrow 0} - \text{evaporation rate} \quad (4.20)$$

where C_s^t gives the surface concentration (atoms.m⁻³) of solute atoms, D is the solute lattice diffusion coefficient (m²s⁻¹), d is the solute monolayer thickness at the surface, taken as the atomic size (m) of the solute atom. $C_{x=0}^t$ is the time varying bulk solute content immediately below the surface and is related to C_s^t by the surface enrichment ratio α . This is the ratio of the concentration of segregant atoms at the surface to that in the bulk. It is of utmost importance to not confuse this with the evaporation coefficient α used in other parts (e.g. section 4.2.2) of this thesis.

This equation assumes that evaporation of the bulk material is negligible and that since the chemical potential of the solute atoms on the surface is equal to that just below the surface, the rate of evaporation is proportional to the bulk solute content in the atom layer just below the surface, namely C_0 .

The evaporation rate is expressed in terms of a dimensionless parameter V , such that

$$\text{evaporation rate} = \frac{VDC_0}{\alpha^2 d} \quad (4.21)$$

where C_0 the concentration just below the surface.

The predicted effect of varying V on the kinetics of surface segregation is shown in figure 4.9. For small times the build-up of segregated atoms is the same for all V values as the concentration gradient is steep and the diffusion flux towards the surface is large. At longer times the diffusion flux becomes smaller due to the solute depletion beneath the surface and the evaporation flux begins to dominate. The segregation level passes through a maximum before falling asymptotically to zero as a result of competition between the two mechanisms of a diffusion limited segregation rate from a depleted zone and an evaporation rate dependent upon the segregated concentration.

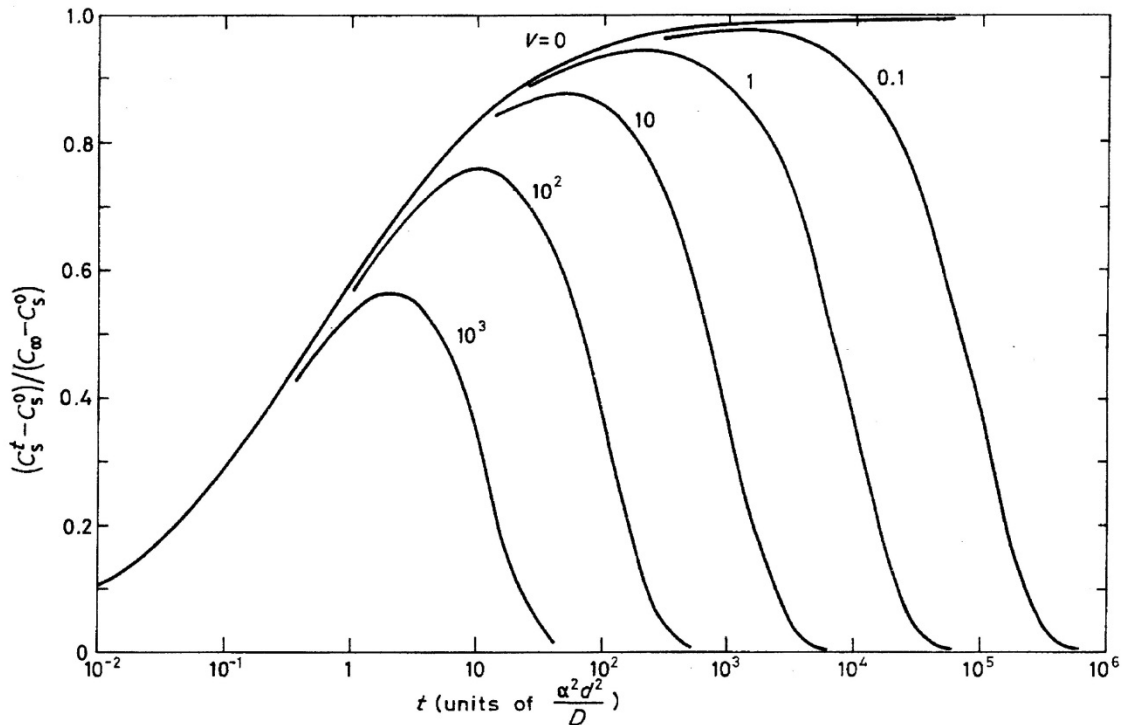


Figure 4.9: The time dependence of the segregation level on a free surface at a series of evaporation rates (Lea and Molinari, 1984). Values of V are shown next to each curve.

In order to test the curves in figure 4.9 it is necessary either to measure V experimentally or to describe it from thermodynamic data.

The equilibrium vapour pressure, p_s , of a dilute solute more volatile than its matrix is related to the pure solute vapour pressure p by

$$p_s = p \exp\left(\frac{\Delta G}{RT}\right) \quad (4.22)$$

where ΔG is the free energy difference between the solute in the dilute alloy and in the pure bulk state at temperature T . To a first approximation p_s varies as the solute content below the surface, assuming Raoult's law (the partial vapour pressure of each component of an ideal mixture of liquids is equal to the vapour pressure of the pure component multiplied by its mole fraction in the mixture) is obeyed

$$p_s \cong pX_{x=0}^t \quad (4.23)$$

If p_s is expressed in Pa, the rate of evaporation of solute from the surface is

$$\frac{2.64 \times 10^{24} p_s}{\sqrt{MT}} \text{ atoms m}^{-2}\text{s}^{-1} \quad (4.24)$$

where M is the atomic mass of the solute. By combining equations 4.21 and 4.24 the temperature dependence of V may be determined, enabling comparison of figure 4.9 with experimental measurements.

Lea and Molinari (1984) studied magnesium diffusion, surface segregation and oxidation in Al-Mg alloys in the temperature range up to 600°C. It was reported that at high temperatures the evaporation rate exceeded the segregation rate and that subsequently the surface layer became depleted of magnesium. Auger electron spectroscopy was used to follow the surface segregation behaviour of magnesium at the surface of the Al-Mg alloys.

To measure the rate of evaporation from the specimen surface and to identify any species evaporated a copper flag was mounted a short distance from the sample surface. This copper rod, mounted on a wobble stick, could, by simple adjustment, be moved such that the flag could be both sputtered cleaned and surface analysed by AES. The experimental procedure was to clean by means of ion sputtering, first the copper flag and then the Al-Mg sample. The sample was then raised to a selected temperature as quickly as possible (up to 3 minutes) and the composition of the surface measured as a function of time. The copper flag was then moved in front of the AES analyser and the amount of evaporated material quantified from the spectra. Figure 4.10 shows the rate of evaporation of magnesium as measured by Lea and Molinari (1984) as a function of temperature.

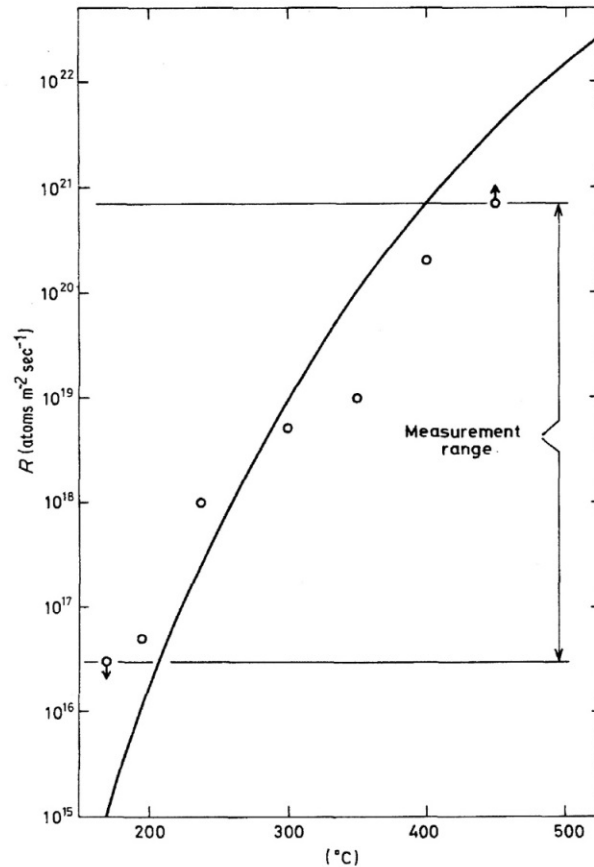


Figure 4.10: The rate of magnesium evaporation from an Al-0.8Mg alloy. The curve was calculated from equation 4.24 using standard vapour pressure data (from Lea and Molinari, 1984).

The quantified segregation data obtained during the study is shown in figure 4.11. At 195°C it can be observed that evaporation is significant and that the surface concentration of Mg is observed to decrease as a function of time.

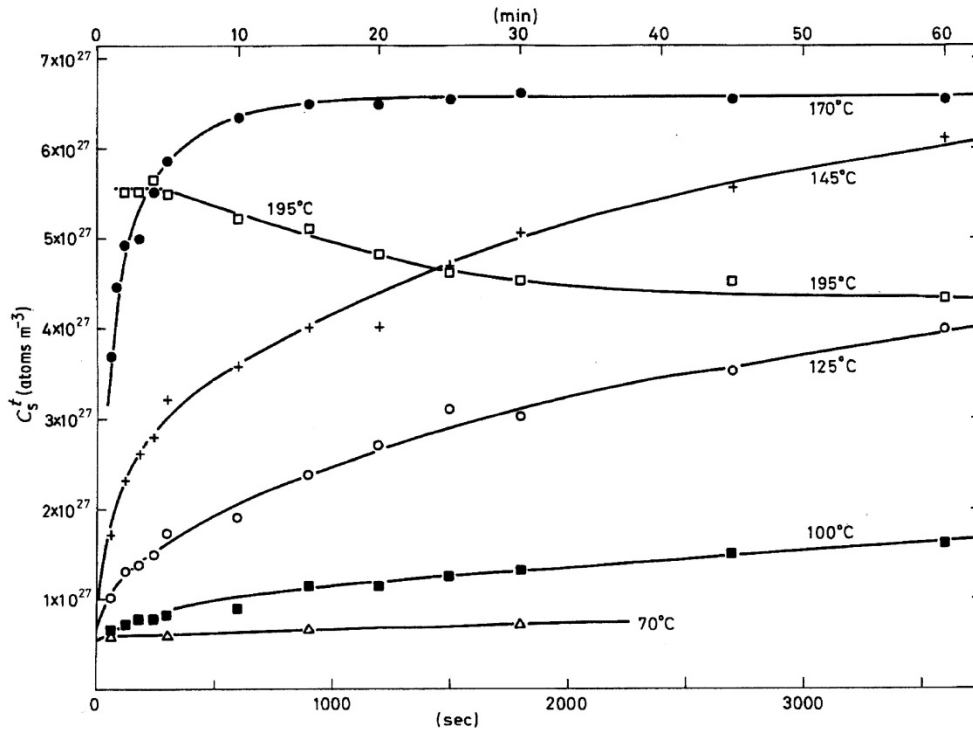


Figure 4:11. The magnesium concentration in the surface atomic layer of the Al-0.8Mg alloy as a function of time. (Lea and Molinari, 1984)

From the experimental measurements shown in figure 4.10, figure 4.11 and equation 4.23 the authors then derived values for the evaporation parameter V . It was ascertained that for the temperature ranges shown in figure 4.10, V varied between 1 and 100.

Surface segregation measurements of magnesium on the Al-0.8Mg alloy plotted in the form of the universal segregation-evaporation curves of figure 4.9 are shown in figure 4.12.

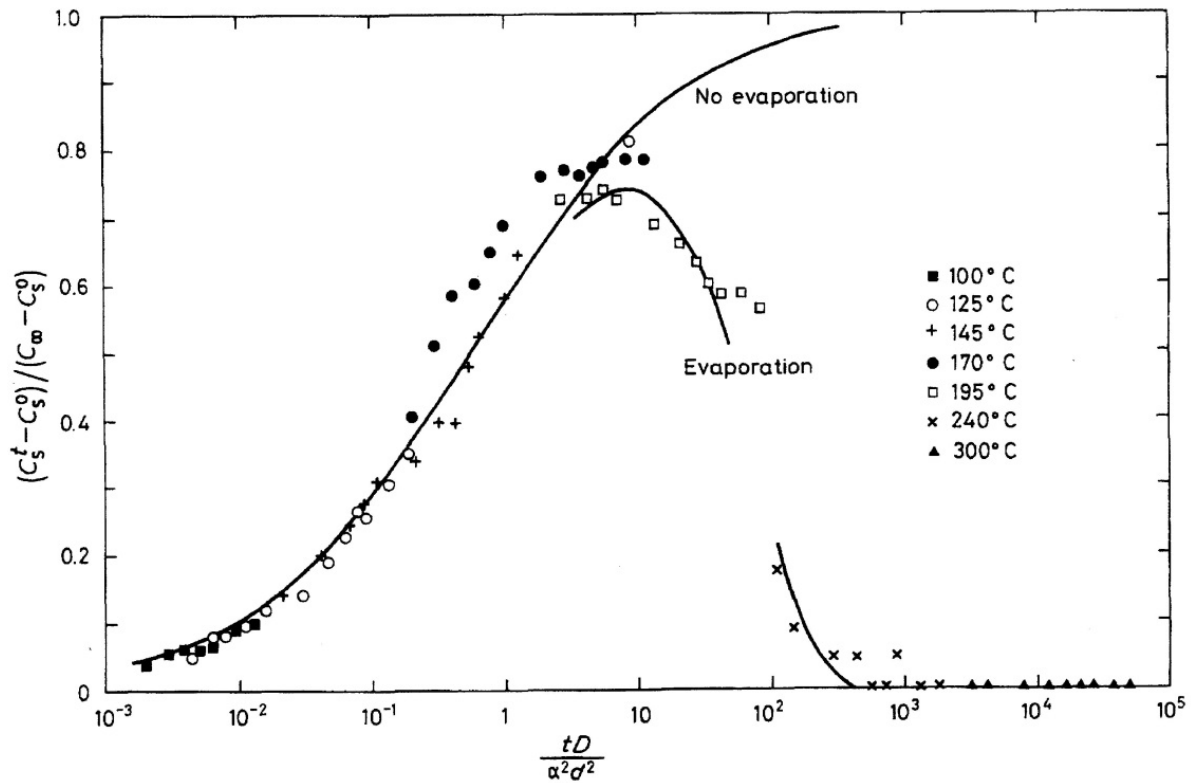


Figure 4:12. Surface segregation measurements of magnesium on the Al-0.8Mg alloy plotted in the form of the universal segregation-evaporation curves of figure 4.5. (Lea and Molinari 1984)

At temperatures in excess of 170°C the evaporation of magnesium became significant. At temperatures above approximately 200°C the evaporation rate exceeds the segregation kinetics and the magnesium enrichment of the sample surface rises to a maximum before decreasing to zero. At temperatures above approximately 250°C surface enrichment is not observed. The authors state that it is only in a very narrow temperature range 100°C-300°C that curves of the form shown in figure 4.7 might be experimentally obtained. The mismatch in data in figure 4.12 are accounted for by the uncertainty in the quantification of the AES, as well as the values of V , α and D .

4.3.3 Stinespring and Lawson (1985)

Stinespring and Lawson (1985) developed a theoretical model describing the combined effects of surface segregation and evaporation in binary alloys. Using this model, parameter regimes dominated by segregation, evaporation, or competitive segregation and evaporation were

described. General criteria for performing meaningful segregation measurements were discussed as well as studies aimed at rigorously testing the theory.

The suggested model was based on a description of the segregation process developed by Hofmann and Erlewein (1978) which utilizes input parameters which in principle can be calculated using theoretical analyses of solids and surfaces and in certain cases, which may be established experimentally. This segregation model is based upon a free energy diagram similar to the one shown in figure 4.13.

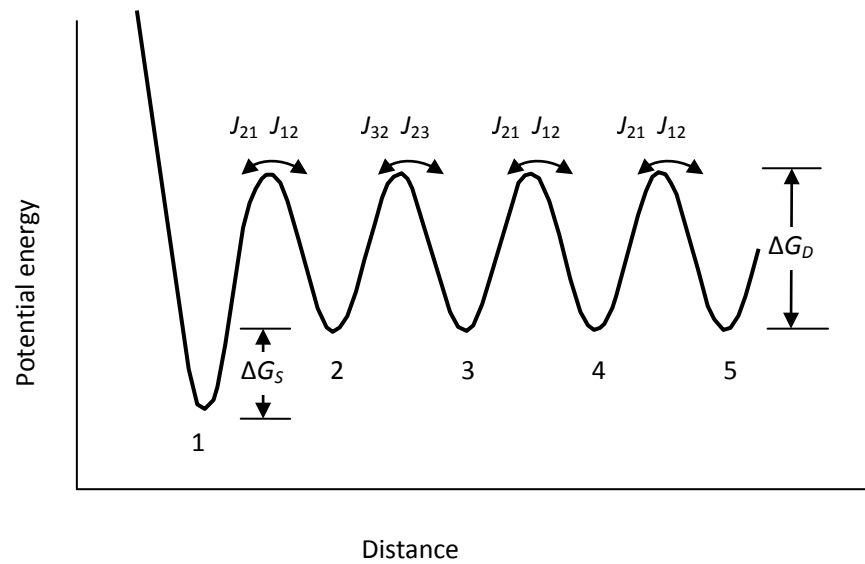


Figure 4.13: The potential energy diagram as a function of depth into the crystal indicating a very steep potential barrier for atoms escaping into the vacuum.

Here the free energy of the segregant is plotted as a function of depth in the alloy. The indices 0, 1, 2etc. identify the gas phase (0), the surface (1), and the interior bulk planes (2, 3,...etc.) of the solid. ΔG_s is the free energy of segregation and ΔG_D is the free energy of diffusion. The energy gradient at the surface arises from lattice strain and bond breaking. The energy zero in this figure is defined as the minimum of the interior free energy. Thus ΔG_s is negative while ΔG_D is positive. Stinespring and Lawson (1985) incorporated the evaporation process into the model by introducing ΔG_v , the evaporation energy (see figure 4.14). The potential barrier between the

surface layer and vacuum is thus finite, making evaporation possible. For evaporation to take place the energy barrier $\Delta G_v - \Delta G_s$ has to be exceeded.

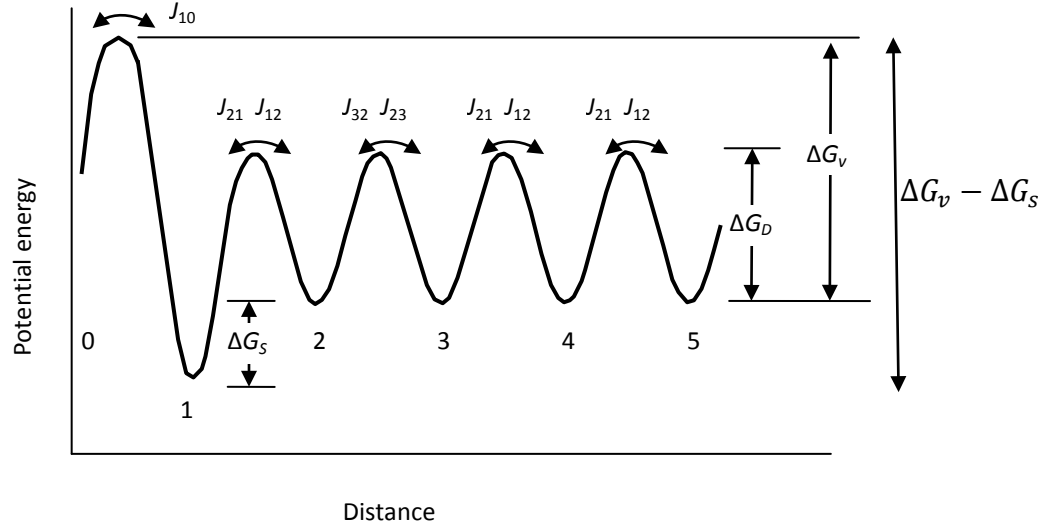


Figure 4.14: The potential energy diagram as a function of depth into the crystal indicating a finite potential energy barrier between the surface layer (1) and vacuum (0) allowing evaporation to take place.

In the same manner as Hofmann and Erlewein (1978), the authors used the free energy diagram as shown in figure 4.14 and reaction rate theory to determine the flux of segregant atoms between adjacent planes. The flux between the surface layer and the vacuum i.e. the evaporating segregant atoms is given by

$$J_{10} = N_s X_1 \vartheta_1 \exp[-(\Delta G_v - \Delta G_s)/RT] \quad (4.25)$$

where N_s is the total number of available surface sites, X_1 is the surface mole fraction of the segregant ϑ_1 is the effective jump frequency.

According to the authors, estimates of ΔG_v may be made using data for the pure solute element and free energy solution ΔG_{sol} data for the system under discussion. As the paper discussed the model in terms of Cu evaporation from a Ni-Cu system, ΔG_v is given by

$$\Delta G_v = \Delta G_v^{Cu} - \Delta G_{sol} = (\Delta H_v^{Cu} - \Delta H_{sol}) - T(\Delta S_v^{Cu} - \Delta S_{sol}) \quad (4.26)$$

where ΔH and ΔS represent the appropriate enthalpy and entropy terms. The flux $J_{i,i\pm 1}$ of segregant atoms between adjacent planes are given by

$$J_{12} = a_1^{-2} X_1 W_{12} v_1 \exp \left[-\frac{\Delta G_D - \Delta G_s}{RT} \right] \quad (4.27)$$

$$J_{21} = a_2^{-2} X_2 W_{21} v_2 \exp \left[-\frac{\Delta G_D}{RT} \right] \quad (4.28)$$

$$J_{23} = a_2^{-2} X_2 W_{23} v_2 \exp \left[-\frac{\Delta G_D}{RT} \right] \quad (4.29)$$

⋮

$$J_{i,i\pm 1} = a_i^{-2} X_i W_{i,i\pm 1} v_i \exp \left[-\frac{\Delta G_D}{RT} \right] \quad (4.30)$$

where v_i is the frequency of the normal vibrational mode resulting in a jump from the i^{th} to the $(i \pm 1)^{th}$ plane, $W_{i,i\pm 1}$ is the corresponding jump probability and a_i is the lattice constant for the i^{th} plane.

Although a rigorous validation of the model was not attempted, predictions of the theory were compared with and found to be qualitatively similar to the measurements of Webber and Chadwick (1980) for the Ni-Cu system. The authors however conceded that the available data on Ni-Cu were not sufficient to quantitatively test the model. To quantitatively test this theoretical model as a whole would not only require independent measurements of the surface concentration as a function of time but also ΔH_S , ΔH_D , ΔG_v and D_0 where ΔH_S and ΔH_D are the enthalpies of segregation and diffusion respectively.

4.4 The Darken model with evaporation

Considering the preceding sections and chapters a number of issues should now be clear:

1. The Modified Darken model's ability to predict both kinetic and equilibrium segregation qualifies it as a prime model for further development.
2. Previous research, although limited, indicates the need to include the effects of evaporation when modelling segregation.
3. Evaporation behaviour from a pure element can in theory be predicted by using the Hertz-Knudsen equation in unison with an equation which predicts the vapour pressure of the specific element as a function of temperature.
4. The current models, which considers the effects of surface evaporation during segregation treat the evaporation largely as if it takes place from a pure element. In some cases e.g. Stinespring and Lawson (1985) this is largely due to the lack of data relating to the various enthalpy and entropy terms used in the proposed model.

Considering the above, a new form of the Hertz-Knudsen equation can now be introduced which makes provision for the situation where an impurity atomic layer evaporates from a pure elemental substrate. The evaporation rate is given by

$$J_S = 3.513 \times 10^{22} \frac{Kp}{\sqrt{MT}} \text{ (atoms. cm}^{-2}\text{. s}^{-1}\text{)}. \quad (4.31)$$

The parameter K can be considered a function of among other parameters the following:

- The original evaporation coefficient α as used in the original Hertz-Knudsen equation.
- The difference in atom bonding strength between the impurity atom and the substrate when compared to the pure elemental bonding strengths involved for the impurity.
- Any interaction parameters involved due to the influence of additional impurities on the surface layer.

If only a partial surface coverage of impurity atoms is present on the substrate equation 4.31 becomes

$$J_S = 3.513 \times 10^{22} \frac{KpX_F^S}{\sqrt{MT}} \text{ (atoms. cm}^{-2}\text{. s}^{-1}\text{)}. \quad (4.32)$$

where X_F^S is the fraction of the surface coverage of the impurity species atoms present, if compared to a complete surface coverage of the impurity atoms.

Note that the evaporation rate is proportional to the actual surface concentration of the impurity itself. This assumption is different to that of Lea and Seah (1977) which assumed the rate of evaporation to be proportional to the bulk solute content in the atom layer just below the surface. The approach used in this study is however closer to physical reality and corresponds to the approach of Stinespring and Lawson (1985).

With due regard given to the units used, equation 4.32 can now be incorporated into the Modified Darken model in terms of the surface layer concentration. Referring back to section 3.4.2, the Modified Darken model gives an expression for the flux of atoms between two adjacent layers, namely

$$J_i^{(j+1 \rightarrow j)} = m_i X_v^j C_i^{(j+1)} \left(\frac{\Delta \mu_i^{(j+1 \rightarrow j)}}{d} \right). \quad (4.33)$$

For a time interval t the surface concentration will change by $J_i^{(2 \rightarrow 1)}$ atoms per unit area for species i , where $J_i^{(2 \rightarrow 1)}$ is the amount of atoms of species i per unit area moving from the layer just below the surface to the actual surface layer in the time interval t . Implementing the Modified Darken model thus gives the new surface concentration of species i after time t as

$$J_i^{(1,t)} = J_i^{(1,0)} + J_i^{(2 \rightarrow 1,t)} \quad (4.34)$$

Considering the loss of atoms of species i due to evaporation from the surface for the time interval t , equation 4.32 can be incorporated into equation 4.34 which gives the new surface concentration after a time t with the effects of evaporation considered.

$$J_i^{(1,t)} = J_i^{(1,0)} + J_i^{(2 \rightarrow 1,t)} - J_S^t. \quad (4.35)$$

The change of the Modified Darken model software to incorporate evaporation in this way is described in Appendix A.

4.5 Summary

The kinetics of materials evaporation is important in many areas such as vacuum metallurgy, welding, electron beam processing and thin film technology. Developing the fundamental knowledge of evaporation kinetics is thus of crucial importance. In theory the evaporation rate of materials can be predicted by the Hertz-Knudsen equation. Certain aspects of this equation however appear to be poorly understood. Furthermore it has been found that surface impurities, crystallographic faults and the surface atomic structure might affect evaporation rates.

In a number of binary alloy systems, surface evaporation during segregation experiments has been reported. The effect of evaporation has however received very little attention in previous experimental studies. It is clear that more research on this topic is required to validate the few proposed segregation/evaporation models that has been published.

It has been described in this chapter and proposed how to incorporate the Hertz-Knudsen equation, with some small but significant modifications, into the Modified Darken model. This new model will enable researchers to predict both kinetic and equilibrium segregation whilst including the effects of surface evaporation of the segregating solute.

4.6 References

Arblaster J.W. [2007] *Platinum Metals Review* **51(3)** p130.

Briant C.L. [1988] *Auger Electron Spectroscopy (Treatise on Materials Science and Technology)*, Academic Press.

Burton J.J., Helms C.R. and Polizzotti R.S. [1976] *Journal of Vacuum Science & Technology* **13** p204.

Das S. [2003] *Advanced Engineering Materials* **5(10)** p701.

Das S. [2001] On Some Physical Aspects of Process Control in Direct Selective Laser Sintering of Metals, Part II *Internal publication*, Department of Mechanical Engineering University of Michigan.

Du Plessis J. [1990] *Solid State Phenomena, surface segregation* **(11)**.

Dushman S. [1966] *Scientific Foundations of Vacuum Technique*, John Wiley and Sons.

Goldberg D.C. [1970] *Trends in Usage of Antimony*, NMAB.

Herman M.A., Richter W. and Sitter H. [2004] *Epitaxy: Physical Principles and Technical Implementation*, Springer-Verlag.

Hirth J.P. and Pound G.M. [1957] *Journal of Chemical Physics* (26) p1216.

Hofmann S. and Erlewein J. [1978] *Surface Science* 77 p59.

Honig R.E. [1957] *RCA Review* (18) p195.

Honig R.E. and Kramer D.A. [1969] *RCA Review* 30 p285.

Kaye G. and Ewen D [1913] *The Sublimation of Metals at Low Pressures*, Royal Society of London.

Lea C. and Molinari C. [1984] *Journal of Materials Science* 19 p2336.

Lea C. and Seah M.P. [1977] *Philosophical Magazine* 35 p213.

Lide D.R. [2008] *CRC Handbook 89th edition*, CRC Press.

McLean D. [1957] *Grain Boundaries in Metals*, Oxford University Press.

Pound G.M. [1972] *Journal of Physical and Chemical Reference Data* **1(1)** p135.

Rahimi P. and Ward C.A. [2005] *International Journal of Thermodynamics* **8(1)** p1.

Safarian J and Engh T.A. [2013] *Metallurgical and Materials Transactions A* **44(2)** p747.

Schrage R.W. [1953] *A Theoretical Study of Interphase Mass Transfer*, Columbia University Press.

Stinespring C.D. and Lawson W.F. [1985] *Surface Science* **150** p209.

Tabe M. and Nakamura H. [1979] *Journal of Applied Physics* **50** p5292.

Webber P.R. and Chadwick D [1980] *Surface Science* **94** pL151.

Yaws C.L. [1995] *Handbook of Vapor Pressure, Vol 4, Inorganic Compounds and Elements*, Gulf Professional Publishing.

Chapter 5

Experimental Setup and Procedures

5.1 Introduction

In this chapter the experimental techniques and procedures used during this study will be discussed. The experimental work can be divided into 4 sections:

- The preparation of samples used for segregation and evaporation/sublimation measurements.
- The design, construction and testing of equipment used to measure evaporation/sublimation fluxes at low rates.
- The actual measurement of the evaporation/sublimation that takes place during a typical segregation measurement.
- The use of additional techniques to verify and support the main experimental results.

Some of the techniques used during this study are well known, and subsequently only a brief overview will be given. As far as possible the procedures and techniques will be discussed in the sequence used to obtain the experimental results. The design, construction and testing of equipment that can be used to measure evaporation/sublimation flux at low orders of magnitude will be discussed in detail as it forms an integral part of this study. During this study Cu single crystals with various surface orientations and polycrystalline Cu samples doped with Sb were

studied in addition to pure Sb. The preparation of these Cu samples will be discussed in the next paragraph.

5.2 Sample preparation

Sample preparation is a very important aspect of any experimental study. In this section, an account of the sample preparation and the experimental procedures that were followed will be given.

It is well known that Sb segregates to the surface in a Cu crystal (Terblans, 2001; Asante, 2005). This together with the high vapour pressure of Sb (see figure 5.1) and low vapour pressure of Cu makes this system ideal for an investigation regarding surface evaporation during segregation studies.

was also performed on the unpolished side of the Cu single crystals. The copper samples were subsequently doped with Sb to a bulk concentration of below 0.1 at%. This was done by first evaporating a thin layer of Sb onto the Cu sample by means of Electron Beam Physical Vapour Deposition (EBPVD) and then annealing the sample until a homogeneous distribution of the Sb in the Cu bulk was achieved.

5.2.1 Evaporation of Sb

Sb was evaporated onto the roughened side of the Cu samples. This was done in order to avoid any damage to the highly ordered surface of the single crystals. By using this rough side the adhesion probability of the Sb onto the Cu was also increased.

To adhere to the modified Darken model conditions for a Cu/Sb system, the following conditions were observed:

- The Sb concentration must be below the solubility limit of Sb in Cu, (less than about 1 at% Thaddeus, 1990),
- The Sb concentration must be low enough to form an ideal solution,
- The Sb concentration must be uniformly distributed throughout the bulk of the Cu-crystal,
- The Sb concentration must allow segregation to occur within a convenient time frame,

It was proposed that the Cu be doped with less than 0.1 at% Sb (Terblans, 2001).

To determine what the corresponding thickness of the deposited thin film must be, it is necessary to first determine the mass of Sb needed. This can be done using

$$m_{Sb} = \frac{m_{Cu} X_{Sb} M_{ASb}}{(1 - X_{Sb}) M_{ACu}} \quad (5.1)$$

where m_{Sb} is the mass of Sb to be evaporated onto the Cu, m_{Cu} is the mass of the Cu substrate and X_{Sb} is the fractional concentration of Sb in the Cu/Sb sample. M_{Asb} and $M_{A_{Cu}}$ refer to the atomic masses of Sb and Cu respectively.

During EBPVD the thickness of the deposited Sb is measured. This measurement together with the surface area of the Cu substrate can be used to determine the volume of Sb evaporated on to the Cu. A correlation between the thickness of the Sb layer and m_{Sb} can thus be made using

$$d_{Sb} = \frac{m_{Sb}}{A_{Cu}\rho_{Sb}} \quad (5.2)$$

where d_{Sb} is the thickness of the Sb layer, A_{Cu} is the surface area of the Cu sample and ρ_{Sb} is the density of Sb.

Using equations 5.1 and 5.2 the mass and thickness of Sb that had to be evaporated onto the Cu crystals to result in a concentration of 0.1 at% Sb in Cu were calculated. The dimensions were determined using a vernier calliper and all mass measurements were performed using a Mettler Toledo XS205 DualRange Analytical Balance. These results are shown in table 5.1.

Table 5.1: Mass and thickness of the Sb layer to be evaporated onto Cu crystals in order to produce a dopant concentration of 0.1 at% Sb. Material parameters used as indicated in Askeland (1998).

Orientation	Mass of Cu crystal (g)	Surface area of Cu Crystal (mm²)	Mass of Sb (mg)	Thickness of Sb (kÅ)
(110)	0.51755	51.78	0.993	28.6
(111)	0.51700	51.91	0.992	28.5
(100)	0.50001	50.76	0.959	28.2
Polycrystalline 1	0.49228	50.83	0.944	27.7
Polycrystalline 2	0.49194	50.76	0.944	27.7
Polycrystalline 3	0.49054	51.02	0.941	27.5

Based on the results shown in table 5.1 it was decided to aim for a dopant concentration of 0.05 at% Sb which translates to an approximate thickness of 14 kÅ or deposited Sb mass of 0.49 mg. This decision was made in light of the possible Sb/Cu adhesion problems that might arise from the evaporation of a layer of Sb greater than 25 kÅ. In addition, Cu crystals doped with such a concentration of Sb will form a Sb/Cu system as discussed.

5.2.2 The evaporation system

Photographs of the evaporation system used are shown in figures 5.2 and 5.3. During EBPVD, a current is passed through a tungsten filament, heating the filament so that electrons are released. These electrons are then accelerated with a high voltage and directed with a magnetic field into a crucible containing high purity (99.999%) Sb purchased from Mateck in Germany. This causes the Sb to melt and then evaporate onto the Cu crystal positioned above the crucible. The thickness of the evaporated Sb layer is measured with an Inficon deposition controller which utilizes a gold coated quartz crystal to detect any material that is deposited onto the crystal surface. When mass is added to the face of this resonating quartz crystal, the resonance frequency is reduced. This change in frequency is very repeatable and is precisely understood for specific oscillating modes of quartz. This phenomenon leads to an measurement and process

control tool that can detect the addition of less than an atomic layer of an adhered foreign material (Inficon XTC/3 Manual) and is described in detail in section 5.3.4.



Figure 5.2: The evaporation system showing some of the external parts: a) electron gun filament current controller, b) Pirani gauge control unit, c) Varian pressure gauge control unit, d) Inficon thickness monitor, e) glass dome cover, f) High voltage feeds troughs connecting the electron gun filament to the controller, g) linear crucible manipulator, and h) stainless steel vacuum chamber. Not visible on photo: turbo molecular and rotary vane pump system. Adapted from (Joubert, 2010).

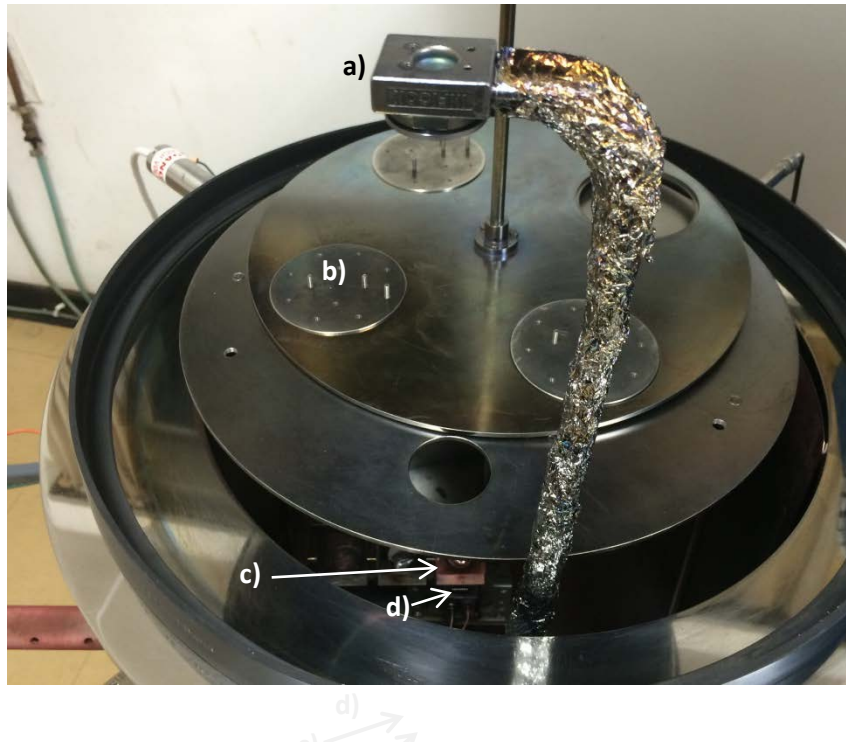


Figure 5.3: The evaporation system showing some of the internal parts: a) Inficon quartz crystal holder, b) Mounted samples on sample plate, c) Crucible containing material to be evaporated, d) Electron gun filament.

Before the Cu crystals were mounted in the EBPVD system they were first cleaned for 15 minutes in an ultrasonic bath containing acetone, where after they were rinsed with ethanol. The mounted samples are shown in figure 5.4.



Figure 5.4: Cu crystals mounted on a sample plate.

After mounting the samples the EBPVD system was evacuated to a base pressure of $\sim 10^{-5}$ torr where after Sb was deposited onto the Cu crystal. After the evaporation process, the crystals were once again weighed in order to determine the mass of Sb evaporated onto the Cu surface. These results are shown in table 5.2. Figure 5.5 shows Cu crystals with Sb evaporated onto the surfaces compared to a clean Cu crystal.

Table 5.2: Mass and thickness of Sb layers.

Orientation	Mass before evaporation (g)	Mass after evaporation (g)	Mass Sb deposited (mg)	Calculated thickness of Sb (kÅ)	Expected Sb concentration (at%)
(110)	0.51755	0.51819	0.64	18	0.065
(111)	0.51700	0.51772	0.72	21	0.073
(100)	0.50001	0.50051	0.50	15	0.052
Polycrystalline 1	0.49228	0.49301	0.73	21	0.077
Polycrystalline 2	0.49194	0.49240	0.46	14	0.049
Polycrystalline 3	0.49054	0.49123	0.69	20	0.073

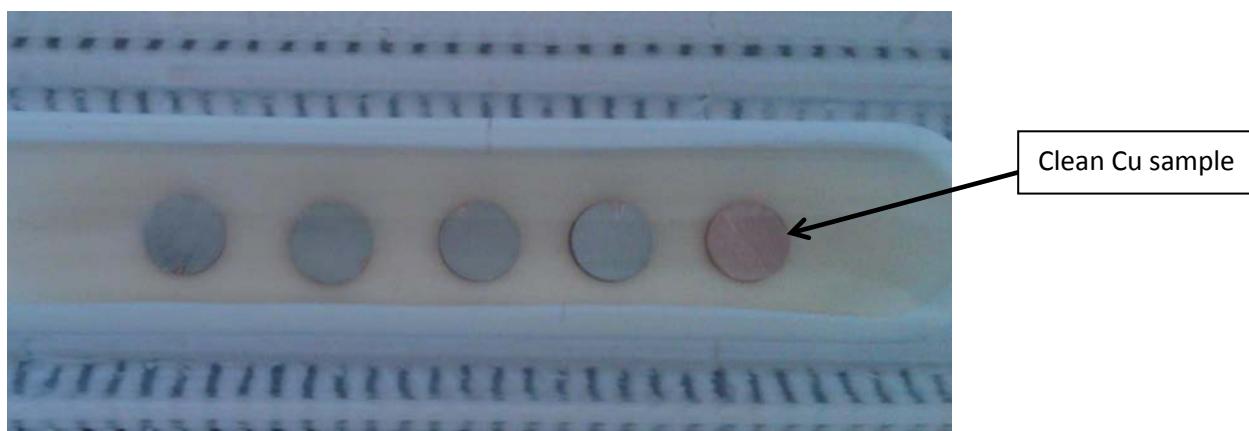


Figure 5.5: Cu samples with an evaporated layer of Sb compared to a clean Cu sample.

5.2.3 Verification of deposited thickness by means of mass calculations

An experiment was conducted to determine if a simple mass/volume calculation could be used to accurately verify the thickness evaporated onto a substrate. A thin layer of Sb was evaporated simultaneously onto a polycrystalline copper sample and a piece of Si substrate. The dimensional details of the copper disk and details regarding the mass of the Sb evaporated onto the disk are given in table 5.3. Once again the dimensions were determined using a vernier caliper and all mass measurement were performed using a Mettler Toledo XS205 DualRange Analytical Balance.

Table 5.3: Measurements used to determine accuracy of mass measurements in calculating deposited layer thickness.

Cu crystal diameter (mm)	Cu crystal thickness (mm)	Cu mass before evaporation (g)	Cu mass after evaporation (g)	Sb mass evaporated onto surface (mg)	Expected thickness(μm)
8.135	0.990	0.44538	0.44588	0.50	1.4

Due to the poor adhesion of the Sb layer to the highly polished Si substrate, the delaminated Sb layer could be carefully mounted sideways on a microscope stub allowing the thickness to be determined with a Shimadzu SSX-550 scanning electron microscope (SEM) utilizing the secondary electron detector. An image of the Sb layer with the thickness indicated at various points is shown in figure 5.6. Comparing this figure with the results shown in table 5.3 shows that simple volume and mass calculations can be used to accurately determine the thickness of a deposited layer as the calculated thickness and measured thickness are the same.

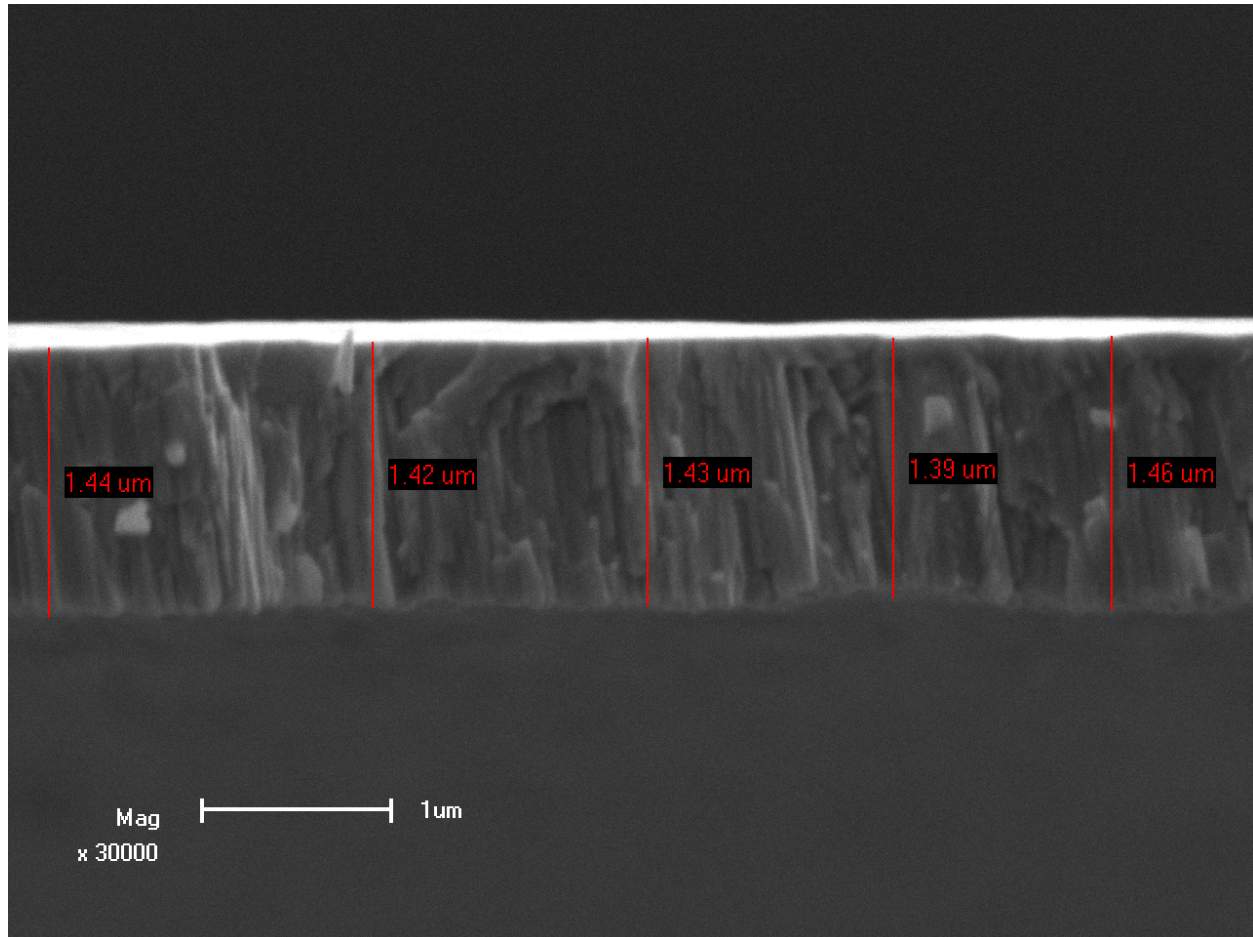


Figure 5.6: SEM image of Sb layer indicating the thickness of the deposited Sb.

5.2.4 Annealing of Cu crystals

To ensure a uniform Sb distribution through the Cu bulk, the samples were annealed. This was done by first sealing the samples in quartz vials filled with argon to prevent oxidation of the samples, and then using a Lindberg furnace to anneal the samples over a period of time.

Sealing of the samples in an argon atmosphere was done in the following manner:

- A high purity quartz tube open at one side and with an inlet and outlet on the closed side is used after being cleaned with acetone (see figure 5.7).

- The samples are placed inside this tube, where after the large open end is sealed by a glass blower. The samples must be kept away from the opening being sealed in this step in order to minimize any heat damage arising from the gas flame used (see figure 5.8).
- A high purity argon source is now connected to the inlet. Argon is flushed through the quartz vial at a rate of 25L/min in order to displace any oxygen rich air. This is done for 5 minutes after which the flow rate is reduced to 5 L/min with the glass blower first sealing the outlet and then the inlet.
- The whole quartz tube was then immersed in a beaker of acetone to check for leakage.
- This process should result in the sample being sealed in a positive pressure argon atmosphere (see figure 5.9).

The services of United Glass Blowers in Johannesburg, South Africa were used during this study.

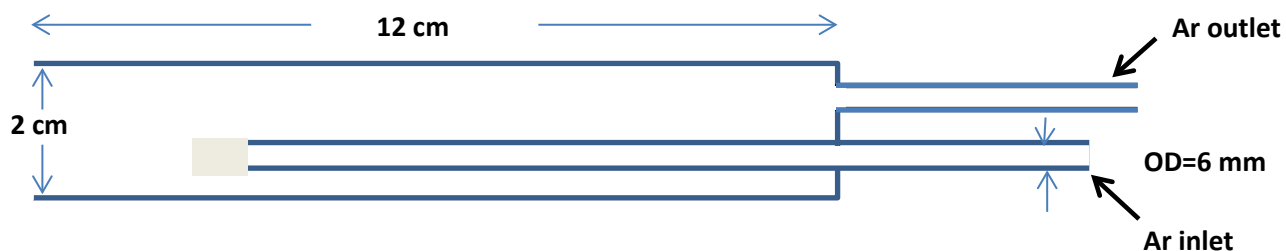


Figure 5.7: Schematic diagram of quartz tube.



Figure 5.8: Quartz tube with samples ready to be sealed.

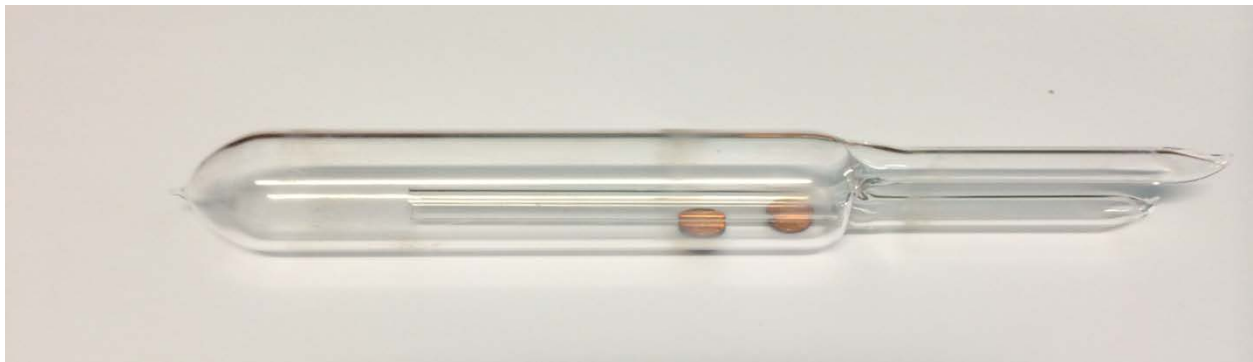


Figure 5.9: Quartz tube with samples after sealing procedure.

The sample vials could then be annealed using a Lindberg furnace as shown in figures 5.10 and 5.11.



Figure 5.10: The Lindberg furnace used during the sample annealing process.

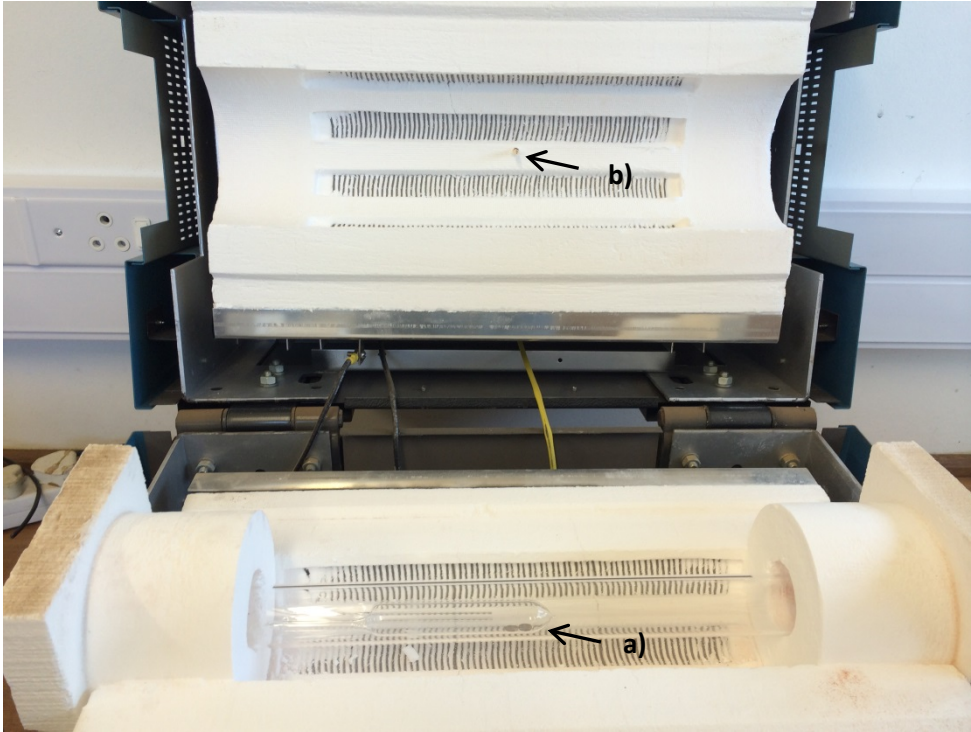


Figure 5.11: An internal view of the Lindberg furnace. a) the argon filled vial with samples, b) the thermocouple used for temperature measuring

5.2.5 Determining the annealing time and temperature

Numerous models exist to calculate the concentration profiles of Sb in Cu for various annealing temperatures and times. For this study however, the finite model with a limited diffusion source is the most appropriate. For a full discussion relating to the choice of this model the reader is referred to Terblans (2001) and Crank (1975).

Consider a Cu crystal with thickness L , where the surface is at $x = 0$. Assume that initially no Sb atoms are present in the Cu bulk. The Sb thin film on the surface of the Cu has a thickness h .

The boundary conditions are as follows:

$$0 \leq x \leq L \quad (5.3)$$

$$C(x) = 0 \text{ for } x > h \text{ and } t = 0 \quad (5.4)$$

$$C(x) = C_0 \text{ for } 0 \leq x \leq h \text{ and } t = 0 \quad (5.5)$$

$$\frac{\partial C}{\partial x} = 0 \text{ at } x = L \text{ for } t \geq 0 \quad (5.6)$$

The above mentioned conditions can be used in Fick's second law

$$\frac{\partial C}{\partial t} = D \frac{\partial^2 C}{\partial x^2} \quad (5.7)$$

to obtain the following solution

$$C = C_0 \sum_{n=-\infty}^{\infty} \left[\operatorname{erf} \left(\frac{h+2nL-x}{2\sqrt{Dt}} \right) + \operatorname{erf} \left(\frac{h-2nL+x}{2\sqrt{Dt}} \right) \right] \quad (5.8)$$

as shown in Crank (1975). This solution shows the concentration of Sb atoms which diffused into the Cu-crystal. The homogeneity of the Sb concentration in the Cu crystal is given by

$$\text{Homogeneity} = \frac{C_{x=L}}{C_{x=0}} \quad (5.9)$$

Using equation 5.8 and the set of parameters indicated in figure 5.12 it was possible to obtain the homogeneity curve. Choosing $T = 1173 \text{ K}$ and using approximate diffusion values (Terblans, 2001), the graph in figure 5.12 indicates that annealing at 1173 K for 30 days is necessary to obtain a homogeneity of 99.9 % for a crystal 1 mm thick. The calculation was done for the thickest Sb layer as shown in table 5.2.

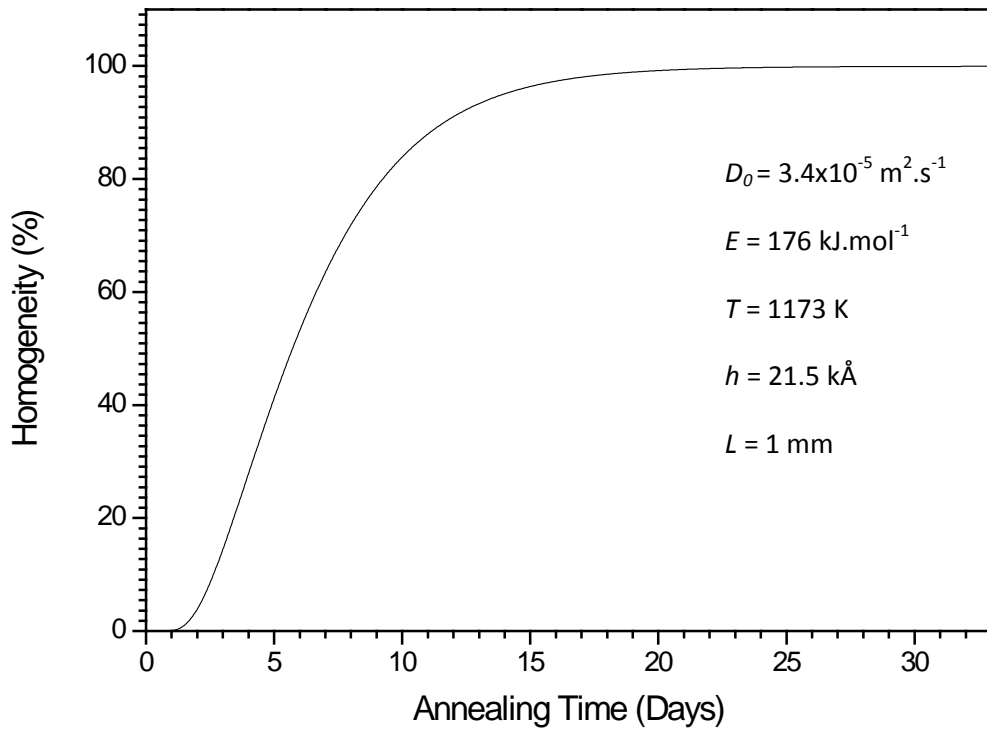


Figure 5.12: The graph indicates the homogeneity of a Sb doped Cu crystal as a function of annealing time at 1173 K (Software developed by J.J. Terblans).

To ensure sufficient homogeneity the samples were annealed for 35 days at 1173 K .

Unfortunately problems arose with the annealing of two sample sets. These samples are shown in figure 5.13 and figure 5.15. In figure 5.13 it can be observe that the evaporated Sb layers did not adhere to the Cu substrates. This prevented the Sb layers diffusing into the Cu substrates.



Figure 5.13: Failed sample preparation. The antimony did not adhere to the copper crystal.

As all the Cu substrates underwent the same roughening of the surface onto which the Sb where deposited, and seeing that all the Sb layers where of similar thicknesses the reason why these samples failed cannot be explained at this point of time.

Figure 5.14 shows a sample set with typical signs of oxidation. As this quartz tube showed no signs of leaking when tested in acetone, it can only be concluded that the filling of the quartz tube with argon was not successful.



Figure 5.14: Failed sample preparation showing possible oxidation of samples.

Only a third of the attempted sample preparation proved successful. It should thus be clear that the sample preparation technique used in this study and used in studies like Asante (2005), has room for improvement. One possible option is to make use of equipment like that described by Jafta *et al.*, (2010) which uses a large quartz tube which is first evacuated by means of vacuum pumps and then pressurized with argon.

5.3 Equipment to measure evaporation/sublimation during segregation

An AES system was modified to allow the user to perform standard segregation measurements, but also to measure the evaporation rate of any material that might evaporate from the surface of a sample during a temperature ramp. While the main objective of this study is to investigate evaporation during segregation, these modifications may prove useful in any study where evaporation is investigated. The modifications not only allow the user to determine the chemical composition of the sample surface before or after evaporation, but it also enables the user to clean the surface of any contaminants by means of Ar^+ sputtering before an evaporation run is started.

The modifications were done by employing an Inficon XTC/3s Deposition Controller which utilizes a gold coated quartz crystal to detect any material that is deposited onto the crystal surface. This thickness monitor was mounted in the AES system (see figure 5.15) in such a way that the specimen mounted on a resistance heater could be repositioned from a position in front of the AES electron gun/analyser to a position underneath the gold coated crystal. This was achieved by making use of a manipulator with a flip mechanism.

The modifications made consist of four main parts:

- The original AES system
- Sample stage and manipulator
- The sample heater
- The thickness monitor

These parts will now be discussed in detail.

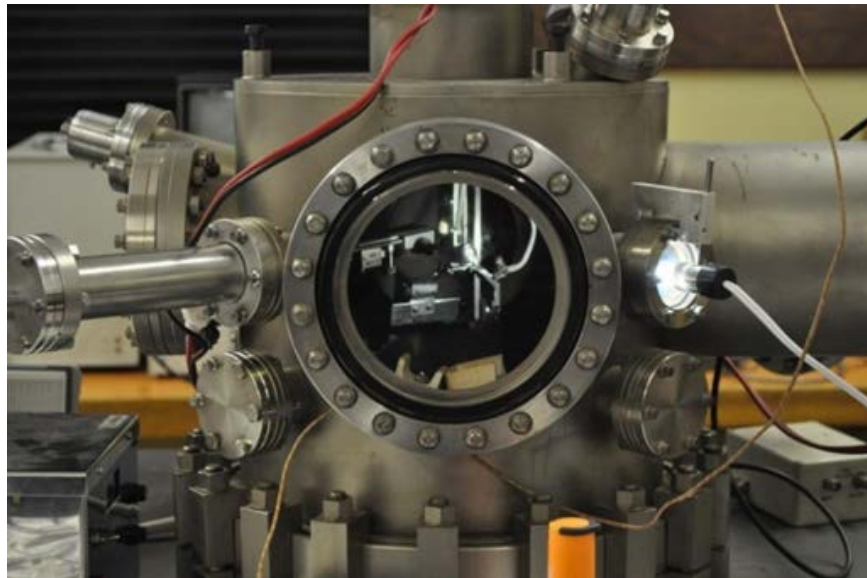


Figure 5.15: The modified AES system.

5.3.1 The AES system

The fundamental principles of AES are well understood and can be obtained in a number of literature sources (Davis *et al.*, 1976). Consequently only a brief description of the system and settings used will be given.

A photo of the AES system used during this study is shown in figure 5.16 with a schematic diagram of the system's main components shown in figure 5.17.

This AES system was originally computerised by J.J. Terblans. A complete description of this can be found in Terblans (1997). Use was however made of updated software developed by W.D. Roos and C.J. Jafta.



Figure 5.16: The AES system used during this study.

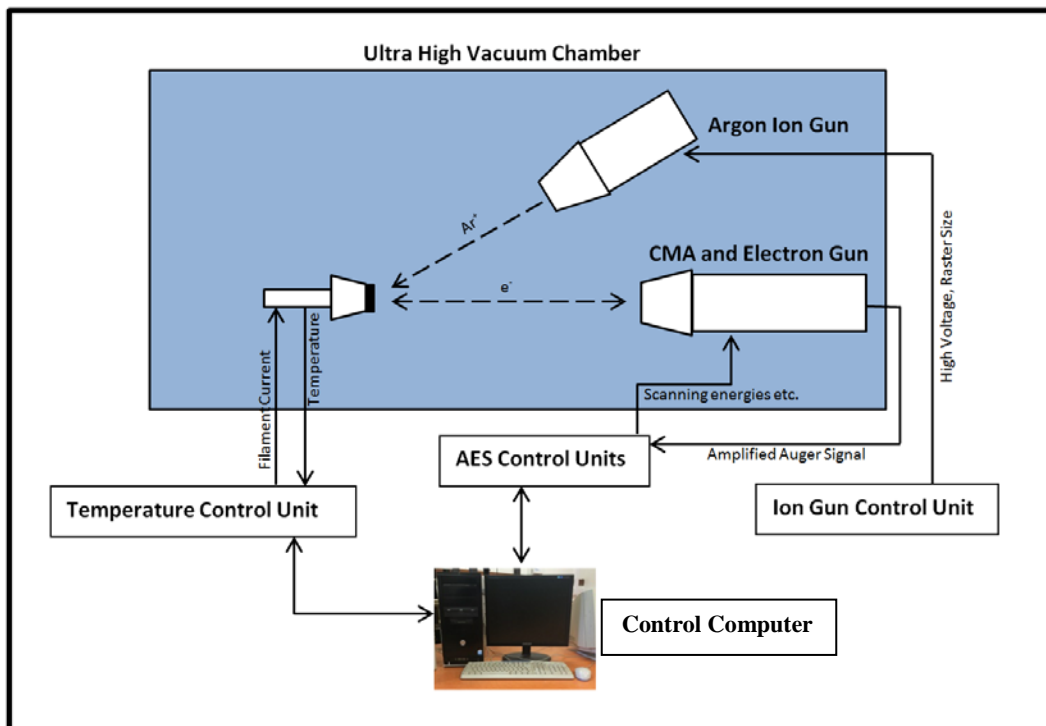


Figure 5.17: The schematic diagram of the computer controlled AES system.

In a broad sense the AES consist of the following parts:

- An ultra high vacuum chamber with vacuum pump system
- An argon ion gun used for cleaning the sample surface and for performing depth profiles
- An electron gun with single stage cylindrical mirror analyser
- Control units for the above
- Sample stage with resistance heaters (see sections 5.3.2 and 5.3.3)

The following individual components were used during this study:

1. A Varian ultra-high vacuum system consisting of a rotary vane- and turbo molecular pump pre-vac system with an ion pump (240l/s) capable of reaching a vacuum of $\leq 1 \times 10^{-9}$ torr.
2. An argon ion gun with a PHI 20-115 Ion Gun Control unit. The system was used with a 2 kV beam voltage with an emission current of 25 mA. The raster size was set at 8 mm x 8 mm. The non-differentially pumped ion gun was used by first back filling the vacuum chamber with argon gas until the ionization pressure gauge read 5.0×10^{-5} torr.
3. An electron gun with an analog Perkin Elmer AES gun control, model number 20-320. The primary energy of the electron beam used was set at 3 keV and 2 keV during the measurement of the Auger spectra and elastic peak respectively. The electron gun filament current was kept constant at 3.5 A and the emission current was kept constant at 1.5 mA.
4. A single pass Perkin Elmer cylindrical mirror analyser (CMA) model number 15-110B. The apertures in the analyser were set at the small settings position.
5. A Perkin Elmer 11-500A Auger System Control. This unit controls the voltages on the inner- and outer cylinders of the analyser, so that only electrons with specific kinetic energies can pass through to the electron multiplier. A modulation voltage of 4 eV peak to peak was used.
6. A Stanford Research systems Model PS325 high voltage digital power supply unit for the electron multiplier. The multiplier voltage was set at 1200 V for measuring the Auger spectra.

7. A PHI model 32-010 lock-in amplifier. The sensitivity with amplification factor set at 100X for obtaining the Auger spectra and 1X for the elastic peak. A time constant of 1 second was used.

5.3.2 The sample stage and manipulator

The first modification made to the AES system (see section 5.3.1) was the fitting of a sample stage manipulator that allowed the user to reposition a sample mounted on a resistance heater from a position in front of the electron gun/analyser to a position underneath the thickness monitor. The manipulator fitted allows the user to adjust the spatial position of the sample with reference to the laboratory frame of reference with the X direction along the optical axis of the analyser. These adjustments are not only by means of adjustments in the horizontal (X, Y) and vertical (Z) directions, but also by rotation of the sample stage through 360 degrees in the horizontal plane, and 90 degrees in the vertical plane. These movements can be precisely controlled as the manipulator has vernier micrometers with millimetres or degree scales on each adjustment arm. Figure 5.18 shows the fitted manipulator.



Figure 5.18: The fitted manipulator.

Figure 5.19 show a schematic diagram indicating movements necessary to align the specimen for measurements.

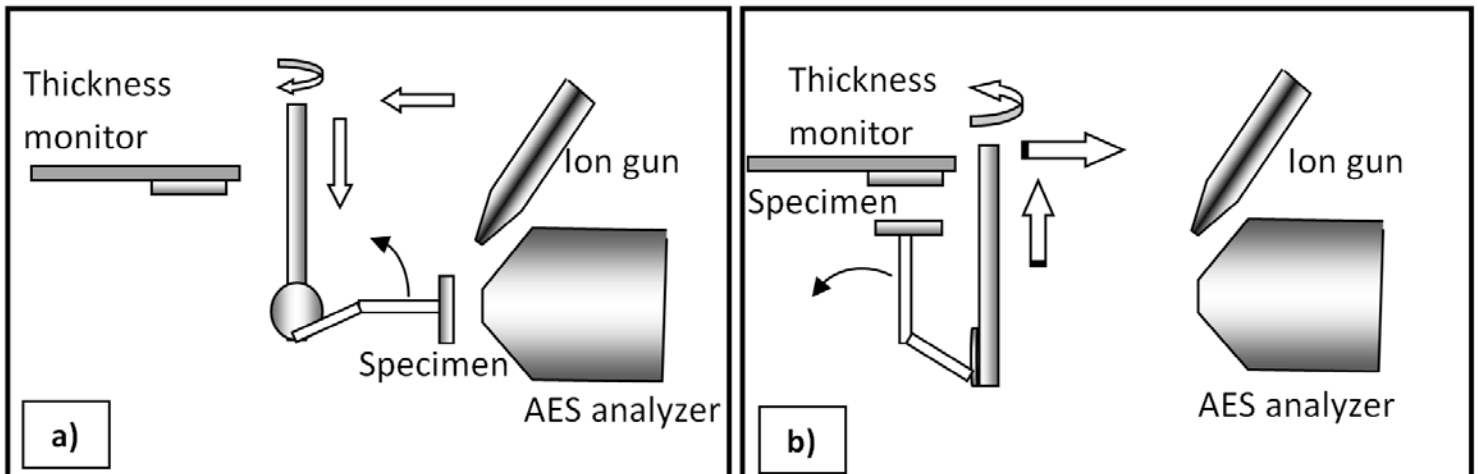


Figure 5.19: A schematic of the thickness monitor as it relates to the AES. **a)** The arrows indicate the movements necessary to align the specimen for evaporation measurements. **b)** The arrows indicate the movements necessary to align the specimen for AES measurements.

Figure 5.20 shows photos with descriptions of the modifications made and their relation to each other.

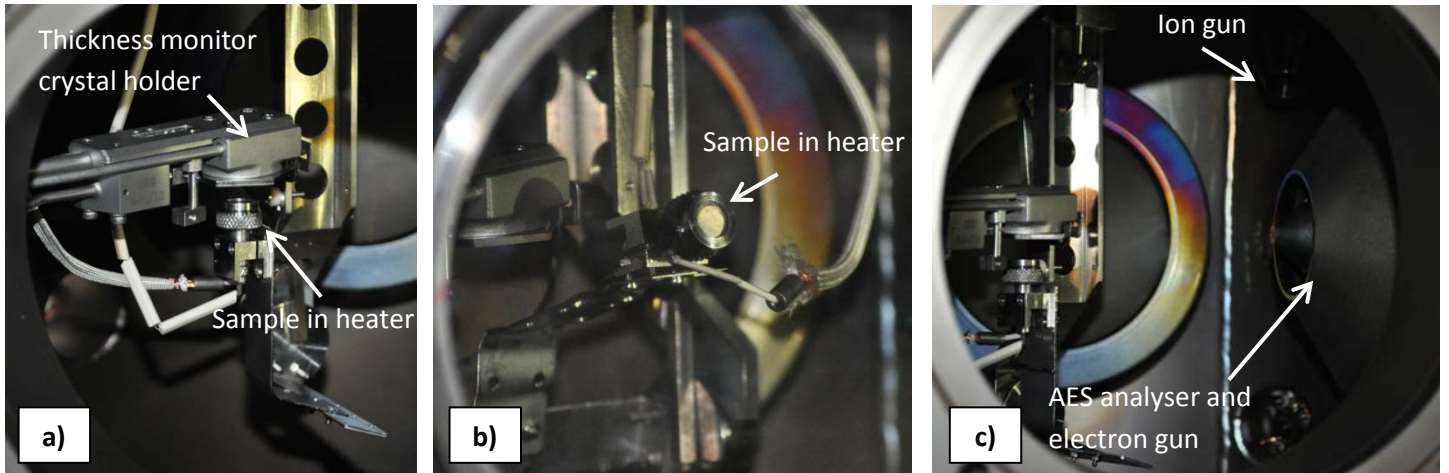


Figure 5.20: The different parts of the modifications made and how they relate in terms of position to each other.

5.3.3 The resistance heater

The heater used in the modification follows the basic design as developed by Terblans (2001). It consists of a cupped shape sample holder with a screw top machined out of non-magnetic 316 stainless steel, backed by an alumina housing isolating the tungsten filament. The setup is arranged in such a way that the thermocouple measures the temperature directly at the back of the crystal and that the crystal can be changed easily without damaging the filament or thermocouple connections. The screw-on cup opening also masks the crystal in such a way that the evaporation surface area is kept constant. The heater and its various parts are shown in figure 5.21.

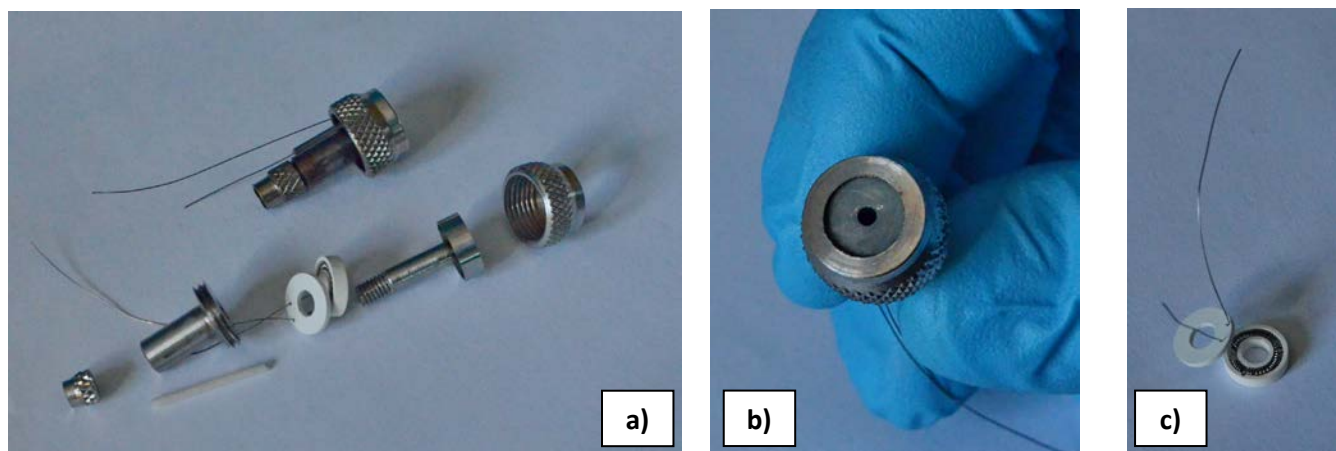


Figure 5.21: a) An exploded view of the resistance heater. The hole in figure b) is where the thermocouple will protrude to press against the back of the sample. c) The tungsten filament and alumina housing.

5.3.4 The thickness monitor

The Quartz Crystal Monitor (QCM) is a commonly used instrument in vacuum deposition systems to determine the thickness of the deposited layer on the substrate. Such a device was built into the modified AES system in order to measure the amount of segregant that evaporates off the surface of a sample during a segregation run. The QCM was positioned to prevent any possible contamination of the AES analyser. The various parts of the device are shown in figures 5.22 and 5.23.



Figure 5.22: Inficon XTC/3s Deposition Controller unit



Figure 5.23: The deposition monitor arm with water cooling tubing, electrical connections and sensor holder.

According to the Inficon XTC/3s Manual the QCM utilizes the piezoelectric sensitivity of a quartz crystal to added mass to measure the deposition rate and displays the thickness of the deposited layer.

When a voltage is applied across the faces of a properly shaped piezoelectric crystal, the crystal is distorted and changes shape in proportion to the applied voltage. At certain discrete frequencies of applied driving voltage, a condition of very sharp electromechanical resonance are encountered (Inficon XTC/3s Manual).

When mass is added to the face of a resonating quartz crystal, the frequency of these resonances is reduced. This reduction in frequency when mass is added to the crystal is very repeatable and is precisely understood for specific oscillating modes of quartz. Using this principal it is possible detect the addition of less than an atomic layer of an adhered foreign material to the surface of such a quartz crystal (Inficon XTC/3s Manual).

In the late 1950's it was noted by Sauerbrey and Lostis that the change in frequency

$$\Delta F = F_q - F_c \quad (5.10)$$

of a quartz crystal with coated and uncoated frequencies F_c and F_q respectively, is related to the change in mass from the added material, M_f as follows

$$\frac{M_f}{M_q} = \frac{(\Delta F)}{F_q} \quad (5.11)$$

Where M_q is the mass of the uncoated quartz crystal. Simply substitutions lead to the equation that was used with the first frequency measurement instruments

$$T_f = \frac{K(\Delta F)}{\rho_f} \quad (5.12)$$

where the film thickness T_f is proportional to the frequency change ΔF and inversely proportional to the density of the film, ρ_f . The constant K is given by

$$K = \frac{N_{at}\rho_q}{F_q^2} \quad (5.13)$$

Where ρ_q is the density of single crystal quartz and N_{at} is the frequency of AT cut quartz. As an example a crystal with a starting frequency of 6.0 MHz will display a reduction of its frequency by 2.27 Hz when 1Å of Aluminium is added to the surface. In this manner the thickness of a deposited layer is inferred from the measurement of the crystal's frequency shift (Inficon XTC/3s Manual).

Although equation 5.12 was very useful, it was soon noted that equipment using it had a very limited range of accuracy (Inficon XTC/3s Manual). Advances in both the understanding of the resonating quartz and deposited film system as a one-dimensional continuous acoustic resonator and advances relating to electronics, namely the micro-processor allowed the development and real time implementation of the Z-Match equation

$$T_f = \left(\frac{Nat\rho_q}{\pi\rho_f F_c} \right) \arctan \left(Z \tan \left[\frac{\pi(F_q - F_c)}{F_q} \right] \right) \quad (5.14)$$

where $Z = \left(\frac{\rho_q u_q}{\rho_f u_f} \right)^{\frac{1}{2}}$ is the acoustic impedance ratio and u_q and u_f are the shear moduli of the quartz and film respectively. Most deposition controllers sold today including the one used during this study make use of equation 5.14. This means that the most important input parameters for the deposition controller is the density of the material deposited and the Z-ratio, both which can be obtained for a number of elements and compounds from the XTC/s Operating Manual. In this study a gold coated quartz crystal with a starting frequency of 6.0 MHz was used.

Figure 5.24 shows a gold coated quartz crystal before and after deposition.

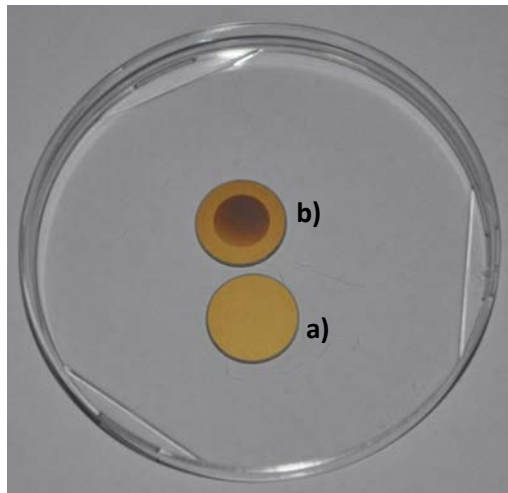


Figure 5.24: Gold coated quartz crystals a) as new b) after deposition of Sb.

5.4 Some considerations when measuring evaporation

5.4.1 Heat effects on the thickness monitor

As discussed the thickness of a deposited layer is inferred from measurements of the shift in the resonance frequency of the quartz crystal. As heating effects should in theory result in an increase in frequency and thus show a decrease in the amount of deposited material the influence of the resistive heater temperature on the QCM was investigated.

A silica disk of similar dimensions to the copper samples used in this study was placed inside the resistive heater. As silica has an extremely low vapour pressure even at high temperatures this material was deemed ideal for an experiment of this nature as no evaporation of material should take place. Any “deposition” or change in frequency detected by the QCM would be directly due a temperature effect.

Three heating runs were performed at different standoff distances lower than the recommended minimum specified by the manufacturer, where the standoff distance d_s is the distance between the top of the heater cap and the bottom of the quartz crystal holder. This distance could be accurately determined due to the measuring scale on the vertical-axis of the manipulator. The

QCM quartz crystal was water cooled with a flow rate of 1L/min at 16 °C as the temperature of the silica disk was gradually increased. At each measuring temperature the system was allowed to stabilise for 5 minutes, and the thickness monitor observed for an additional 5 minutes taking a deposition rate measurement every 10 seconds and averaging the measurements over a 5 minute time interval. The results are shown in figure 5.25.

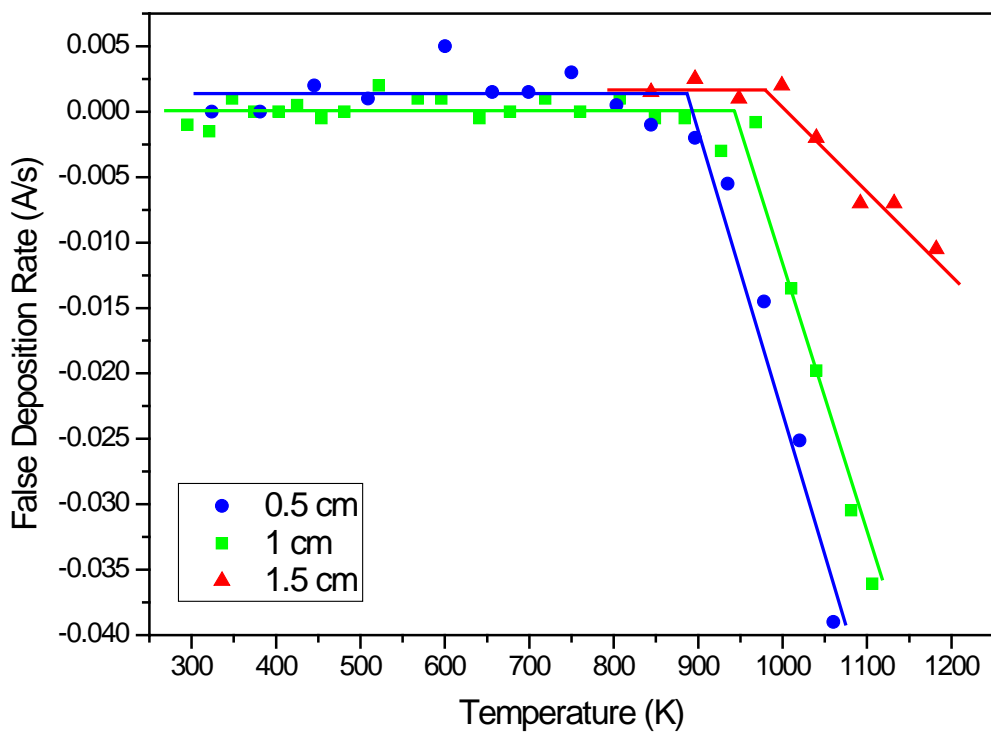


Figure 5.25: False deposition readings as a result of temperature effects.

As can be seen in figure 5.25 no temperature effects can be detected below 900 K. Above a temperature of 900 K an increase in crystal frequency is detected resulting in the QCM recording a negative deposition rate. For a Sb/Cu system, 900 K represents the upper temperature limit during a linear temperature ramp, and subsequently the heating effect on the thickness monitor can be ignored during the study.

5.4.2 Calibration of the QCM

Due to the fact that the flow of material from a deposition source is not uniform, it is necessary to account for the different amount of material flow onto the sensor compared to the substrate. The thickness difference is due to the geometric distribution of material flux, from the source. One such scenario is where the substrate and the crystal are not at the same distances from the deposition source. The tooling parameter is a correction factor used for correlating the rate and thickness accumulation on the crystal with the thickness accumulation on the substrate. The tooling factor is calculated using the equation:

$$Tooling = TF_i \times \left(\frac{T_m}{T_x} \right) \quad (5.15)$$

where TF_i is the initial tooling factor, T_m is the actual thickness of the deposited layer at the substrate, and T_x is the thickness of the deposited layer on the sensor (Inficon XTC/3s Manual).

To calibrate the system in terms of tooling factor a short deposition run is performed on a test substrate. The thickness of the deposited layer is then determined using a multiple beam interferometer, a stylus-type profilometer or some other method and using equation 5.15 to determine the appropriate tooling factor. This procedure should be repeated a number of times to obtain an average value for the tooling factor.

The default setting for the tooling factor on the XTC/3s controller is 100%, which corresponds to a scenario where the quartz crystal and substrate is at the same distance from the deposition source. This corresponds to the experimental setup used during this study since the quartz crystal also serves as the substrate. A tooling factor of 100% would thus be expected. To verify this value three experimental runs were done where varying Sb films of between 2 and 12 kÅ were deposited onto the quartz crystal. By using the techniques described in section 5.2.1 to determine the mass deposited and subsequently the thickness deposited, an average tooling factor of 106% was calculated. Considering the experimental errors involved in determining the thickness deposited, a decision was made to use the default tooling factor.

5.4.3 Evaporation geometry

The quartz crystal of the deposition controller monitors the thickness and deposition rate of a thin film deposited on the quartz crystal. It is however obvious that in the case of an experimental setup as used during this study, only a fraction of the evaporant leaving the sample surface impinges on the quartz crystal. This means that the amount of material lost from the sample surface is a multiple of the amount of evaporated material detected by the deposition monitor (see figure 5.26 (b)).

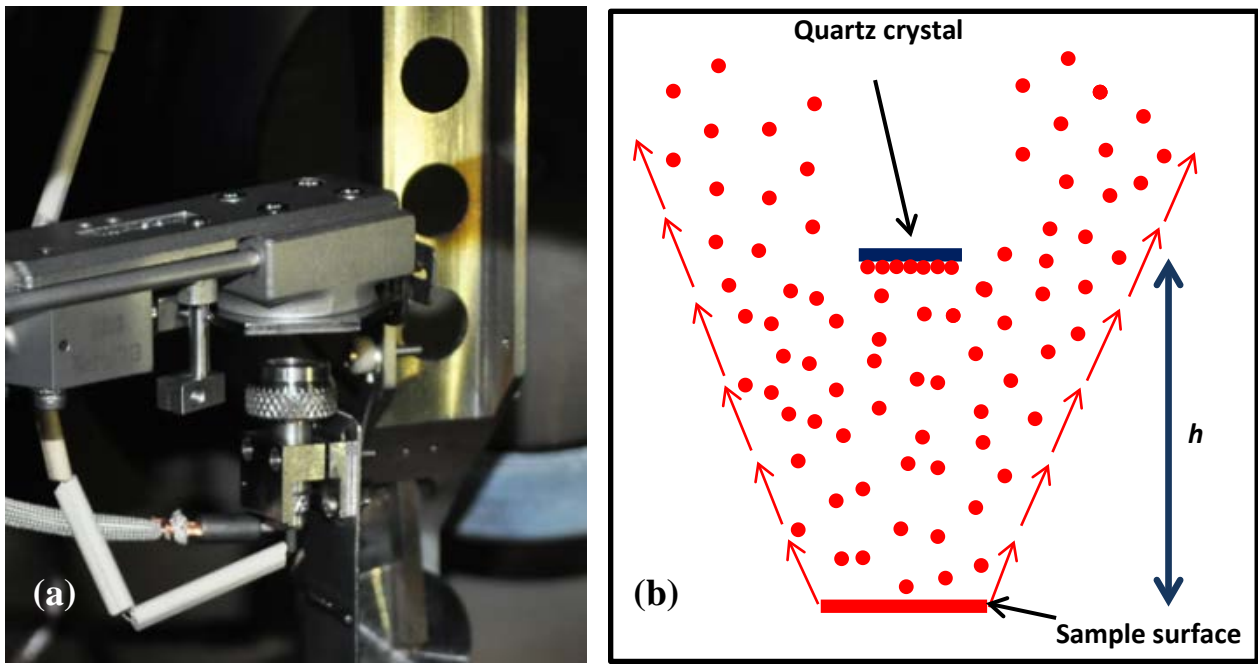


Figure 5.26: (a) The deposition monitor crystal holder position the crystal a distance h from the sample surface. (b) Only a fraction of the atoms or molecules that evaporates from the sample surface are registered by the deposition monitor.

The question now arises what fraction of the evaporated material is incident on the quartz crystal? The main aim is to get the total evaporation rate from the specimen surface. For the purpose of this study it can be assumed that

- A portion of the total evaporated particles is incident on the quartz crystal.
- The particles incident on the quartz crystal has a sticking coefficient of 1.

- The total number of evaporated particles incident on the quartz crystal is related to the angle and distance between the specimen and crystal.
- The evaporated atoms travel in a field free region, thus in straight lines from the specimen.
- The expansion of the evaporated particles into the chamber depends on whether the source is a point source or a surface source.
- The measured deposition rate depends on the orientation of the source relative to the quartz crystal.

5.4.3.1 Point Source

Deposition of thin films involves consideration of both the characteristics of the evaporation source and the orientation and placement of the substrate upon which the evaporated atoms or molecules impinge (Ohring, 2002). Evaporation from a point source is the simplest of situations to model. Consider a point on a surface from which particles are evaporating. The particles may leave with equal probability at any angle (isotropic), or they may follow the so-called cosine law often used for Knudsen cells. The particles may even be directed more strongly upwards from a deep narrow crucible (Ohring, 2002). Figure 5.27 illustrates this.

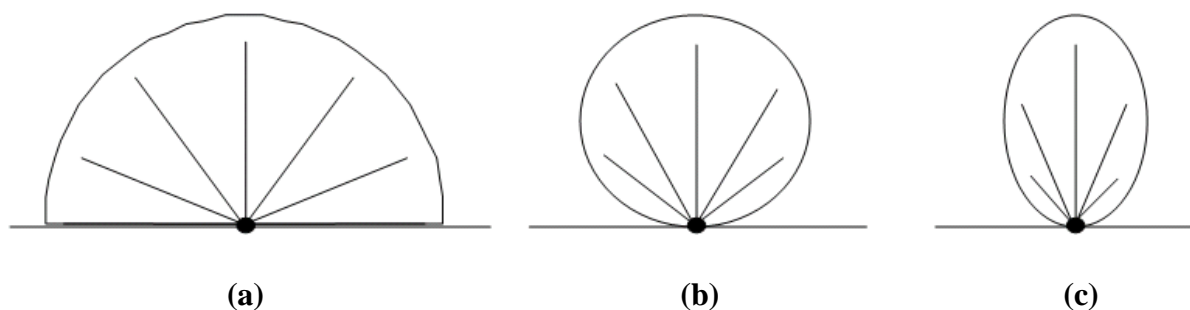


Figure 5.27: Possible angular distribution of particles evaporating from a point on a surface, given by $\cos^n \varphi$ where φ is the angle relative to the surface normal at that point: **(a)** isotropic, $n = 0$; **(b)** $n = 1$, simple model for a surface or Knudsen cell **(c)** $n = 2$, more directed anisotropic source applicable for a narrow deep evaporation source.

(from <http://ece.uwaterloo.ca...>).

If it is assumed that the particles leave a point on the surface with angular dependence $\cos^n \varphi$ where φ is the angle relative to the surface normal at that point, and by integrating over a hemisphere of radius r centred at that point then

$$\iint_{\text{hemi-sphere}} \cos^n \varphi \, da = \int_{\varphi=0}^{\pi/2} \cos^n \varphi (2\pi r^2 \sin \varphi \, d\varphi) = \frac{2\pi r^2}{n+1} \quad (5.16)$$

meaning the fraction of particles reaching an area da on the surface of the hemisphere will be

$$\frac{\cos^n \varphi da}{\left(\frac{2\pi r^2}{n+1}\right)} \quad (5.17)$$

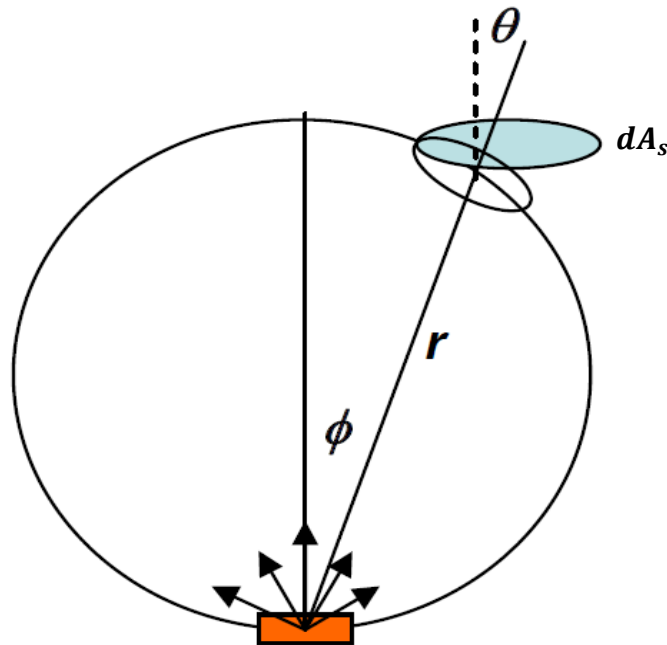


Figure 5.28: Particles evaporating from a surface and collected on an area dA_s

(from www.users.wfu.edu/ucerkb/Nan242/L06-Vacuum_Evaporation.pdf)

If the collecting surface dA_s is orientated with the normal on this surface an angle θ from the normal to the hemisphere, then the effective surface for collecting particles is given by $da = \cos \theta dA_s$ and the fraction of particles collected on a finite area A_s is given by:

$$\int_{A_s} \frac{(n+1) \cos^n \varphi}{2\pi r^2} \cos \theta dA_s \quad (5.18)$$

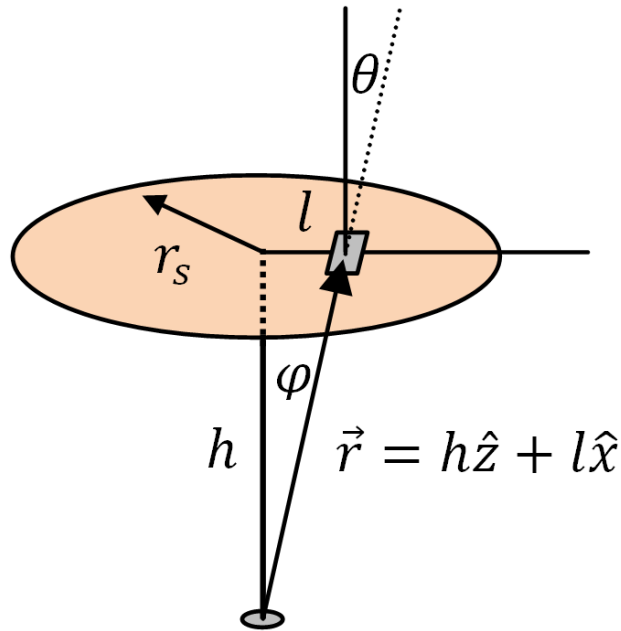


Figure 5.29: Particles evaporating from a point on a surface and being collected on a disk of radius r_s that is a distance h above the source.

Considering a flat collecting surface lying a distance h above and parallel to the emission point. In this case the angles φ and θ are equal, with $\cos \varphi = \cos \theta = \frac{h}{r}$. If the collecting area is a disk

of radius r_s directly above the emission point then the fraction of collected particles will be given by:

$$\int_{l=0}^{r_s} \frac{(n+1) \cos^{n+1} \varphi}{2\pi r^2} (2\pi l dl) = (n+1)h^{n+1} \int_{l=0}^{r_s} \frac{l}{r^{n+3}} dl \quad (5.19)$$

Note that $r = \sqrt{h^2 + l^2}$, so that this integral can be evaluated to

$$1 - \left[\frac{1}{1 + \left(\frac{r_s}{h}\right)^2} \right]^{\left(\frac{n+1}{2}\right)}. \quad (5.20)$$

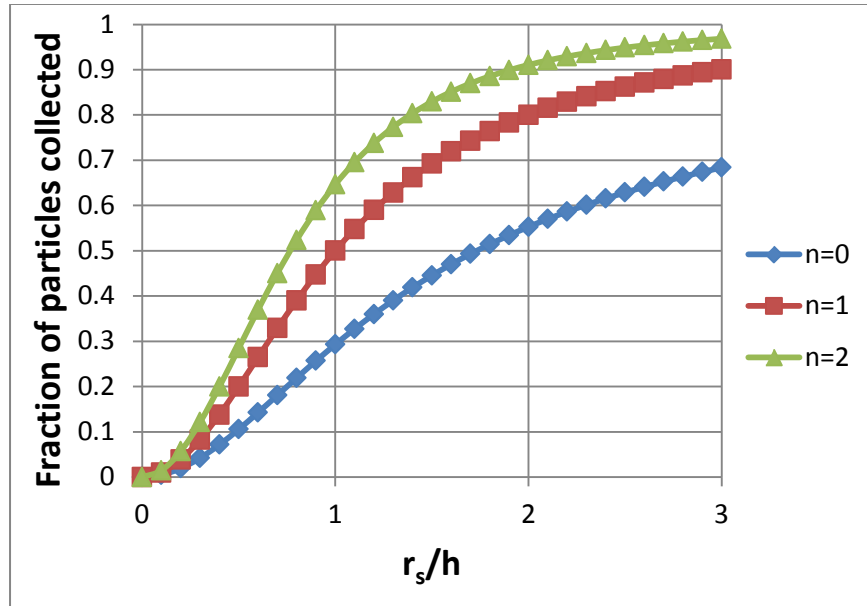


Figure 5.30: The relationship between the exposed quartz crystal radius r_s and distance from the sample h for a point source, where n refers to the power of the cosine function which describes the angular distribution of particles evaporating from a point source.

5.4.3.2 An evaporating surface

The results shown in figure 5.30 assumed the particles evaporated from a point source. If the evaporating surface is small and the collecting surface is far away, that is a reasonable assumption. However, when the collecting surface is close to the evaporating surface which has also has significant size, it is not always justified. Consider then evaporation not from a point source, but a distributed region or surface area. This leads to a situation as shown in figure 5.31.

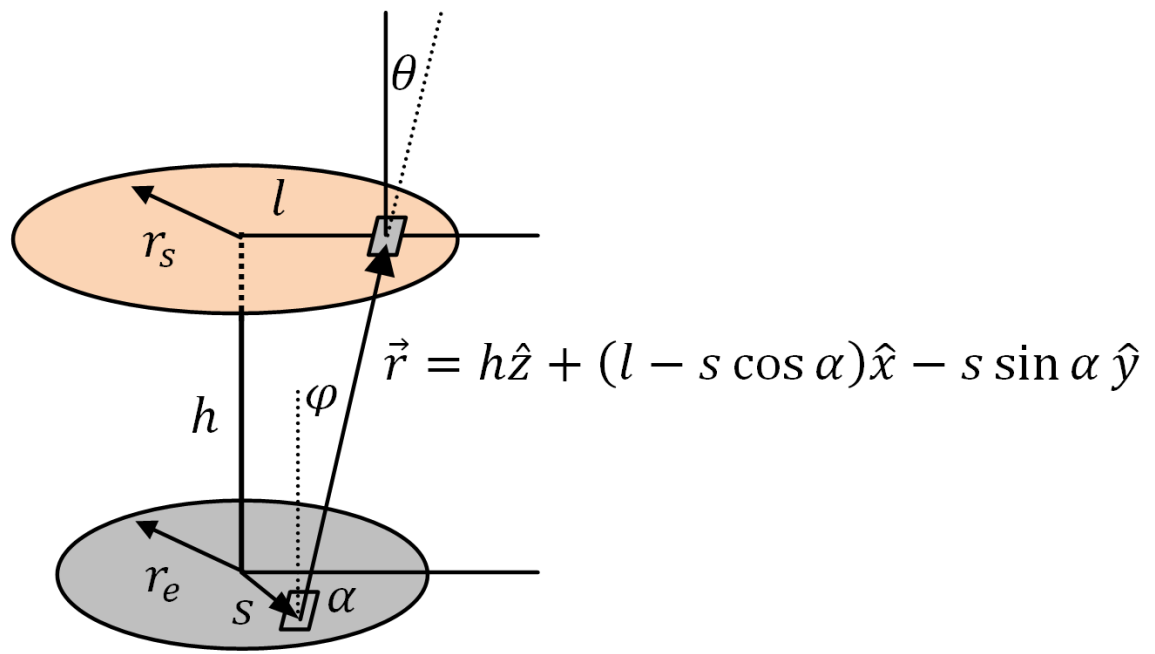


Figure 5.31: Particles evaporating from an extended disk surface of radius r_e and being collected on a disk of radius r_s that is a distance h above it.

The analysis for the fraction of evaporating particles emanating from a finite circular source that impinge on a circular collecting surface directly above was not found in the literature, but developed for this study. Taking the evaporating region as a disk of radius r_e directly below and parallel to the collecting disk, the previous expression needs to be modified by considering how

$\frac{\cos^{n+1} \varphi}{r^2}$ varies as the emission point $(x, y) = (s \cos \alpha, s \sin \alpha)$ varies over the emitting disk.

This results in

$$\int_{l=0}^{r_s} \frac{(n+1)}{2\pi} \left[\frac{1}{\pi r_e^2} \iint_{A_e} \frac{\cos^{n+1} \varphi}{r^2} dA_e \right] (2\pi l dl) \quad (5.21)$$

Again $\cos \varphi = \cos \theta = \frac{h}{r}$, but in this case $r = \sqrt{h^2 + (l - s \cos \alpha)^2 + (-s \sin \alpha)^2}$ so the expression can be written as

$$\frac{(n+1)h^{n+1}}{\pi r_e^2} \int_{l=0}^{r_s} \int_{\alpha=0}^{2\pi} \int_{s=0}^{r_e} \frac{sl}{[h^2 + (l - s \cos \alpha)^2 + (s \sin \alpha)^2]^{\frac{(n+3)}{2}}} ds d\alpha dl \quad (5.22)$$

Given the disk radii r_e and r_s , the parameter n and the distance between the disks h , this integral can be evaluated numerically in the software program Matlab using the function `triplequad` as shown in appendix B.

The value calculated with this expression for the fraction of collected particles for an extended surface is always less than that for the corresponding point source. For example, consider the setup when $n = h = r_s = 1$, for which the point source expression predicts that exactly half the particles will be captured. The more accurate expression allowing for the finite emission area is plotted as a function of emitting radius in figure 5.32.

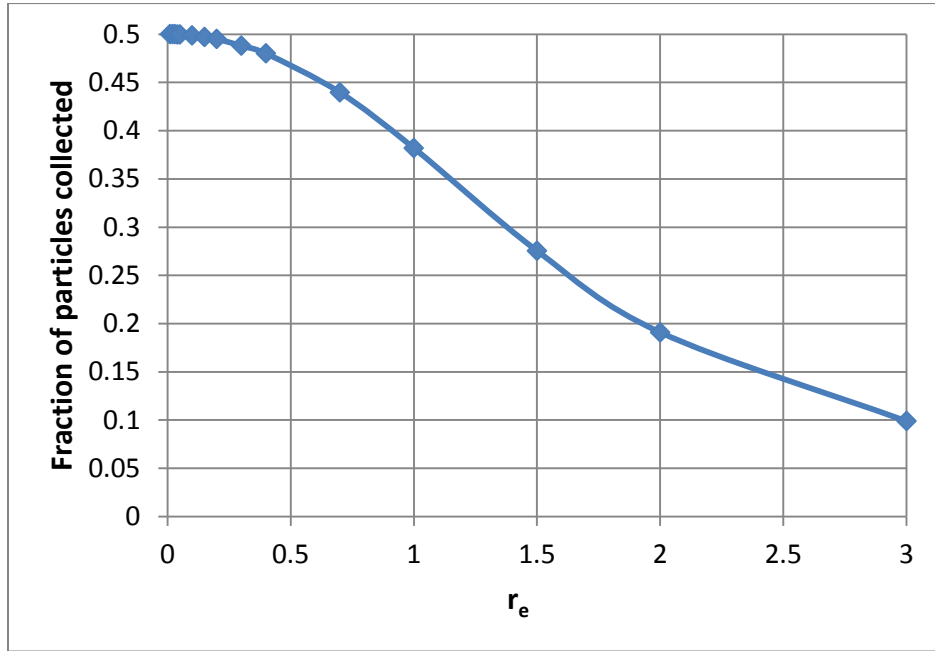


Figure 5.32: Fraction of particles collected as a function of emitting source radius r_e for $n = h = r_s = 1$.

Here again n is a number that determines the geometry of the lobed shaped vapour cloud and the angular distribution of the evaporation flux from such sources. In a case where n is large the vapour flux is highly directed. Physically n is related to the evaporation crucible geometry and scales directly with the ratio of the melt depth below the top of the crucible to the melt surface area (Ohring, 2002). More specifically in the case of this study n is related to the sample holder geometry.

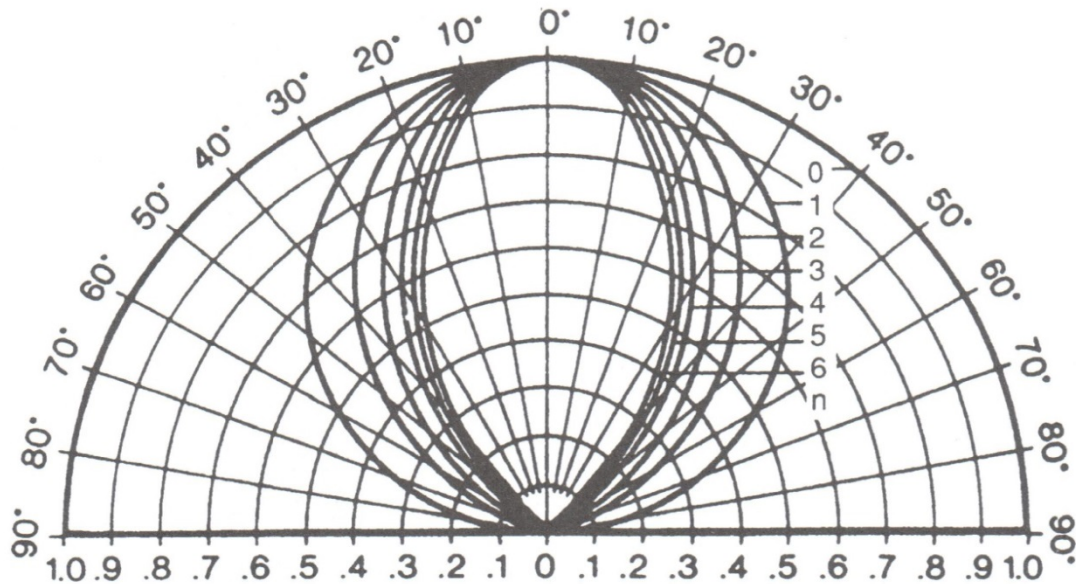


Figure 5.33: Calculated lobe-shaped vapour clouds with various cosine exponents (n) (Ohring, 2002).

One may consider which is the most appropriate value of n to use. The textbook ‘Handbook of Physical Vapor Deposition (PVD) Processing’ 2nd ed by Mattox (2010) states (while referring to water) that “... note that vaporizing species leave the surface with a cosine distribution of the molecular flux” [i.e. $n = 1$] and later it states “In actuality, the flux distribution from a free surface may not be cosine but can be modified by source geometry, collisions associated with a high vaporization rate, level of evaporant in the source, etc.”. It is therefore clear that n can vary according to the circumstances, but using $n = 1$ is a good starting point when there is no clear reason to use a different value.

In the case of this study the heater used (see figure 5.34 and 5.25) masks the sample so that a circular surface area with an average diameter of 7.90 mm which gives $r_e = 3.95$ mm and an evaporation surface area of 49 mm^2 . This surface is however recessed in the sample heater due to the heater cap edge by 1.0 mm. Because n scales directly with the ratio of the melt depth below

the top of the crucible to the melt surface area or in this case the sample surface to the top of the heater cap, a n value of 2 or even 3 might be appropriate.

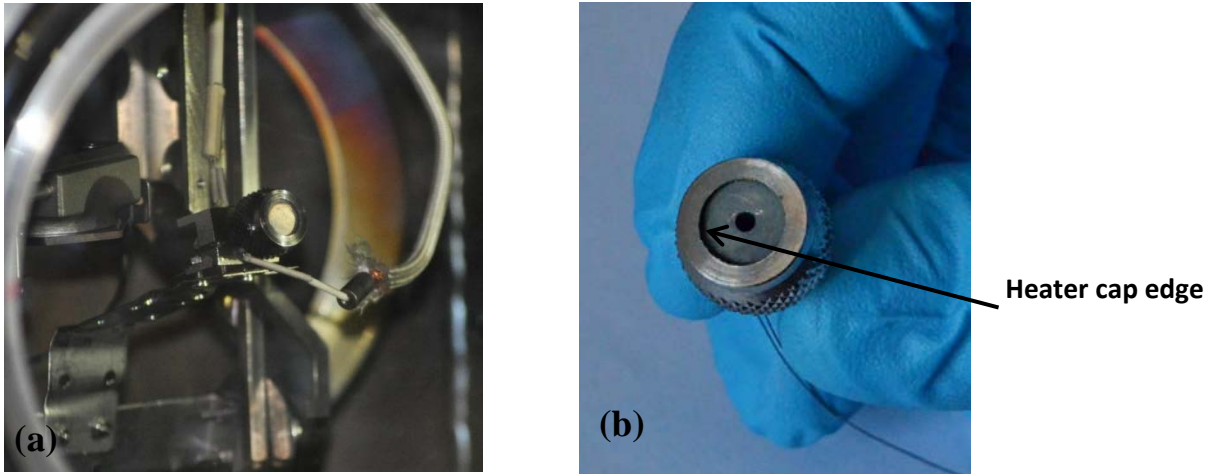


Figure 5.34: A close up view of (a) the sample surface from which evaporation can take place and (b) the heater showing the heater cap edge

Similarly the crystal holder of the deposition monitor masks the quartz crystal so that the evaporant can impede upon a circular surface area with an average diameter of 8.25 mm. This gives a r_s value of 4.125 mm.

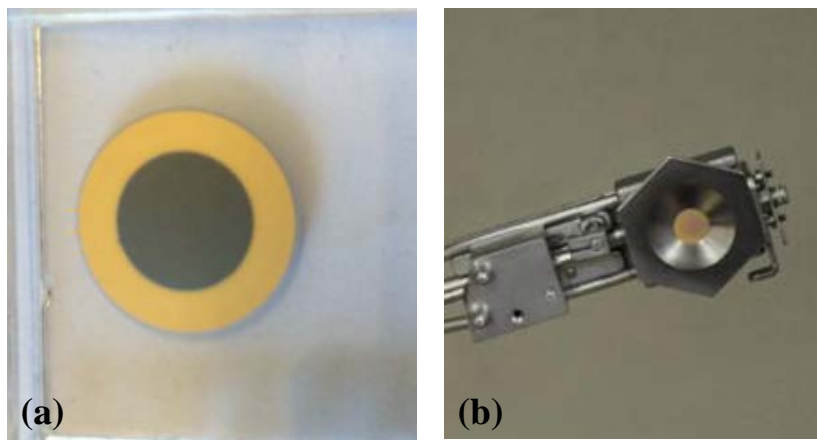


Figure 5.35: A close up view of (a) the gold coated quartz crystal and (b) the crystal holder showing the surface area upon which evaporant impedes on.

Table 5.4 was constructed using these measurements and the Matlab program previously discussed. It shows the fraction of atoms or molecules which evaporated from the sample surface detected by the deposition controller for various n and h values.

Table 5.4: Fraction of particles collected for various n and h values. ($r_e = 3.95$ mm; $r_s = 4.125$ mm)

	$h = 5$ mm	$h = 10$ mm	$h = 15$ mm	$h = 20$ mm
$n = 1$	0.32	0.13	0.07	0.04
$n = 2$	0.42	0.18	0.10	0.06
$n = 3$	0.49	0.23	0.12	0.08

5.4.4 Identification of evaporated species

To detect a specific atomic species the Inficon XTC/3s deposition controller uses various input parameters to determine the deposition rate which corresponds to the measured change in frequency as described in section 5.3.3. While this is satisfactory in a situation where the evaporation/deposition of a pure element is measured, it might not give accurate values in the case where multi component alloys or compounds are used. In such a case the measured deposition rate or evaporation rate might be due to the combined evaporation of two or more components. In addition evaporation may also occur from the surface of the heater used, depending on the material it is manufactured from.

While care was taken when planning this study to choose a binary system where the two components Sb and Cu had vastly different vapour pressures and subsequently evaporation rates for a given temperature (see section 4.2.1) it is still considered important to outline how the system can be utilized to account for multi-component systems where simultaneous evaporation of more than one component takes place.

In the case of a simple system where multicomponent evaporation is not expected such as in the case of this study, it is sufficient to use any number of analytical techniques to ensure that the deposition rate measured by the quartz crystal is in fact due to the evaporation of one element

and one element alone. Figure 5.36a) shows an X-ray Photoelectron Spectroscopy (XPS) spectrum taken using a PHI Versaprobe XPS spectrometer of the surface of a gold coated quartz crystal before using the crystal in the deposition monitor. As expected the spectrum indicates the presence of gold as well as some surface contaminants.

Comparing this spectrum in figure 5.36a) of an unused quartz crystal to the spectrum of a quartz crystal used during an deposition run as shown in figure 5.36b) it can be seen that in addition to the gold and surface contaminant peaks shown in figure 5.36a) the only additional peaks are that of Sb. It is thus reasonable to assume that all the measured evaporation was due to the evaporation of Sb.

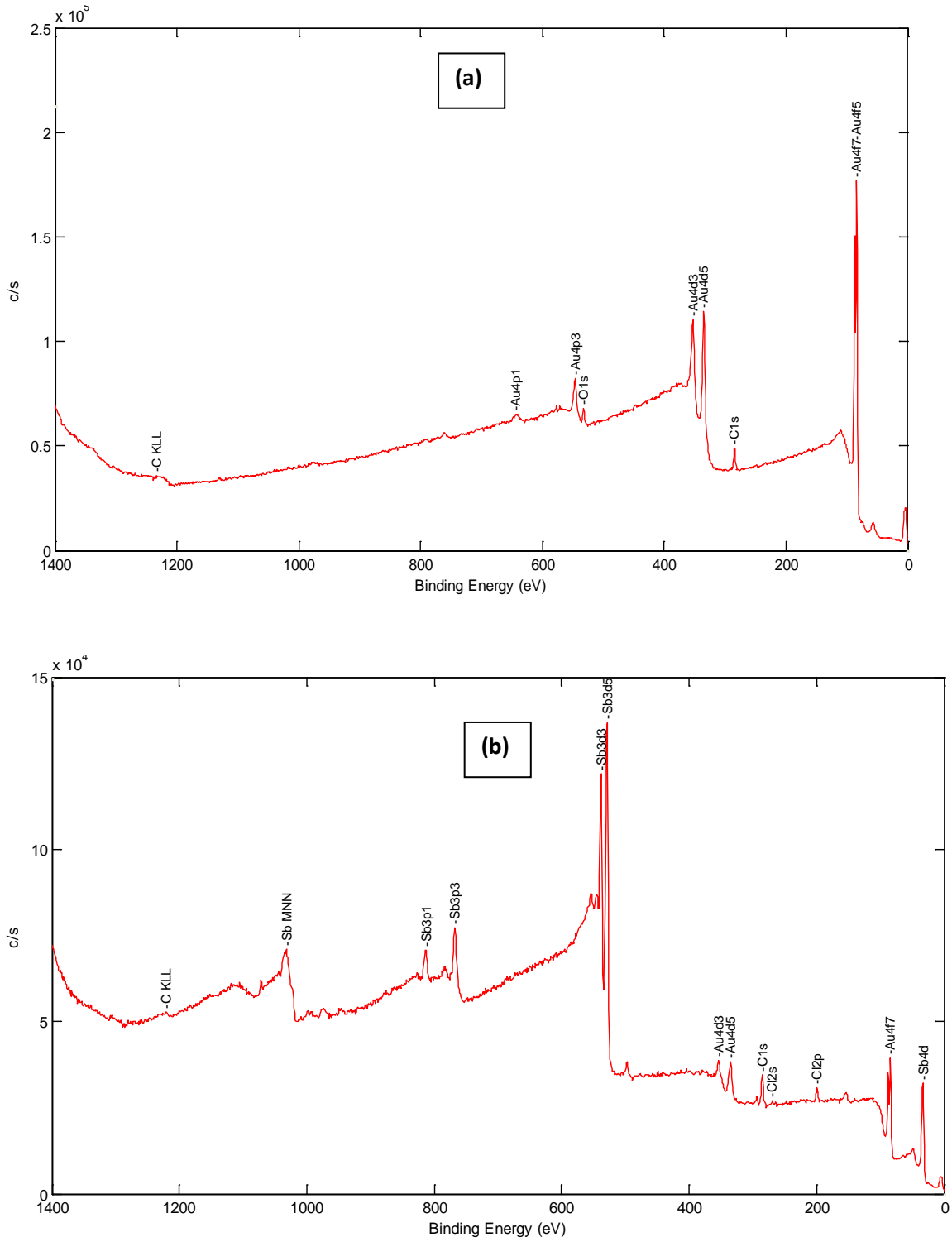


Figure 5.36: XPS spectrum of a gold coated crystal used in the deposition monitor a) before and b) after a deposition run.

Throughout this study each quartz crystal used where analysed with XPS to ensure that all evaporation measured can be attributed to the evaporation of Sb.

If more than one element evaporates a different experimental approach will have to be taken. The individual evaporation rates can still be determined for a specific temperature if a quantitative technique like Interstitial Gas Analysis (IGA) or Glow Discharge Mass Spectrometry (GDMS) is used to determine the relative quantities of each evaporated component on the quartz crystal surface evaporated at that temperature.

5.5 Experimental procedures

5.5.1 Special considerations for sputter cleaning

As mentioned in section 5.3.1 the argon ion gun is used to remove surface contaminants off the sample surface before a measurement is done. In a typical segregation study (Terblans, 2001; Asante, 2005) an ion beam raster size of between 2 mm x 2 mm and 3 mm x 3 mm was used to sputter the surface for between 3 - 4 min until it is sufficiently clean of surface contaminants. While this procedure is perfectly acceptable for a standard segregation measurement it is insufficient in the case where any surface evaporation are measured, the reason being that with the raster sizes commonly used only a portion of the sample surface is cleaned, whereas evaporation will take place from the entire sample surface. Besides the normal concerns associated with the presence of surface contaminants, it is vitally important to ensure that the entire sample surface is free of any Sb from a previous segregation or evaporation run, as any additional Sb on the sample surface will serve as an additional source of Sb available for evaporation besides the Sb segregating from the bulk.

To ensure that the complete sample surface were devoid of Sb the raster size was increased to 8 mm x 8 mm, and because of the lower Ar ion flux, the sputter time was also increased.

To check that the sample surface is indeed free of any contaminants and excess Sb, AES spectra were taken after sputtering at five positions on the sample surface as shown in figure 5.37. These positions are determined by first taking an AES spectrum at the center of the sample surface and then moving the sample stage up, down, left or right as required to obtain an AES spectrum close to the edge of the sample.

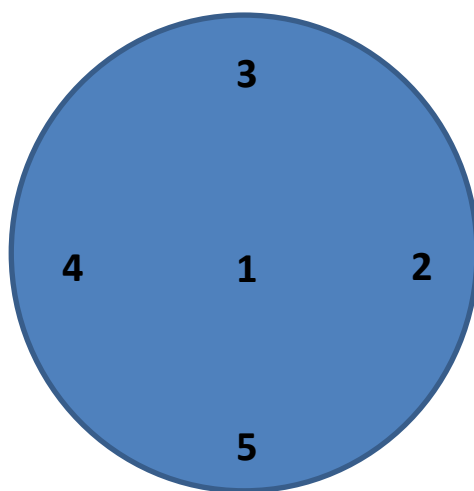


Figure 5.37: Positions for AES spectra to ensure complete clean sample surface.

These positions could be accurately determined by means of not only the micrometers on the fitted manipulator (see section 5.3.2), but also by using the AES spectra itself to note when the electron beam was on the edge of the sample/heater interface. If it were noted that certain areas of the sample required additional sputtering to clean the sample this could then be done.

5.5.2 Segregation measurements

The following steps were followed during segregation measurement:

1. The Cu crystal was mounted in the resistance heater and the vacuum chamber was evacuated to a base pressure of $\leq 5.0 \times 10^{-8}$ torr.
2. The sample was positioned in front of the analyzer.
3. All control units and filaments were switched on, adjusted to the specified parameters and allowed to stabilize for at least one hour before any measurements were taken.
4. The crystal was cleaned of surface contaminants (C, S, O etc) by means of Ar sputtering with the vacuum chamber backfilled with argon to a pressure of 5.0×10^{-5} torr. A modified procedure as described by Asante (2005) and Jafta (2010) was used. The modifications to the procedure were done in view of considerations expressed in section 5.5.1.
 - a) The sample was sputtered at room temperature for 1 hour using 2 keV Ar ions rastered over an area of 8 mm x 8 mm.
 - b) It was then heated to a temperature of 823 K to desorb surface trapped O₂ and sputtered again for 30 minutes.
 - c) The temperature of the sample was increased to 923 K and annealed for 10 minutes without sputtering so as to level off any concentration gradient.
 - d) The crystal was then cooled down to 823 K and sputtered for 30 minutes at that temperature.

Step 4 was repeated six times before a clean surface was obtained.

5. The sample was annealed at 973 K for 12 hours to allow for the vacancy concentration to reach equilibrium and for the vacancies to be distributed homogeneously in the crystal.
6. The sample was allowed to cool down to a temperature of 473 K.
7. The sample surface was once more sputtered for 15 minutes.
8. Immediately after the sputtering the vacuum chamber was pumped down to $\leq 5 \times 10^{-8}$ torr and the segregation measurement was started.
9. Steps 5 - 8 were repeated for each segregation measurement.

5.5.3 Evaporation measurements

Different procedures were followed depending on whether a single crystal sample or pure Sb sample was used:

5.5.3.1 Pure Sb

1. The Sb sample was mounted in the resistance heater and the vacuum chamber was evacuated to a base pressure of $\leq 5 \times 10^{-8}$ torr.
2. The sample was positioned in front of the analyzer.
3. All control units and filaments were switched on, adjusted to the specified parameters and allowed to stabilize for at least one hour before any measurements were taken.
4. The sample surface was cleaned of surface contaminants by means of ion gun sputtering at room temperature for 1 hour using 2 keV Ar ions rastered over an area of 8 mm x 8 mm.

5. Auger spectra were taken at five different locations on the sample surface as explained in section 5.5.2.
6. The sample was immediately moved to a position below the Inficon thickness monitor.
7. The sample temperature was gradually increased in increments. At each measuring temperature the system was allowed to stabilise for 5 minutes, and the thickness monitor observed for an additional 5 minutes taking a measurement every 10 seconds and averaging it over the 5 minute time period to obtain every data point.

5.5.3.2 Cu single crystal –linear heating method

1. Steps 1-7 of section 5.5.2 were performed.
2. The sample was immediately moved to a position below the QCM sensor whilst the vacuum chamber was pumped down to $\leq 5 \times 10^{-8}$ torr.
3. The sample was heated at a linear rate of 0.1K.s^{-1} and a deposition measurement taken every 10 seconds.

5.5.3.3 Cu single crystal – equilibrium surface concentration method

1. Steps 1-7 of section 5.5.2 were performed.
2. The vacuum chamber was pumped down to $\leq 5 \times 10^{-8}$ torr.
3. The sample was heated for a predetermined temperature and time which will ensure a equilibrium surface concentration. The sample was allowed to cool down to room temperature.

4. The sample was then immediately moved to a position below the QCM sensor. The temperature was then gradually increased in increments. At each measuring temperature the system was allowed to stabilise for 5 minutes, and the thickness monitor observed for an additional 5 minutes taking a measurement every 10 seconds and averaging it over the 5 minute time period to obtain a data point.

5.6 Summary

In this chapter the experimental techniques and procedures used during this study were discussed. The doping of Cu crystals with Sb were discussed in regards to evaporation of a predetermined Sb thin films onto the Cu substrates by means of EBPVD, and the subsequent annealing procedure to ensure a homogeneous distribution of solute Sb atoms in the sample. The sample preparation proved challenging with a number of samples failing due to oxidation. A Sb doped Cu(100) sample was prepared successfully.

The modifications made to an AES system to measure evaporation were discussed in detail. This entailed the use of an Inficon XTC/3s deposition controller. The calibration and other considerations of using this device in the AES system are discussed in detail. Particular emphasis is placed on the evaporation geometry between the XTC/3S sensor and the evaporation source used. An assessment of the maximum heating of samples close to the QCM sensor without inducing false readings was made.

Experimental procedures for performing segregation measurements while considering surface evaporation are given.

5.7 References

Asante J.K.O [2005] *Surface segregation of Sn and Sb in the low index planes of Cu*, PhD thesis, University of the Free State.

Askeland D.R. [1998] *The Science and Engineering of Materials*, Stanley Thornes Ltd.

Jafta C.J., RoosW.D., Terblans J.J. and Hugo A.B., [2010] *Instrumentation Science and Technology*, **4** p261.

Crank J. [1975] *The Mathematics of diffusion*, 2nd edition, Elsevier.

Davis L.E., MacDonald N.C., Palmberg P.W., Raich G.E. and Weber R.E. [1976] *Handbook of Auger Electron Spectroscopy*, 2nd Edition, Wiley.

Honig R.E. and Kramer D.A. [1969] *RCA Review* **30** p285.

Jafta C.J. [2010], *Segregation in a Cu bicrystal*, MSc dissertation, University of the Free State.

Joubert H.D. [2010] *A theoretical and experimental investigation on the effect that slow heating and cooling has on the inter-diffusion parameters of Cu/Ni thin films*, PhD thesis, University of the Free State.

Massalski T.B. [1990] *Binary Alloy phase diagrams* Volume 2, ASM International.

Mattox D.M. [2010] *Handbook of Physical Vapor Deposition (PVD) Processing* 2nd Edition, Elsevier.

Ohring M. [2002] *Materials Science of Thin Films* 2nd Edition, Academic Press.

Terblans J.J. [1997] *Die ontwikkeling van 'n sagtewarepakket vir die beheer van en dataverwerking vanaf 'n skandeeraugerelektronmikroskoop*, MSc dissertation, University of the Free State.

Terblans J.J. [2001], *Modellering en eksperimentele ondersoek van Sb – oppervlak segregasie in Cu-enkelkristalle*, PhD thesis, University of the Free State

http://ece.uwaterloo.ca/%7Ebcui/content/NE%20343/Chapter%209%20Thin%20film%20deposition%20_%20II.pptx accessed 3 January 2015.

www.users.wfu.edu/ucerkb/Nan242/L06-Vacuum_Evaporation.pdf accessed 3 January 2015.

Chapter 6

Segregation Results and Discussion

6.1 Introduction

In this chapter the segregation measurements of Sb to the surface of a Cu(100) crystal are shown. These segregation curves are fitted with the existing Modified Darken model. Throughout the segregation measurements the presence of any additional contaminants was also monitored. Figure 6.1 shows an AES spectrum of the Cu(100) surface before and after a LTR was performed (450 K – 950 K).

As can be seen in figure 6.1(a) the surface cleaning procedure as suggested in section 5.5.1 for use during segregation studies where evaporation is to be considered was successful. It should however be kept in mind that due to the lower Ar ion flux impinging on the sample surface when using a 8 mm x 8 mm raster size it will also be more difficult and take longer to obtain a perfectly clean sample surface when compared to the use of a more typical 3 mm x 3 mm raster size.

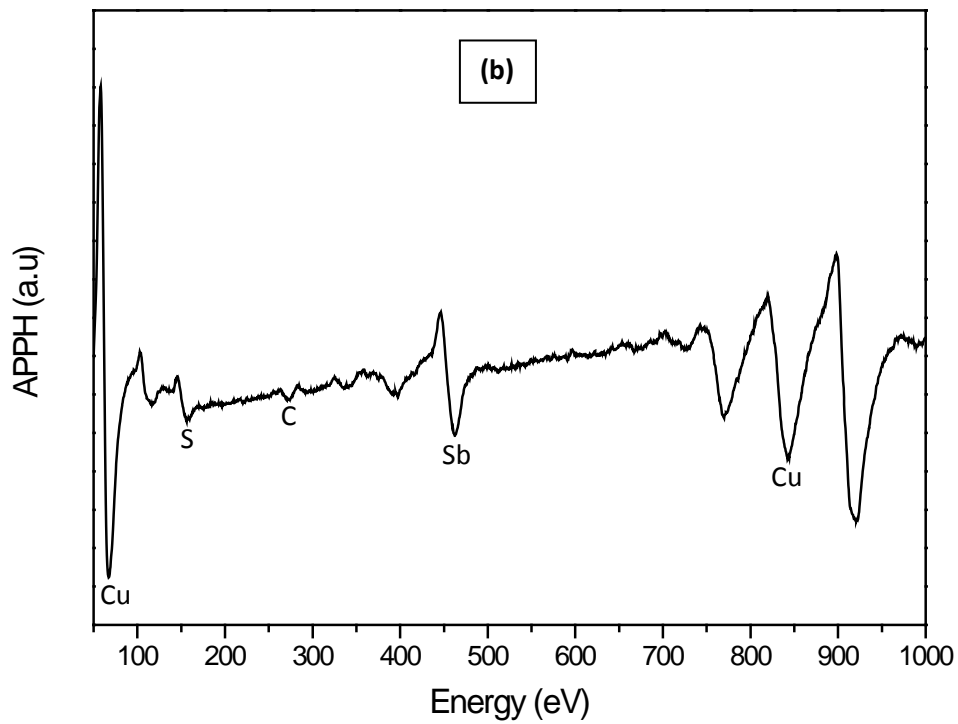
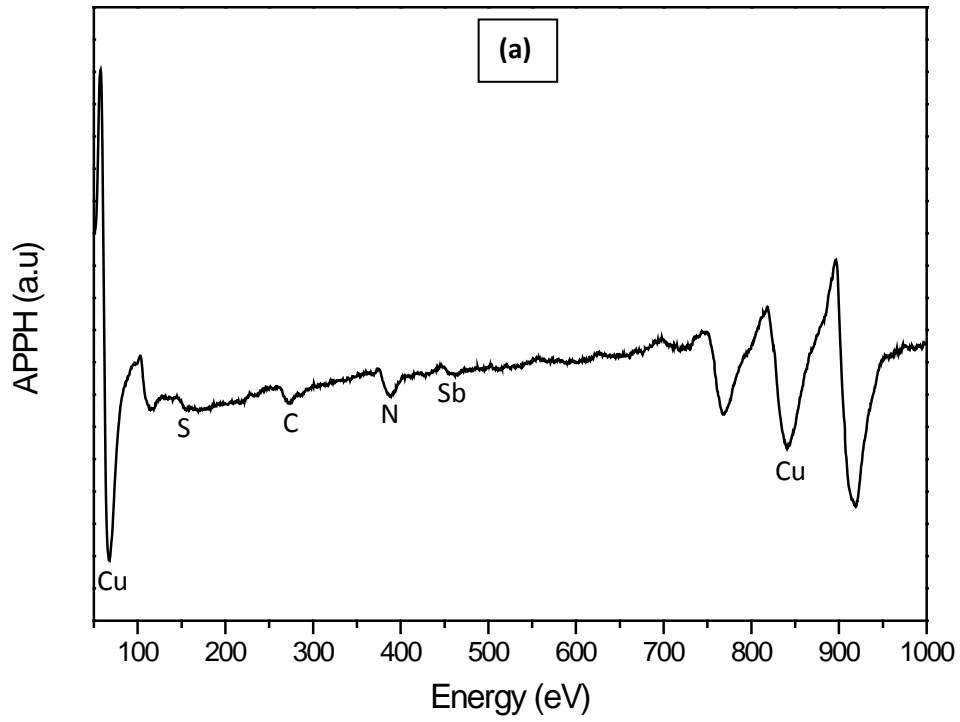


Figure 6.1: AES of Cu(100) surface (a) before and (b) after a linear temperature ramp to 950 K.

When comparing figure 6.1(a) to 6.1(b) it can be noticed that unfortunately the sample contained some traces of contaminants, mostly in the form of S. The effect of these traces of

S is however considered to be minute as no sharp decrease in the equilibrium concentration of Sb was observed during the segregation measurements which would be due to the S displacing the Sb from the surface after maximum surface coverage is reached (Jafta, 2010). Some decreases in the maximum Sb concentration were observed above 930 K which might indicate that any presence of S contaminant will only start to influence interactions on the crystal surface at this high temperature. In this study, segregation parameters will be compared that were obtained by modelling experimental data with and without the influence of surface evaporation taken into account. The slight influence that any presence of S might have is considered of secondary importance and has been neglected. The presence of C can possibly be attributed to the rotary vane pump used on the AES system (Holton, 2012).

6.2 AES segregation data analysis procedure

The following steps were used to obtain segregation profiles from the measured AES data, to fit the Modified Darken model to the segregation profiles and subsequently to extract the relevant segregation parameters:

1. The Auger peak to peak height (APPH) is extracted from the AES spectra obtained during the LTR.
2. The AES data was quantified with Low Energy Electron Diffraction (LEED) data obtained from literature to determine the maximum surface coverage of Sb for a specific orientation of Cu substrate. It is known from literature that Sb forms a (2x2) overlayer structure on Cu(100) (Higashi et al., 2008). If one considers the unit cell of the overlayer of Sb, the ratio of the segregated atoms to that of the Cu substrate is 1:4. The maximum coverage is therefore 25%.
3. The kinetic part of the segregation profile was fitted with Fick's semi-infinite diffusion model to extract the pre-exponential factor D_0 and the activation energy E .

4. The equilibrium part of the segregation parameter was fitted with the Bragg-Williams equation to extract the segregation energy ΔG and interaction parameter Ω . The Bragg-Williams equation was used because the Langmuir-McLean equation cannot account for the interaction parameter Ω between Cu and Sb.
5. The parameters extracted in steps 3 and 4 are used as starting parameters for the Modified Darken fits.
6. The segregation data is then fitted with the Modified Darken model, from which the pre-exponential factor, D_0 , the activation energy E , the segregation energy ΔG and the interaction parameter Ω are obtained.

6.3 Fit using Fick's Integral equation

It is known that the low temperature region of the segregation profile is not sensitive to the segregation energy ΔG and interaction parameter Ω (Du Plessis, 1990). This low temperature region can thus be modelled using Fick's semi-infinite diffusion model as discussed in Chapter 3 section 3.2.1

$$X^S = X^B \left[1 + \frac{2}{d} \sqrt{\frac{Dt}{\pi}} \right]. \quad (6.1)$$

Using the diffusion equation $D = D_0 \exp\left(\frac{-E}{RT}\right)$, the enrichment factor introduced by Viljoen and Du Plessis (1999), namely $\beta = \frac{c^S - c^B}{c^B} = \frac{X^S - X^B}{X^B}$ and the relation between temperature and time t in an LTR, namely $T = T_0 + \alpha_T t$, the Fick Integral equation

$$\frac{\beta^2}{2} = \frac{2 D_0}{\pi \alpha_T} \int_{T_0}^{T_E} \exp\left(\frac{-E}{RT}\right) dT \quad (6.2)$$

can be derived (Roos and Asante, 2007) where α_T is the heating rate and T_0 is the starting temperature used during the LTR. Equation 6.2 can be solved numerically and yields the pre-exponential factor D_0 and the activation energy E . This was done for the segregation profile of a Cu(100) crystal using software developed by W.D. Roos (see figure 6.2). From this fit the starting parameters of the pre-exponential factor D_0 and the activation energy E for use in the Modified Darken model were extracted as shown in table 6.1. The input parameters used during the fit include the bulk concentration C_{Sb}^B of the sample used (0.05 at%) as shown in table 5.2 and the interplanar spacing $d = 1.81 \text{ \AA}$ for the (100) planes of Cu (Viljoen, 1995).

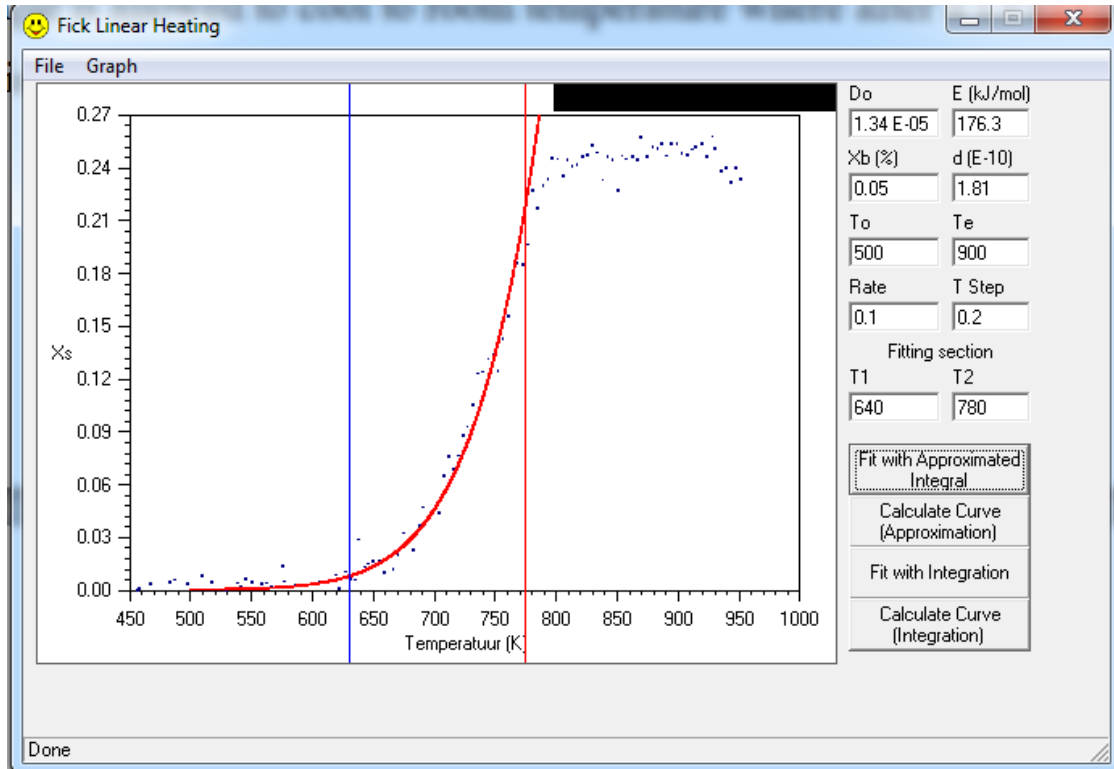


Figure 6.2: Kinetic region of measured Sb segregation for a Cu(100) LTR at a constant heating rate of $0.1 \text{ K}\cdot\text{s}^{-1}$ with the fitted Fick Integral equation.

Table 6.1: Segregation parameters extracted from the Fick Integral model.

D_0 ($\text{m}^2.\text{s}^{-1}$)	1.34×10^{-5}
E ($\text{kJ}.\text{mol}^{-1}$)	176.3

6.4 The Bragg-Williams fit

From the equilibrium section of the segregation profile, the segregation energy ΔG and interaction parameter Ω were extracted using the Bragg-Williams equation

$$\frac{X_1^s}{1 - X_1^s} = \frac{X_1^B}{1 - X_1^B} \exp \left[\frac{\Delta G + 2\Omega_{12}(X_1^s - X_1^B)}{RT} \right] \quad (6.3)$$

(see Chapter 3 section 3.3 for a complete description). Later these values were used as starting parameters for the Modified Darken model. The simulated Bragg-Williams fit is shown in figure 6.3 and the extracted parameters which were used as starting parameters for the Modified Darken model are shown in table 6.2.

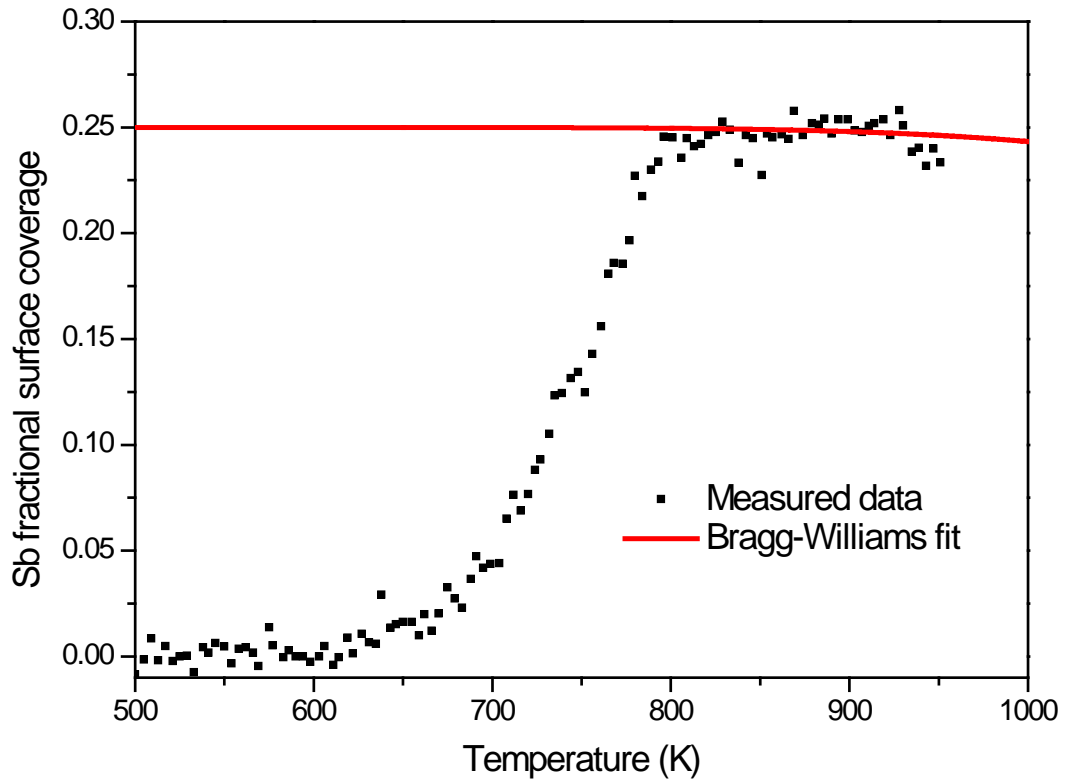


Figure 6.3: Equilibrium region of measured Sb segregation for a Cu (100) LTR at a constant heating rate of 0.1 K.s^{-1} with the fitted Bragg-Williams equation extended to low temperatures.

Table 6.2: Segregation parameters extracted from the Bragg-Williams equation fit for Sb on a Cu(100) surface at an equilibrium condition.

$\Delta G \text{ (kJ. mol}^{-1}\text{)}$	-95
$\Omega \text{ (kJ. mol}^{-1}\text{)}$	-1

6.5 The Modified Darken Fit

Using the starting values obtained from the Fick Integral and Bragg-Williams fits in sections 6.3 and 6.4, a reasonable fit was obtained with the Modified Darken model software developed by J.J. Terblans. The simulated Modified Darken fit is shown in figure 6.4 and the extracted segregation parameters are shown in table 6.3.

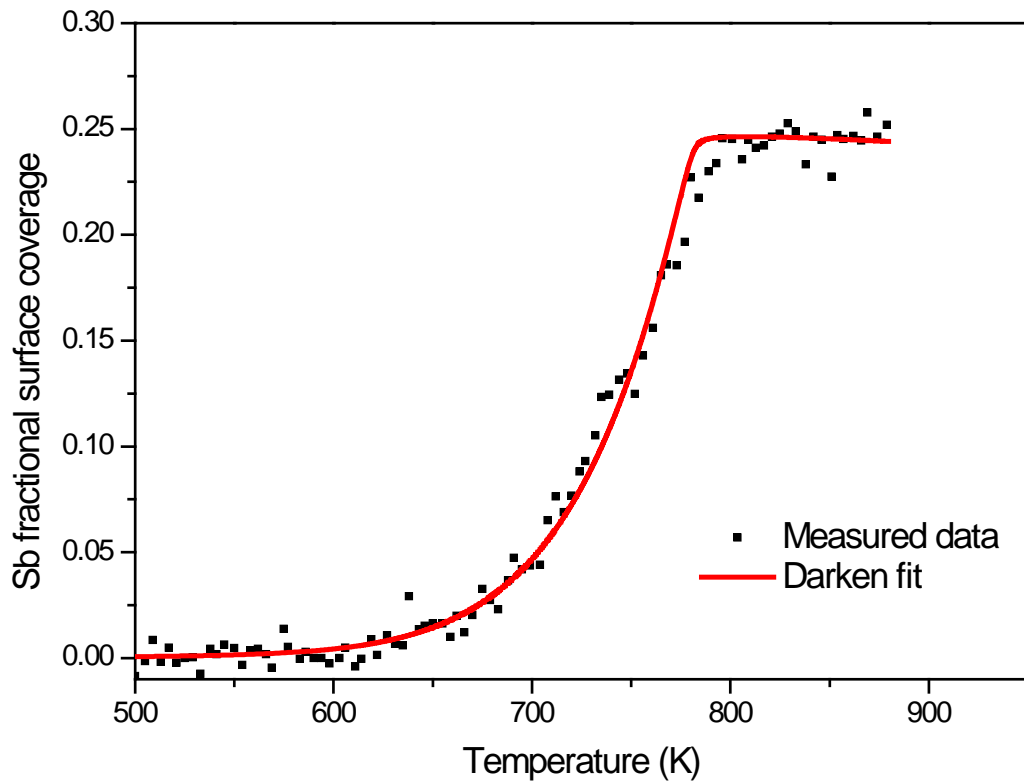


Figure 6.4: Kinetic and equilibrium regions of the measured Sb segregation for a Cu(100) LTR at a constant heating rate of 0.1 K.s^{-1} fitted with the Modified Darken model.

Table 6.3: Segregation parameters extracted from the Modified Darken model.

ΔG (kJ.mol^{-1})	-89 ± 5
Ω (kJ.mol^{-1})	-3 ± 1
D_0 ($\text{m}^2.\text{s}^{-1}$)	$(1.5 \pm 0.2) \times 10^{-5}$
E (kJ.mol^{-1})	177.0 ± 1

A comparison of the starting values obtained for the segregation parameters ΔG , Ω , D_0 and E using the Fick Integral and Bragg-Williams models to the final segregation parameters obtained using the Modified Darken model is shown in table 6.4.

Table 6.4: A comparison of segregation parameters obtained using the Fick Integral, Bragg-Williams and Modified Darken models.

	Starting	Final Modified Darken
ΔG (kJ.mol ⁻¹)	-95	-89 ± 5
Ω (kJ.mol ⁻¹)	-1	-3 ± 1
D_0 (m ² .s ⁻¹)	1.34x10 ⁻⁵	(1.5 ± 0.2) x10 ⁻⁵
E (kJ.mol ⁻¹)	176.3	177.0 ± 1

The values for the pre-exponential factor D_0 and the activation energy E obtained with the Fick Integral model, compares closely to the values for these two segregation parameters obtained using the Modified Darken model. Some dissimilarity is noticeable in the case of the values obtained for the segregation energy ΔG and the interaction parameter Ω from the Bragg-Williams fit when compared to the values obtained using the Modified Darken model.

A more definitive set of values for ΔG and Ω could have been obtained using the Bragg-Williams equation had a negative linear temperature ramp (NLTR) been performed on the sample. In this procedure a standard positive LTR ramp as performed during this study is immediately followed by the linear cooling of the sample at equilibrium. This extends and better defines the equilibrium region of the available data points which allows a more precise Bragg-Williams fit (Asante, 2005). In this study the Bragg-Williams equation was merely used to obtain starting values for the Modified Darken model. The obtained segregation parameters using the Bragg-Williams equation were accurate enough to accomplish this goal.

A substantial body of work has been completed at the Department of Physics at the University of the Free State regarding the segregation of Sb from Cu, not only in binary systems but also in ternary systems (Asante, 2000; Terblans, 2001; Jafta, 2010). Special emphasis had been placed during these studies regarding the role of crystal orientation on the

segregation process. Even so, as far as could be ascertained the results reported in this chapter are the first in-house published segregation parameter values for the Cu(100) orientation and are therefore of importance to complement these studies. A comparison of these results with previous in-house results for the other low index planes of CuSb binary systems are shown in table 6.5. All researchers used the LTR method in combination with the Modified Darken model, with the exception of the values given from the *CRC Handbook 63rd edition F-53* which provide Sb¹²⁴ tracer diffusion data.

Table 6.5: A comparison of segregation and diffusion parameters for the CuSb binary system.

Reference	Heating Rate K.s ⁻¹	Bulk Concentration (at%)	Crystal Orientation	ΔG (kJ.mol ⁻¹)	Ω (kJ.mol ⁻¹)	D_0 (m ² .s ⁻¹)	E (kJ.mol ⁻¹)
Current work	0.1	0.05	(100)	-89	-3	1.5x10⁻⁵	177
Terblans, 2001	0.05	0.0877	(110)	-82.75	—	1.13x10 ⁻⁶	156.75
Jafta, 2010	0.075	0.1	(110)	-90	-5	2.3x10 ⁻⁵	197
Jafta, 2010	0.1	0.1	(110)	-90	-5	2.0x10 ⁻⁵	194
Terblans, 2001	0.1	0.0877	(110)	-89.37	—	1.10x10 ⁻⁴	180.83
Terblans, 2001	0.2	0.0877	(110)	-76.80	—	1.09x10 ⁻⁶	153.05
Terblans, 2001	0.05	0.0816	(111)	-80.70	—	3.49x10 ⁻⁵	183.52
Jafta, 2010	0.075	0.1	(111)	-89	-3	1.1x10 ⁻³	233
Jafta, 2010	0.1	0.1	(111)	-88	-3	1.1x10 ⁻³	232
Terblans, 2001	0.1	0.0816	(111)	-87.70	—	1.09x10 ⁻⁴	189.72
Terblans, 2001	0.2	0.0816	(111)	-82.30	—	5.09x10 ⁻⁵	183.18
CRC	—	—	Single	—	—	3.4x10 ⁻⁵	175.73

The values obtained during this study for the various segregation parameters for the Cu(100) orientation show good agreement with the values obtained in previous studies regarding the CuSb binary system in general as shown in table 6.5. This is especially true if the wide variances of values obtained are considered. The values are however difficult to directly

compare when considering the differences in heating rate, bulk concentrations and experimental conditions used to obtain these results. In addition some of the studies did not consider the influence of the interaction parameter Ω . The excellent agreement between the values for the pre-exponential function D_0 and the activation energy E obtained in this study and obtained from *CRC Handbook 63rd edition F-53* should be noted. Regrettably the single crystal orientation used to obtain the radioactive tracer diffusion data is not specified in the reference.

6.6 Summary

In this chapter the experimental segregation measurements of Sb to the surface of a Cu(100) crystal are presented. The segregation profile was fitted with the existing Modified Darken model using starting values for the various segregation parameters obtained by first fitting the experimental data with the Fick Integral equation and the Bragg-Williams equation. Although the technique used is the same as in some previous studies the results presented are the first numerical values for the segregation parameters of Sb to a Cu(100) surface and are therefore of particular importance to complement previous studies of Sb segregation to other Cu surfaces. These values compare favourably to previous results reported in the literature for other orientations of Cu. The results illustrate that experimental segregation data can be successfully fitted with the Modified Darken model to extract segregation parameters as has been done in the past. Despite a good fit between experimental data and the Modified Darken model, the values of the extracted segregation parameters can be questioned because the current model neglects surface evaporation. In chapter 8 the results of this chapter are compared to those of the updated Modified Darken model including evaporation developed in this study.

6.7 References

Asante J.K.O. [2000] *The determination of ternary segregation parameters using a linear heating method*, MSc dissertation, University of the Orange Free State.

Asante J.K.O. [2005] *Surface segregation of Sn and Sb in the low index planes of Cu*, PhD thesis, University of the Free State.

Du Plessis J. [1990] *Solid State Phenomena*, **11** p76.

Higashi S., Tochiara H., Shneerson V.L. and Saldin D.K. [2008] *Surface Science* **602** p2473.

Holton R. [2012] *Personal correspondence*, Vacutec South Africa.

Jafta C.J. [2010], *Segregation in a Cu bicrystal*, MSc dissertation, University of the Free State.

Roos W.D. and Asante J.K.O. [2007] *Surface Review and Letters* **14(4)** p681-685.

Terblans J.J. [2001] *Modellering en eksperimentele ondersoek van Sb – oppervlak segregasie in Cu-enkelkristalle*, PhD thesis, University of the Free State.

Viljoen E. [1995] *Lineêre verhittingstudies van oppervlaksegregasie in binêre allooie*, PhD thesis, University of the Orange Free State.

Viljoen E.C. and Du Plessis J. [1999] *Surface Science* **431** p128.

Weast R.C. [1982] *CRC Handbook 63th edition*, CRC Press.

Chapter 7

Evaporation Results

7.1 Introduction

The results in this chapter includes evaporation measurements done on pure Sb as well as evaporation experiments performed on the Sb doped Cu(100) crystal. These experimental results are used to test the procedure and equipment developed in chapter 5 as well as to verify the theory presented in Chapter 4 which deals with evaporation of pure elements. The results are also used to test the approach used in contemporary segregation/evaporation models to assume that the evaporation behaviour of the segregant is similar to that of the pure element which was also dealt with in Chapter 4.

7.2 Evaporation of pure Sb

The evaporation of pure Sb was measured according to the procedure described in Chapter 5. Similar to the comments made in Chapter 6 the surface cleaning procedure, as suggested in Chapter 5 section 5.5.1 for use during segregation studies where evaporation is to be considered was successful when applied to the surface of the Sb sample used during this study. It should however be kept in mind that due to the lower Ar ion flux impinging on the sample surface when using an ion beam raster size of 8 mm x 8 mm it will also be more difficult and take longer to obtain a perfectly clean sample surface when compared to the use of a more typical 3 mm x 3 mm raster size. Figure 7.1 shows a representative AES spectrum of the Sb sample surface before and after sputter cleaning.

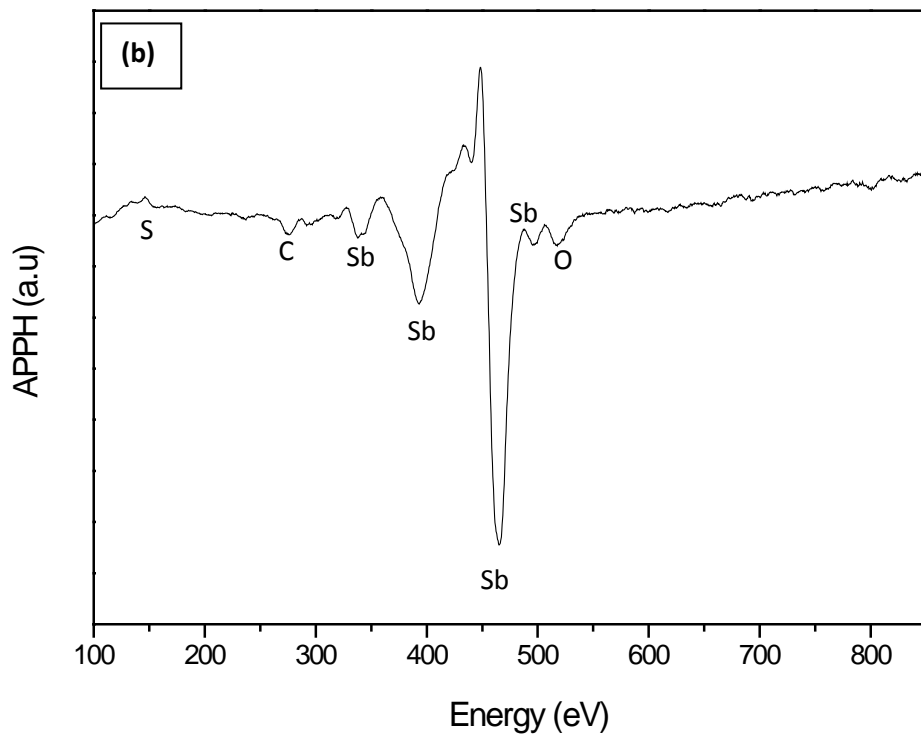
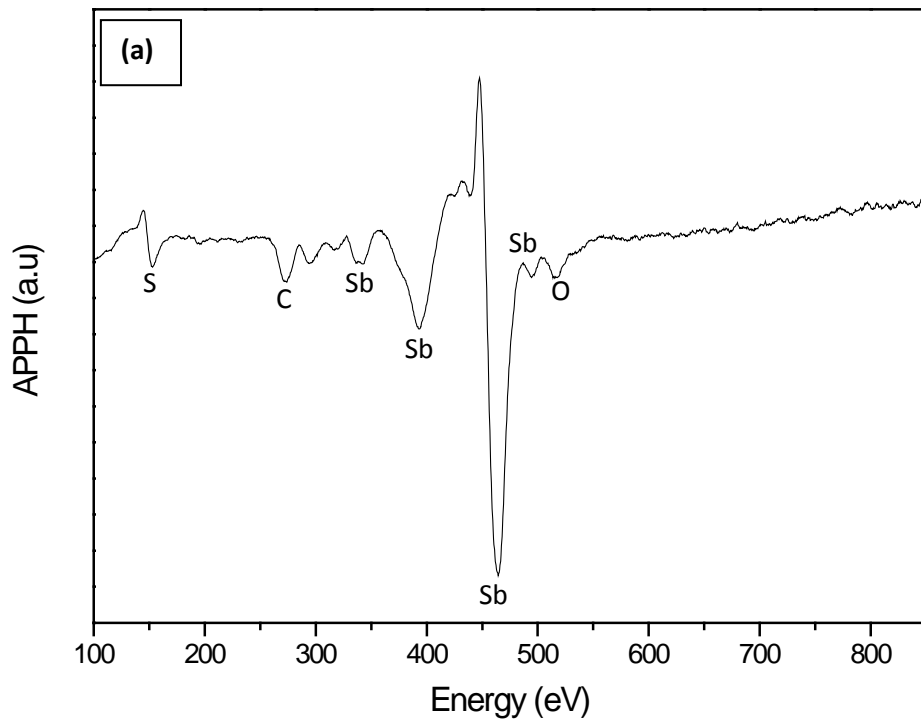


Figure 7.1: AES spectrum of pure Sb sample surface a) before and b) after sputter cleaning.

Figure 7.2 shows a typical deposition rate ($\text{\AA}\cdot\text{s}^{-1}$) vs the source or sample surface temperature (K) graph obtained during an evaporation run when the sample was a distance $h = 1.5$ cm from the gold coated crystal. It should be noted that the vertical-axis shows the measurement from the QCM.

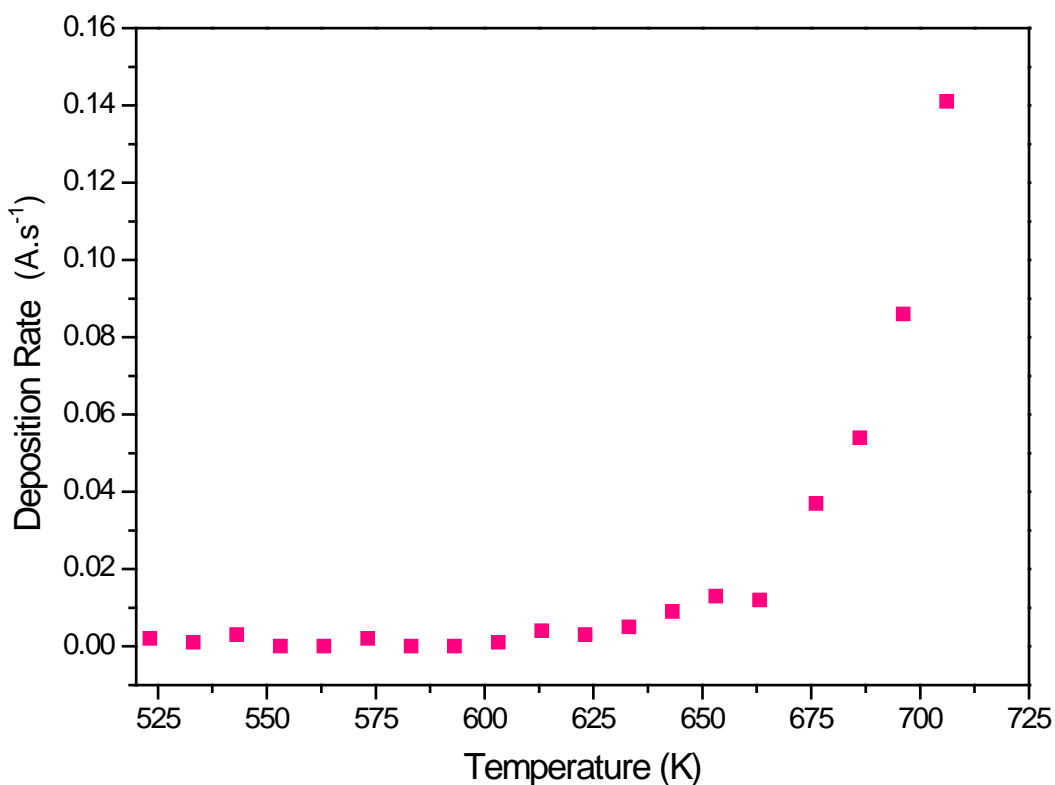


Figure 7.2: Typical results from a pure Sb evaporation run showing the deposition rate as monitored by the QCM.

The graph in figure 7.2 shows a typical profile from an evaporation run, with the deposition rate (which is linked to the evaporation rate from the sample with the geometry of the system) increasing with an increase of source temperature. The procedure of first ensuring that the sample surface is free of surface contaminants, and then performing an evaporation run were repeated a number of times. These results are shown in figure 7.3a) with the deposition rate plotted on a logarithmic scale in figure 7.3b).

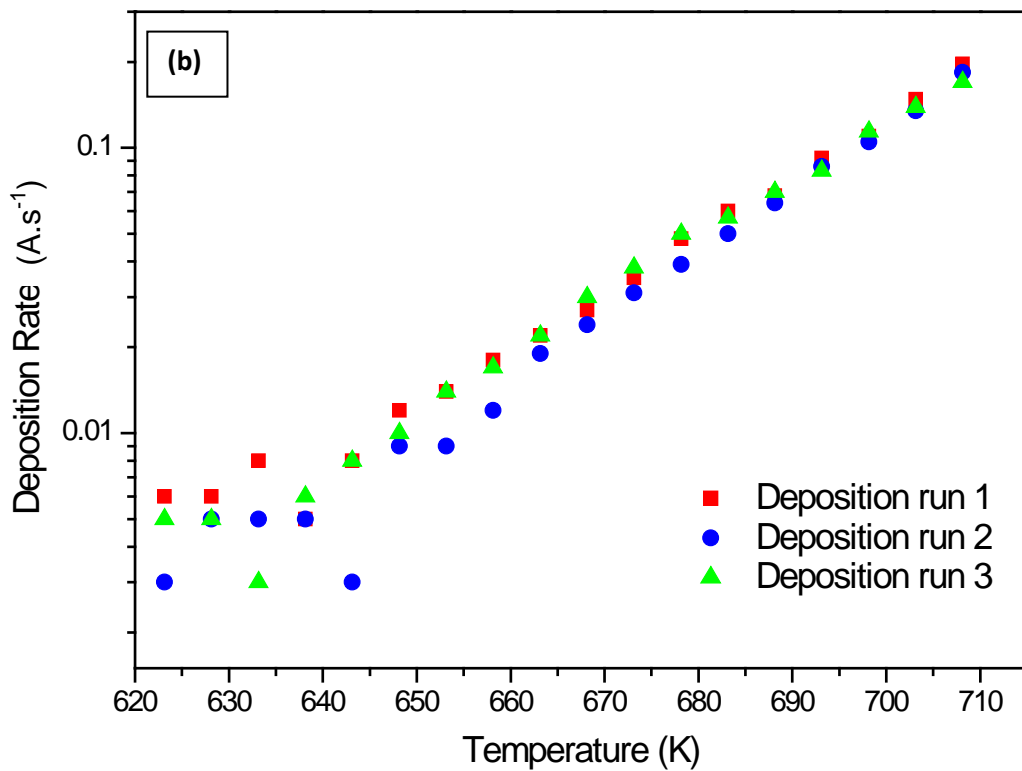
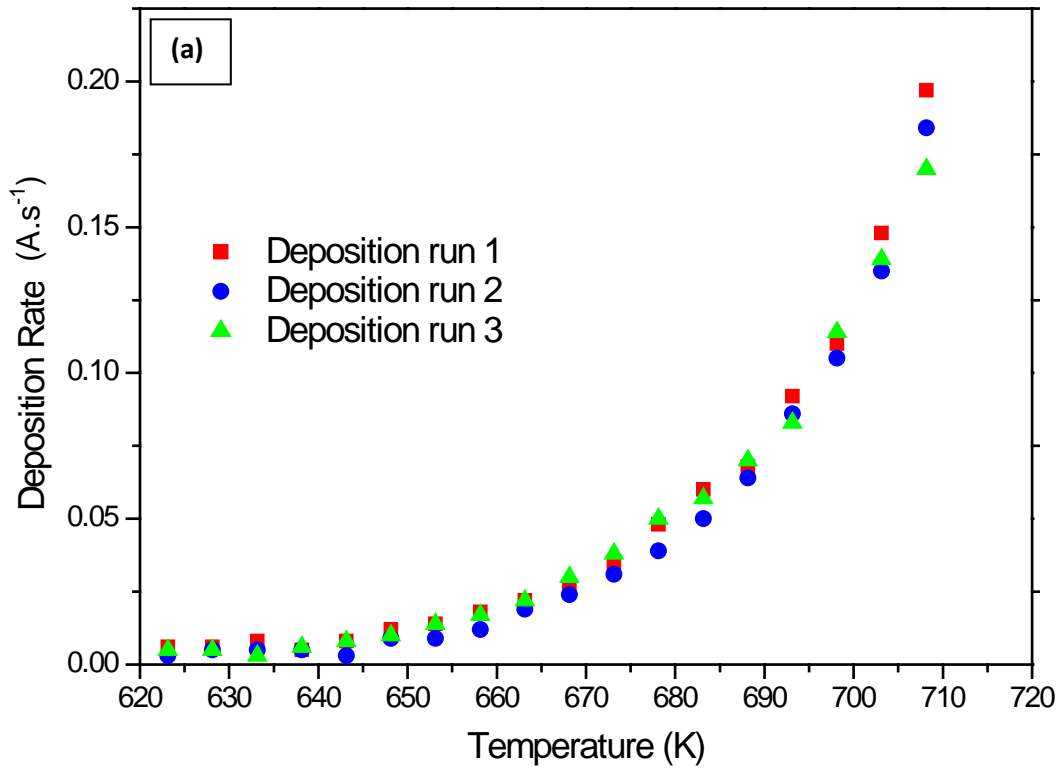


Figure 7.3: Pure Sb evaporation runs showing the deposition rate on a) linear and b) logarithmic scale as monitored by the QCM.

It can be seen in figure 7.3b) that for temperatures below approximately 650 K the reproducibility of the results is poor. This can be attributed to the fact that the deposition rates, as measured by the QCM at these relatively low temperatures, is small enough to fall in the noise/resolution limit of the Inficon XTC/3s system. At higher temperatures the reproducibility of results substantially increases.

Assuming that the values for the deposition rate as shown in figure 7.3b) for temperatures below approximately 650 K can be ignored, average values for the deposition rate on the QCM for Sb as a function of temperature can be obtained. These average values are shown in figure 7.4. as a line plot on the original data.

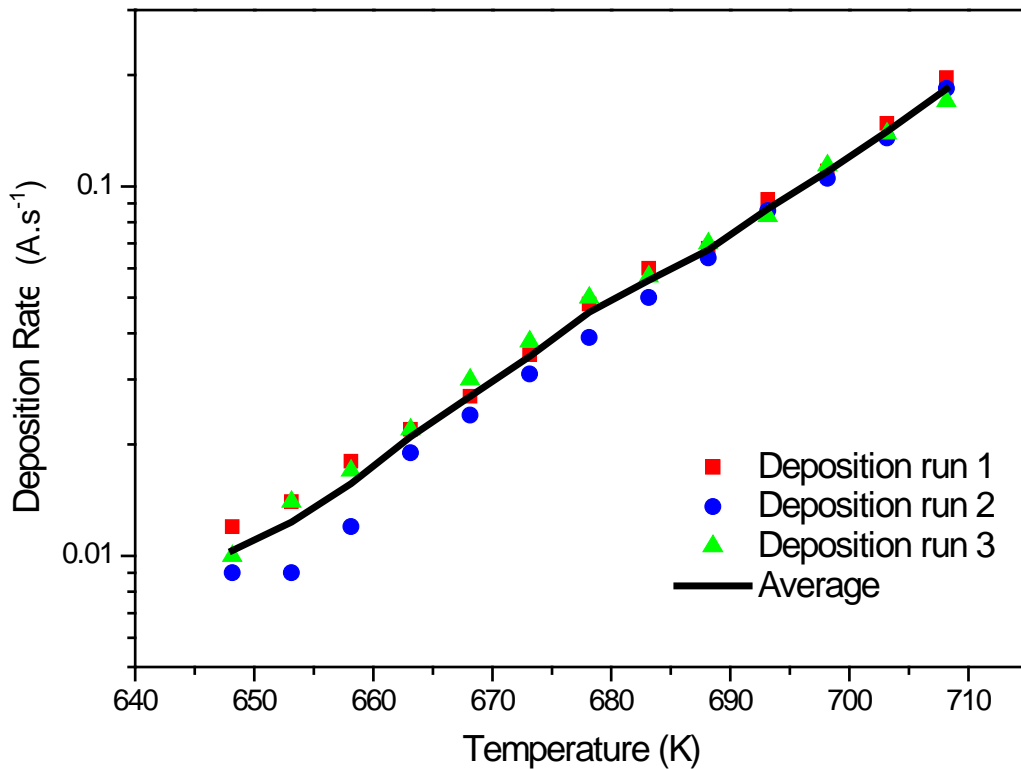


Figure 7.4: Average deposition rate measured as a function of source temperature for an Sb sample a distance $h = 1.5$ cm from the QCM sensor.

Using this average deposition rate, and the geometry between the sample and QCM as discussed in Chapter 5 section 5.4.3 these values can be related to the evaporation flux from the sample surface in terms of mass or number of molecules evaporated. This is done by using the surface area of the quartz crystal (0.53 cm^2) which is not masked by the crystal holder, to determine the volume of 1 \AA layer of material deposited on to the quartz crystal. As the density of the deposited material is known, the mass of 1 \AA of deposited material can be determined. If the mass of such a deposited layer is known the atomic mass of the element can be used to determine the number of atoms in such a deposited layer and subsequently the number of molecules deposited. These values can now be multiplied with the actual measured deposition rate to obtain the deposition rate either in terms of mass or particles whether atoms or molecules. The geometry between the sample and QCM as discussed in chapter 5 section 5.4.3 can then be used to translate these deposition values to evaporation values from the sample surface.

The theoretical evaporation rate shown in figure 7.5, is calculated using equation 4.15 (with the vapour pressure calculated from equation 4.8) in chapter 4. This evaporation flux ($\text{molecules.cm}^{-2}.\text{s}^{-1}$) is then multiplied by the surface area of the sample (0.49 cm^2) used during this study to obtain the evaporation rate of Sb atoms from the sample surface.

The assumption is made that the evaporation is that of the antimony molecule Sb_2 (Dushman, 1966).

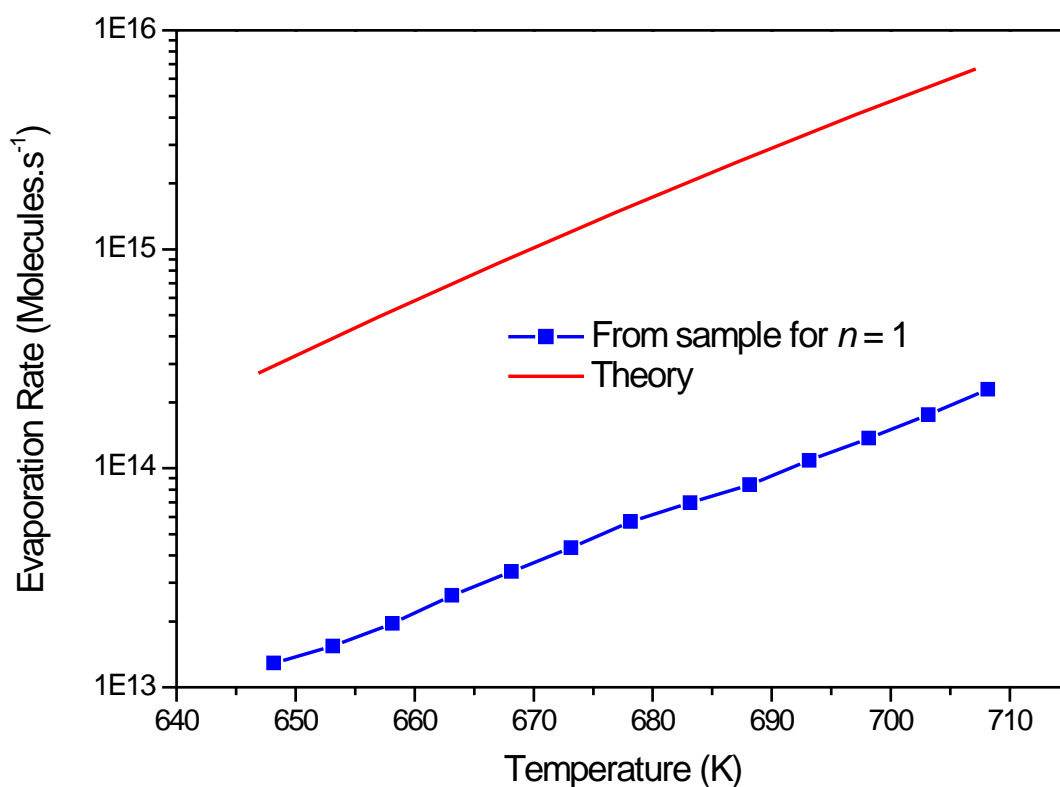


Figure 7.5: Average evaporation rate measured as a function of temperature for the Sb sample a distance $h = 1.5$ cm from the gold coated crystal compared to the theoretical evaporation rate of Sb_2 .

In figure 7.5 the qualitative evaporation behaviour of the pure Sb sample is similar to the theoretical behaviour discussed in chapter 4. There is however a quantitative discrepancy between the measured and calculated results, with the measured evaporation rate being roughly 0.05 of the values expected theoretically. A number of factors or combinations of these factors might explain this discrepancy. Some of these factors are:

1. The source geometry might be misunderstood (Mattox, 2010).
2. Collisions associated with the evaporating particles might affect the evaporation geometry (Mattox, 2010).

3. The QCM calibration might not be linear with temperature.
4. The evaporation coefficient α is not equal to unity. For example, Rosenblatt *et al.* (1966) also found Sb evaporation to be significantly less than expected theoretically, with an evaporation coefficient of $\alpha = 0.2$. However, they assumed Sb evaporated as Sb_4 molecules. An even lower evaporation coefficient of $\alpha = 0.1$ was predicted by L'vov and Novichickhin (1997) based on evaporation of equal numbers of Sb_2 and Sb_4 molecules.
5. The sticking factor of Sb onto the gold coated crystal and onto Sb itself which is temperature dependant (Angelico *et al.*, 2014).
6. The microstructure of the polycrystalline Sb sample used might influence the evaporation rate (Hirth and Pound, 1957).
7. Surface impurities are present which influences the evaporation rate (Pound, 1972).

Many of these factors as pertain to Sb have been largely left unstudied according to the literature (Angelico *et al.*, 2014).

As an example of how any one of these factors might influence the evaporation rate of Sb, four evaporation runs were performed while omitting the sputter cleaning step between each experimental run. This allowed a build up of surface contaminants on the surface, especially contaminants which might segregate to the surface during the continued heating of the sample during the various evaporation runs. The results of these measurements are shown in figure 7.6. As can be seen, with each additional evaporation run performed on the sample, the deposition rate as measured by the QCM and by extension the evaporation rate from the sample surface decreases. This is attributed to the influence of impurity build up on the surface. An AES spectrum (figure 7.7) taken after the fourth consecutive experimental run shows a large concentration of S on the Sb sample surface. This hints at a probable segregation of S from the bulk of the Sb sample to the surface decreasing the evaporation rate.

It should be noted that the measurements shown in figure 7.6 were performed by linearly heating the sample at a heating rate of 0.1 K.s^{-1} and taking a deposition rate measurement with 5 K temperature intervals. This was done in order to minimize the possibility of excessively contaminating the vacuum chamber with Sb due to the higher temperatures used and by extension the increased amounts of Sb that would be deposited in the vacuum chamber. The drastic increase in the evaporation rate of Sb, due to the higher temperatures used, can be seen by comparing figure 7.6 with figure 7.2.

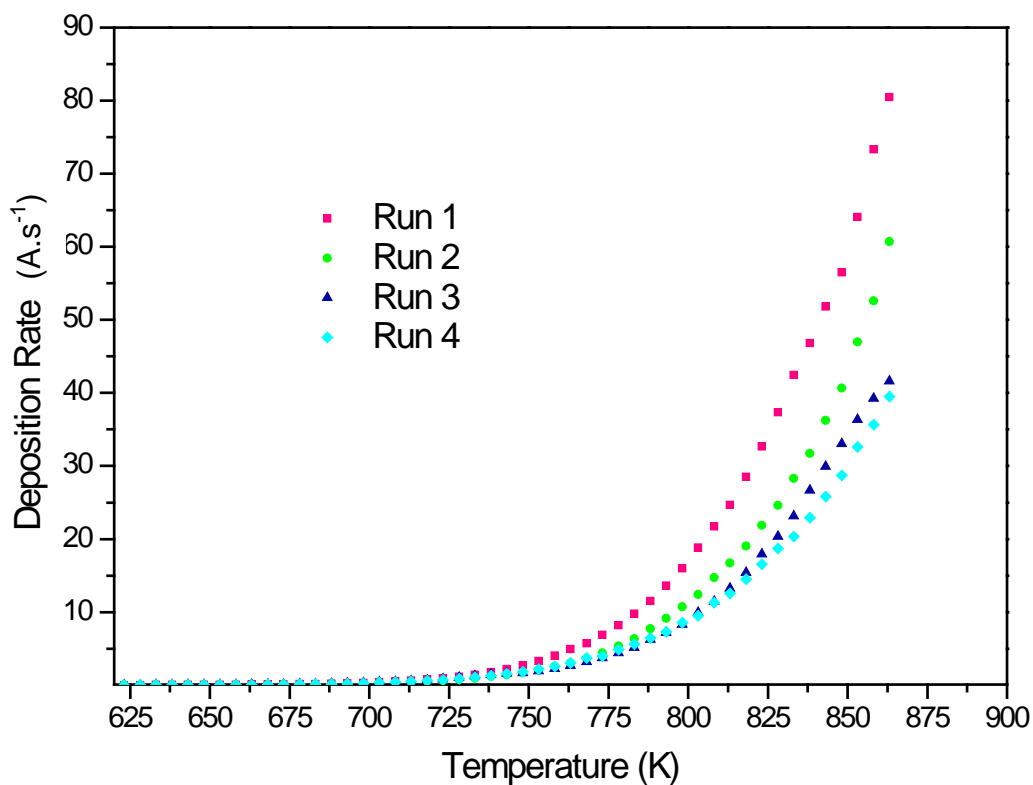


Figure 7.6: Sb evaporation measurements without sputter cleaning the evaporation source between runs.

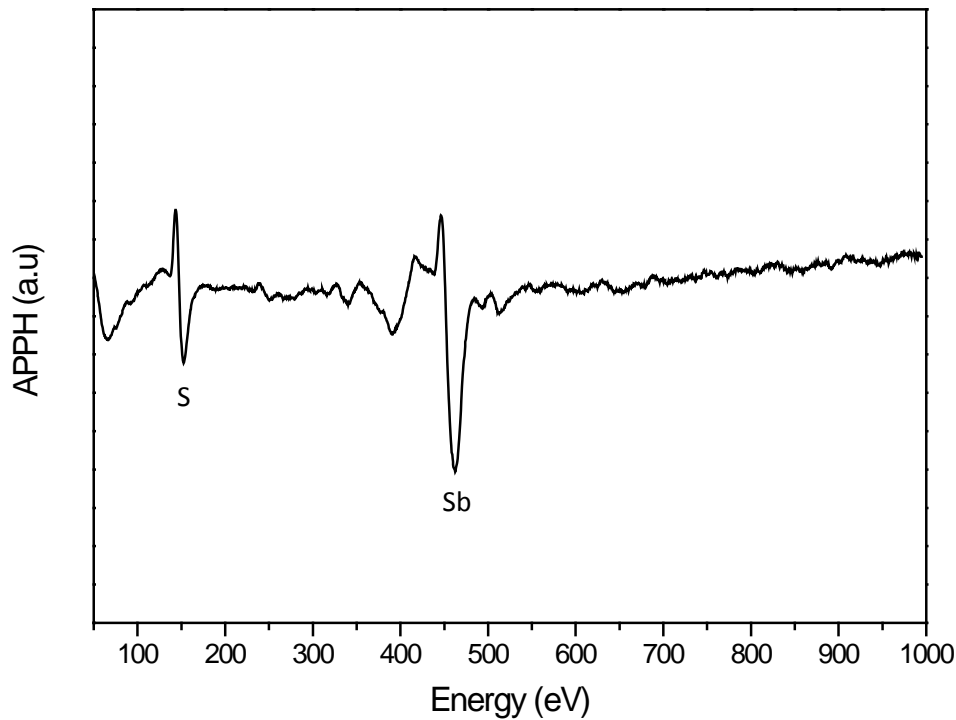


Figure 7.7: An AES spectrum of the pure Sb surface after four evaporation runs, showing high concentrations of S contamination on the surface.

7.3 Evaporation of Sb from doped Cu(100) crystal

An attempt was made to measure the evaporation flux of Sb from the surface of a Cu(100) crystal during a LTR following the procedure given in Chapter 5 section 5.5.3.2. The distance h between the sample surface and the QCM sensor, was varied between 0.5 - 1.5 cm. Numerous attempts were made, but in none of the experimental runs could any definitive measurement of the evaporation flux of Sb from the sample surface be obtained. Since the maximum evaporation flux for a given temperature range will occur when the surface concentration of Sb is at its highest i.e. when the surface is at the equilibrium segregation condition the procedure described in section 5.5.3.3 was used in an attempt to measure the evaporation flux of Sb from the surface of the Cu(100) sample. To do this a set of experimental conditions to ensure that an equilibrium surface concentration was indeed present on the surface of the sample during the evaporation run had to be determined. This

was done by performing a constant temperature (723 K) segregation measurement using the doped Cu(100) crystal. The results of these measurements are shown in figure 7.8.

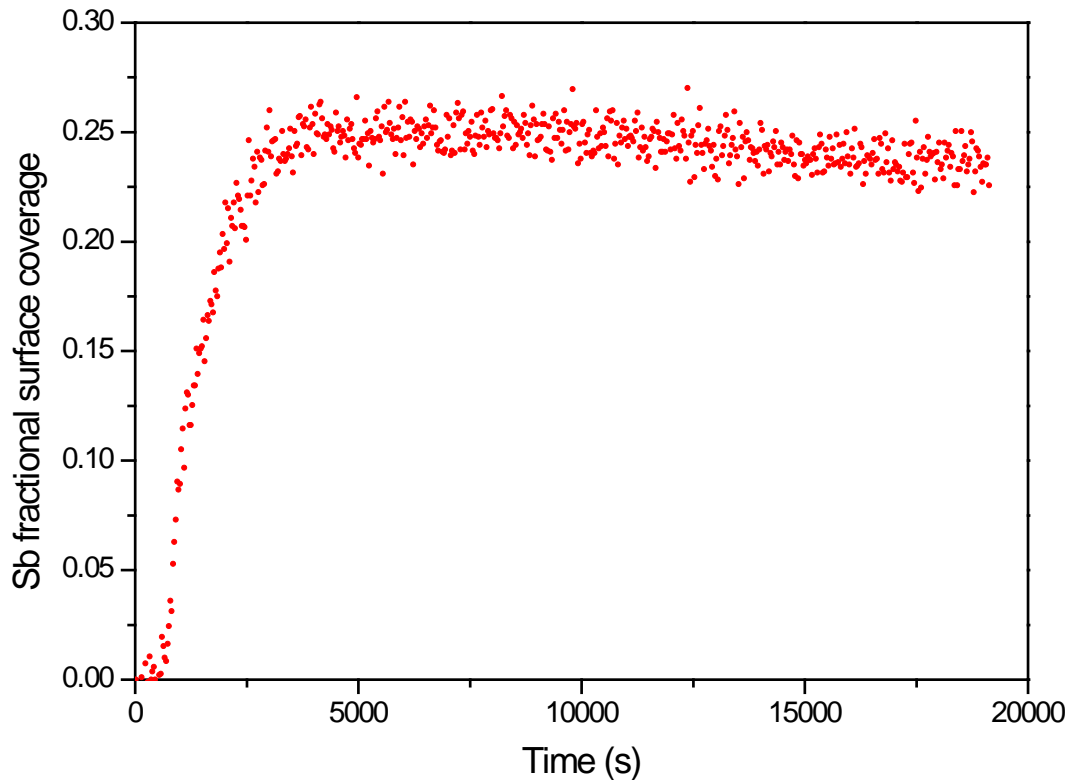


Figure 7.8: The surface coverage of Sb on the Cu(100) surface as a function of time at a constant temperature of 723 K.

From figure 7.8 it can be seen that annealing the sample for 5000 s or approximately one and a half hours at 723 K will result in a maximum surface coverage of Sb. This was done and the procedure described in Chapter 5 section 5.5.3.3 was followed to measure the evaporation flux of Sb. Again the distance h between the sample surface and the QCM sensor, was varied between 0.5 - 1.5 cm and temperatures as high as 973 K were used. As with the case of the linear heating method to measure Sb evaporation from the Cu(100) sample surface, no evaporation flux could be detected using the QCM.

The question arises whether the Inficon XTC/3s deposition controller is in theory sensitive enough to detect the extremely low flux of evaporated solute expected during a segregation run. The QCM used has a thickness and rate resolution of 0.034 \AA over 250 ms sampling

time for a Z-ratio of 1.0 and material density of 1.0 (Inficon XTC/3s operation manual). This resolution is linked to the detectable change in frequency as monitored by the QCM and is thus dependent on the material properties of the evaporant. For example, 100 atoms of an element with a high atomic mass will impart a larger change in frequency than the same number of atoms from an element with a lower atomic mass. A more appropriate approach then might be to consider the deposition rate noise level of the instrument used as an indication of the minimum evaporant flux that can successfully be detected and measured. Figure 7.9 shows a graph of noise versus time of the QCM at room temperature as set for detecting Sb with a new gold coated quartz crystal.

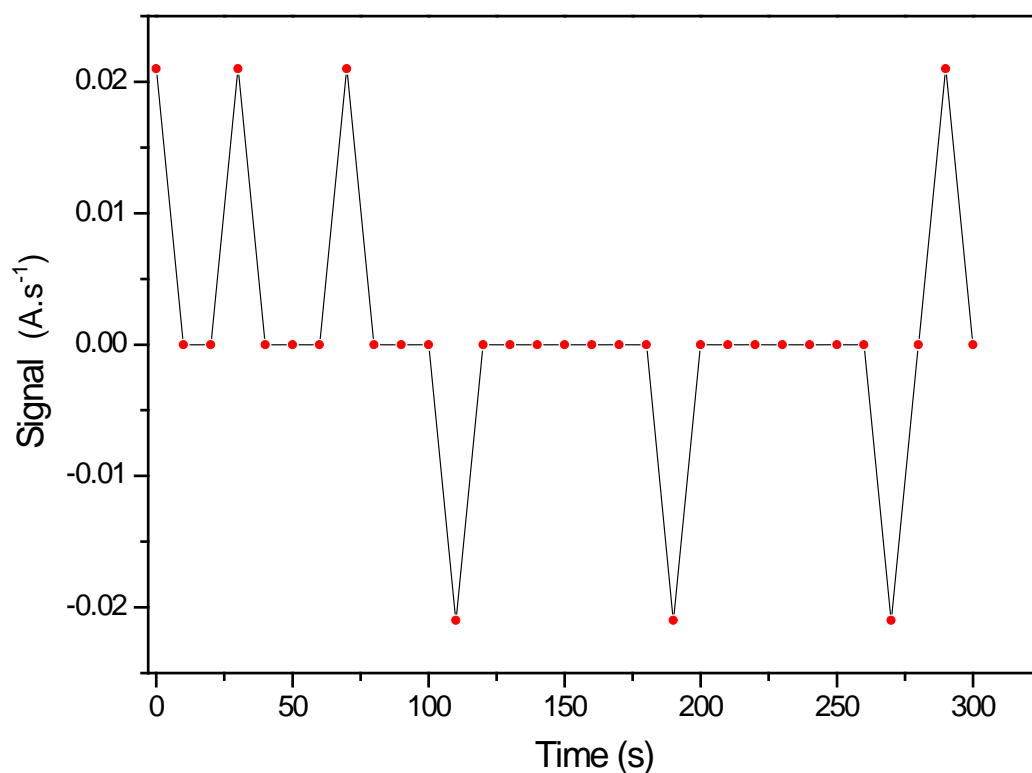


Figure 7.9: Signal levels of QCM at room temperature.

The signal level as seen in figure 7.9 fluctuates between $-0.021 \text{ \AA}\cdot\text{s}^{-1}$ and $0.021 \text{ \AA}\cdot\text{s}^{-1}$. Any evaporation flux from a sample surface must then result in a deposition rate of at least $0.021 \text{ \AA}\cdot\text{s}^{-1}$ or higher on the QCM to produce a meaningful measurement. By using the surface area

of the exposed quartz crystal (0.53 cm^2) and the density of Sb, the minimum deposition rate ($0.021 \text{ \AA}\cdot\text{s}^{-1}$) for meaningful experimental results can be expressed in $\text{g}\cdot\text{s}^{-1}$ or $\text{atoms}\cdot\text{s}^{-1}$ as was explained for figure 7.5. These values are shown in table 7.1.

Table 7.1: Minimum deposition rate required on QCM for meaningful experimental results.

Deposition Rate ($\text{\AA}\cdot\text{s}^{-1}$)	Mass Rate ($\text{g}\cdot\text{s}^{-1}$)	Atomic Rate ($\text{atoms}\cdot\text{s}^{-1}$)
0.021	7.43×10^{-10}	3.68×10^{12}

Using the evaporation geometry as described in section 5.4.3 and assuming that the geometry of the lobed shaped vapour cloud is described by $n = 1$ and that the sample is a distance $h = 1 \text{ cm}$ from the quartz crystal, the values shown in table 7.1 can then be expressed in terms of the minimum evaporation rate required from a sample surface to be detected by the QCM. Using table 5.4 the fraction of particles that evaporate from the sample surface that is collected by the QCM is 0.13 and thus table 7.2 can be obtained

Table 7.2: Minimum evaporation rate of Sb required from Cu(100) surface to allow detection by the QCM.

Mass Rate ($\text{g}\cdot\text{s}^{-1}$)	Atomic Rate ($\text{atoms}\cdot\text{s}^{-1}$)
5.72×10^{-9}	2.83×10^{13}

In the case of evaporation during segregation it must first be established if the concentration of solute atoms on the surface at a given time is sufficiently high to provide the number of atoms for the minimum detectable evaporation rate required as shown in table 7.2. As a first approximation the number of solute atoms on the surface of a sample at segregation equilibrium can be considered.

The maximum fractional surface coverage as it relates to segregated solute atoms for the low index planes of Cu are well known from literature (Terblans, 2001; Higashi *et al.*, 2008). By using the atomic structure of FCC planes in terms the area of a unit cell and the planar density for that particular crystal orientation the number of Cu atoms per unit area and subsequently the number of atoms on the sample surface for different orientations can be calculated. Combining these values with the maximum fractional surface coverage of solute atoms

possible for a specific crystal orientation allows one to calculate the number of Sb values on the sample surface during segregation equilibrium. This is shown in table 7.3. These values assume a sample area of 0.49 cm².

Table 7.3: The maximum surface fraction of solute atoms X_{Sb}^s , the number of Cu atoms N_{Cu}^s on a clean Cu sample surface and the number of Sb atoms on the sample surface at equilibrium N_{Sb}^{eq} , for different crystal orientations for a sample surface area of 0.49 cm².

Sample Surface	Cu(110)	Cu(111)	Cu(100)
X_{Sb}^s (maximum)	0.50	0.33	0.25
N_{Cu}^s (clean sample surface)	5.29×10^{14}	8.67×10^{14}	7.49×10^{14}
N_{Sb}^{eq} (equilibrium sample surface)	2.65×10^{14}	2.86×10^{14}	1.87×10^{14}

Comparing the values in table 7.2 and table 7.3 it can be seen that in a equilibrium state all three low index planes of Cu have enough Sb atoms on a surface to provide sufficient supply of evaporant atoms for the QCM to be used successfully. As the surface concentration at equilibrium can be considered to be constant over short time intervals, the number of Sb atoms on the sample surface at equilibrium shown in table 7.3 can be considered as the number of atoms that can be evaporated at a given second from the surface even if there are no additional solute atoms segregating to the surface from the bulk. These values are also compared in figure 7.10.

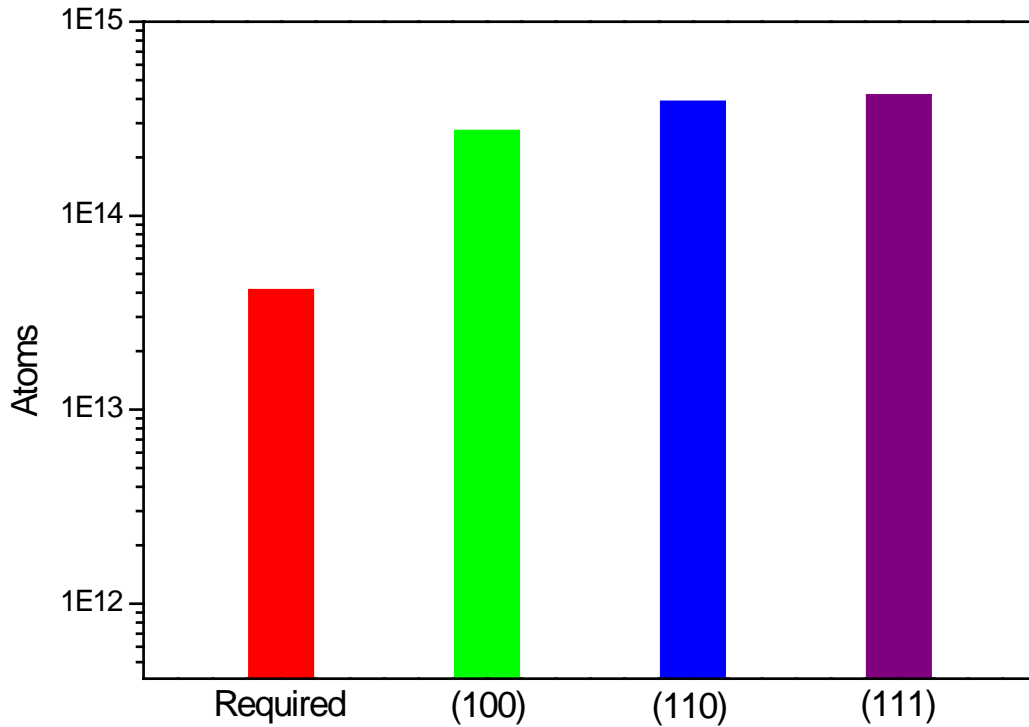


Figure 7.10: The number of Sb atoms on the surface of Cu samples of area 0.49 cm² with different orientations at equilibrium compared to the required number of atoms (per second) that need to evaporate for detectable measurements with the QCM.

This of course assumes that the temperature of the sample is sufficiently high to allow a evaporation rate of Sb atoms equal to, or in excess of 2.83×10^{13} atoms.s⁻¹ from the sample surface. It is assumed that Sb evaporates as Sb₂ (Dushman, 1966) so for Sb₂ this translates to a minimum evaporation rate required of 1.42×10^{13} molecules.s⁻¹ from the sample surface for evaporation to be measured by the QCM.

Using the equation for evaporation flux for a pure metal (Omar, 2011) as discussed in Chapter 4

$$J_N = 3.513 \times 10^{22} \frac{p}{\sqrt{MT}} \text{ (molecules.cm}^{-2}\text{.s}^{-1}\text{)} \quad (7.1)$$

and using Raoult's law as proposed by Lea and Seah (1977)

$$p_s \cong pX_{x=0}^t \quad (7.2)$$

the predicted possible molecule flux of Sb_2 from the Cu sample surface (0.49 cm^2) as used during this study for a can be plotted as a function of temperature as shown in figure 7.11. Again it is assumed for argument's sake that the equilibrium concentration remains relatively constant over a short period of time.

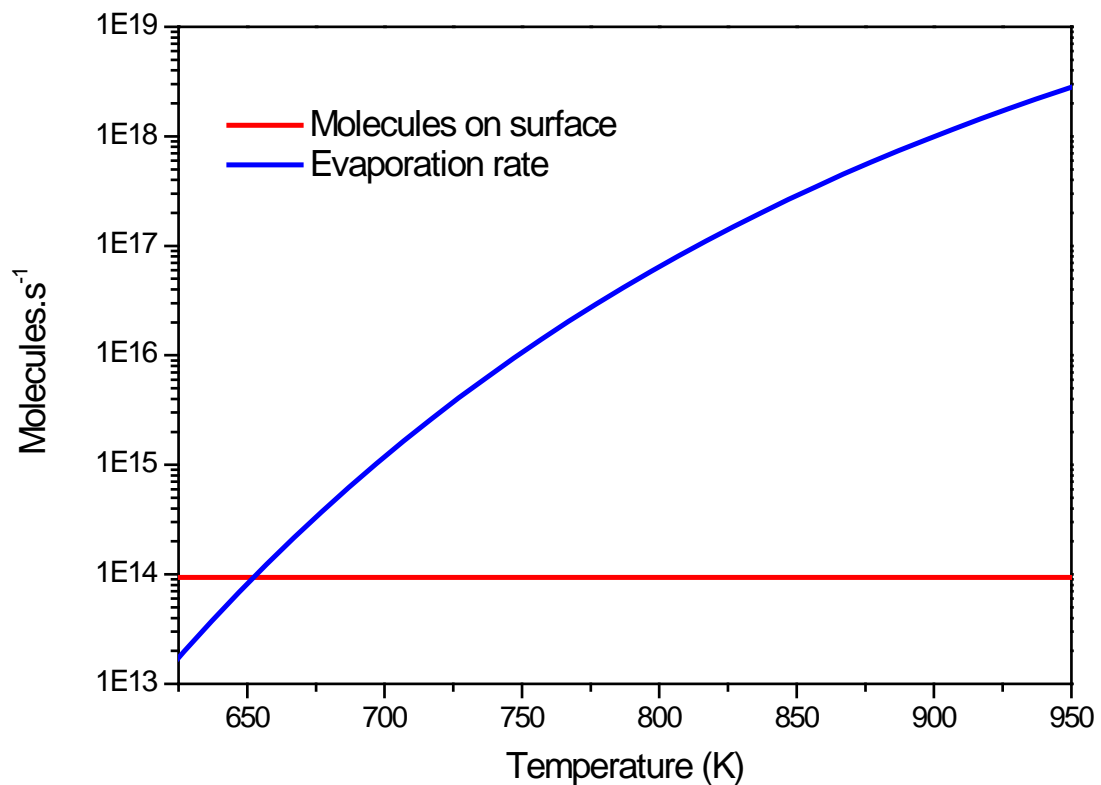


Figure 7.11: The number of Sb_2 atoms on the surface of the Cu(100) sample compared to the calculated evaporation rate according to theory.

From the preceding results it should be clear that the theoretically predicted evaporation flux of Sb is sufficiently high for the Inficon XTC/3s system to detect and measure.

The results in figure 7.11 also indicates that the number of Sb_2 molecules required for the predicted evaporation rate from theory will exceed the instantaneous number of molecules available on the sample surface at a relatively low temperature (± 650 K). As it is obvious from experimental results as shown in figure 7.8 that a drastic decline in surface concentration does not occur, it must be assumed that either the actual evaporation that takes place from the surface is much lower than predicted by theory, or that the segregant flux $J_{\text{Sb}}^{(2 \rightarrow 1)}$ from the layer just below the surface to the surface layer is much higher than previously thought. Considering that no evaporation of Sb could be measured from the Cu (100) crystal and the fact that even in the case of the pure Sb the measured evaporation rate was much lower than the theoretical predicted rate, it must be concluded, that in the case of a CuSb system the Hertz-Knudsen equation highly over estimates the evaporation rate of Sb from the Cu(100) surface. Other assumptions of the theory could be questioned, for instance the suggestion that Raoult's law (equation 7.2) applies as suggested by Lea and Seah (1977).

7.4 Summary

In this chapter evaporation measurements done on pure Sb as well as evaporation experiments performed on the Sb doped Cu(100) crystal are presented. These experimental results are used to test the procedure and equipment developed in Chapter 5. The qualitative evaporation behaviour of the pure Sb sample is similar to the theoretical behaviour discussed in Chapter 4. There is however a quantitative discrepancy between the measured and calculated results with the experimental evaporation being much lower than predicted. This is attributed partly to the presence of S on the surface of the pure Sb sample. This S contamination is most likely the result of S segregating from the Sb bulk which might indicate that the purity of the Sb sample is not as high as initially assumed or specified by the supplier. However, other reports in the literature have also found the experimental evaporation rate of Sb to be much lower than expected and associated this with a low evaporation coefficient.

No Sb evaporation from the Cu(100) doped with Sb could be detected. It is however demonstrated that the modification made to the AES should have detected any evaporation of Sb solute at equilibrium if the evaporation behaviour followed the theory of Hertz-Knudsen and Leah and Seah, (1977). The conclusion is thus made that the evaporation of segregating Sb from a Cu(100) bulk is substantially lower than what is theoretically predicted. Since the evaporation rate of pure Sb is also much lower than theoretically expected, the finding that evaporation of Sb from a Cu(100) surface is lower than expected cannot necessarily be solely related to interaction of Sb with the Cu(100) surface.

7.5 References

Angelico E., Speiglan E. and Yunpeng J. [2014] *Internal publication*, University of Chicago, High Energy Physics.

Higashi S., Tochiara H., Shneerson V.L. and Saldin D.K. [2008] *Surface Science* **602** p2473.

Hirth J.P. and Pound G.M. [1957] *Journal of Chemical Physics* (**26**) p1216.

Inficon XTC/S Operating manual [2006] Inficon Inc.

Lea C. and Seah M.P. [1977] *Philosophical Magazine* **35** p213.

L'vov B.V. and Novichikhim A.V. [1997] *Thermochimica acta* **290** p239.

Mattox D.M. [2010] *Handbook of Physical Vapor Deposition (PVD) Processing* 2nd Edition, Elsevier.

Omar M. [2011] *Introduction to nanomaterials and devices*, Wiley.

Pound G.M. [1972] *Journal of Physical and Chemical Reference Data* **1(1)** p135

Rosenblatt G.M., Lee P. and Dowell M.B. [1966] *Journal of Chemical Physics* **45** p3454.

Terblans J.J. [2001] *Modellering en eksperimentele ondersoek van Sb – oppervlak segregasie in Cu-enkelkristalle*, PhD thesis, University of the Free State.

Chapter 8

Updated Modified Darken simulations including evaporation

8.1 Introduction

This chapter includes new simulated segregation results which are compared to the experimental segregation data presented in Chapter 6. The simulations were obtained using software implementing the Modified Darken model. This software was originally developed by J.J. Terblans for predicting segregation in binary systems, but did not consider evaporation. The software program was upgraded during this study to include the effects of surface evaporation using the equations discussed in Chapter 4 section 4.4. The mathematical foundations for the original programming code used by J.J. Terblans can be found in Appendix A of Terblans, (2001).

The chapter also describes how the concept of evaporation during segregation can be used in understanding and interpreting extracted segregation parameters.

8.2 The Evaporation Parameter K

In Chapter 4 an adapted form of the Hertz-Knudsen equation was introduced which makes provision for the situation where impurity atoms of species i evaporates from a pure elemental substrate. The evaporation rate is given by

$$J_i = 3.513 \times 10^{22} \frac{KpX_F^S}{\sqrt{MT}} \text{ (atoms. cm}^{-2}\text{. s}^{-1}\text{)} \quad (8.1)$$

where X_F^S is the fractional surface coverage of the impurity species present, if compared to a complete surface coverage of the impurity atoms.

The evaporation parameter K included in equation 8.1 can be considered a function of the following:

- The original evaporation coefficient α as used in the original Hertz-Knudsen equation. See Chapter 4 section 4.2.2.
- The difference in atom bonding strength between the solute atom and the substrate when compared to the pure elemental bonding strengths involved for the solute species.
- Any interaction parameters involved due to the presence of additional impurities on the surface layer.

A technical description of the changes made to the original software to allow for the influence of evaporation based on equation 8.1 predicting the evaporating flux from the surface layer is given in Appendix A.

The evaporation flux is proportional to the magnitude of the evaporation parameter K . For $K = 1$ the evaporation flux will be at the theoretical maximum as predicted by the Hertz-Knudsen equation for the specific fractional surface concentration X_F^S of solute of species i present on the surface. If $K = 0$ no evaporation of species i will take place. The influence of varying the value of K on the surface segregation profile obtained using a LTR is shown in figure 8.1. For ease of comparison the segregation profile and parameters used in Chapter 6 for the Sb doped Cu(100) sample were used. In each plot shown in figure 8.1 only the evaporation parameter K was changed.

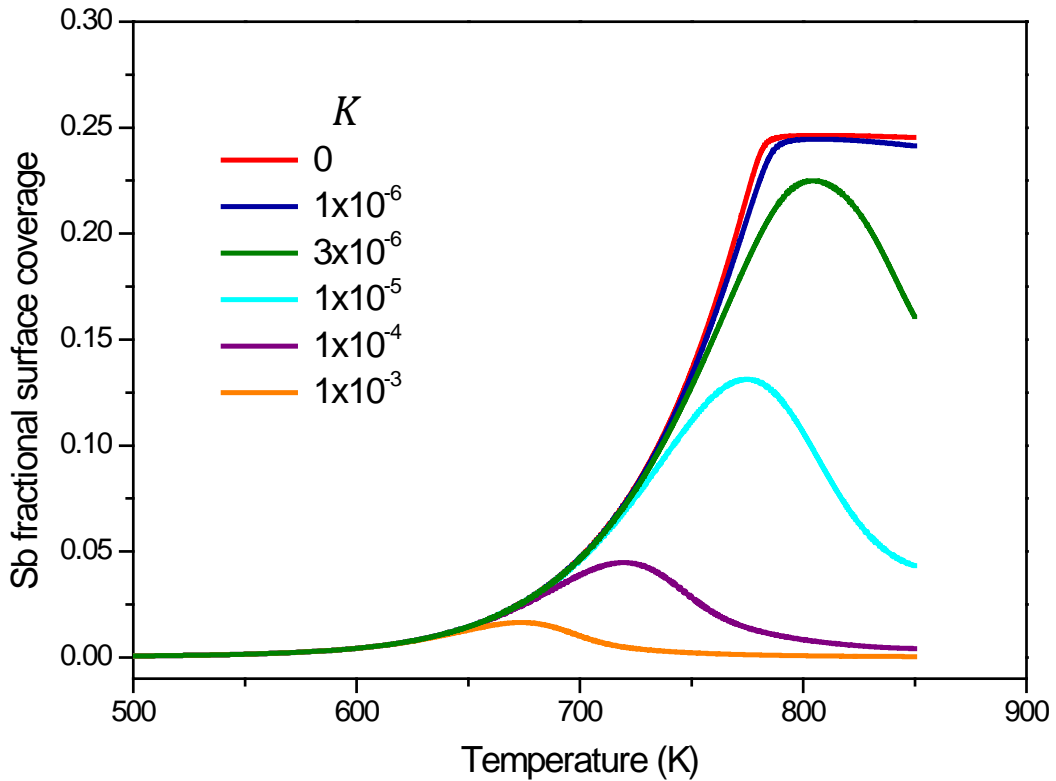


Figure 8.1: The influence of varying magnitudes of K on a segregation profile.

For $K = 0$ no evaporation of the Sb atoms takes place, and as a result the segregation profile obtained is exactly the same as the one used to fit the segregation data in Chapter 6 where evaporation was not considered. It is obvious that even for very low values of K a high evaporation flux of solute atoms from the surface is obtained, having a major effect on the segregation profile. This may be in part due to the results shown in Chapter 7 where it was concluded that the Hertz-Knudsen equation coupled with Raoult's law highly over estimates the evaporation rate of Sb from the Cu(100) surface, but it also shows that the segregation profile is very sensitive to possible evaporation effects and therefore illustrates the extreme importance of including evaporation into the Modified Darken model to obtain physically meaningful fit parameters. For K values higher than approximately 1×10^{-6} equilibrium cannot be reached. This causes the surface concentration to reach a maximum before decreasing to an eventual solute concentration of zero on the surface.

Two scenarios of potential interest in regards to segregation studies in general exist at the extreme ends of the values for K shown in figure 8.1.

First consider the graph with $K = 1 \times 10^{-3}$. In this scenario the evaporation rate is so high when compared to the segregation flux rate that hardly any surface enrichment takes place and only for a short period of time and temperature range. It would be difficult to measure this increase in surface solute concentration using typical surface analytical techniques like AES. If the possible influence of evaporation is neglected, it can easily be assumed that no segregation takes place in that specific system, and that this can wrongly be attributed to factors like atomic sizes and structure prohibiting segregation or even zero segregation energies.

Alternatively in the case where $K = 1 \times 10^{-6}$ the surface enrichment reaches an apparent maximum surface concentration, before declining. This decline from the maximum surface coverage, after surface equilibrium has been reached, has historically been attributed to an additional segregating impurity displacing the segregating solute from the surface (Jafta, 2010). Although even the Bragg-Williams equation predicts such a decline in the equilibrium surface concentration (desegregation) at high temperatures, it is not unreasonable to draw the conclusion that in some systems such a decline in surface solute coverage could be attributed to evaporation. In addition, when using AES, such a situation can lead to the apparent maximum surface coverage being used to quantify the data as if the maximum coverage has in fact been reached. This will of course induce an error in any set of segregation parameters which are extracted from that data.

It is clear from these simulations that even a low evaporation flux (not detected by the QCM) can have a significant influence on the general segregation profile. Even though the experimental segregation data of chapter 6 does not show evidence of extreme evaporation, consistent with the failure to measure Sb evaporation from the Cu(100) surface in chapter 7, a small amount of evaporation in the range corresponding with $K \sim 1 \times 10^{-6}$ may still influence the simulated segregation curve and therefore the fitted segregation parameters appreciably.

8.3 The influence of evaporation on segregation parameters

It was demonstrated in section 8.2 that evaporation of the surface solute during segregation can have a major influence on a simulated segregation profile. This is true even when the evaporation flux is extremely low. This influence becomes more important at higher temperatures due to the high temperature dependence of the evaporation rate. This is especially true in situations where there is a relatively low evaporation rate predicted in relation to the segregation flux, as in the case illustrated in figure 8.1 for $K = 1 \times 10^{-6}$.

Correcting previous segregation parameters extracted from Modified Darken model fits for the evaporation will necessitate obtaining a similar fit to the original profile, but by including evaporation. This will then change the original segregation parameters obtained. This of course assumes that the original fit was reasonable when compared to the measured data, and that a better fit cannot be obtained using the updated Modified Darken model which includes evaporation effects.

At this point in time it is not possible to provide numerical values for the changes in parameters which will occur if the segregation parameters are extracted from a fit close to that of the Modified Darken model, but inclusive of evaporation effects. This is indicative of the need for further research on this topic. General guidelines can however be given regarding to how the inclusion of evaporation effects will affect the extracted parameters. This is shown in the following subsections. While each of the segregation parameters is treated as separate entities, it should be remembered that they do have inter-dependent influence on the profile. As mentioned previously the influence of even low fluxes of evaporation becomes particularly apparent at higher temperatures. The results presented will concentrate on these higher temperatures, in a region between the kinetic and equilibrium regions. In all the graphs shown in the sub-sections of section 8.3, the original fit obtained with the segregation parameters in Chapter 6 are shown in red without the influence of evaporation being include i.e. $K = 0$. A segregation profile using the same segregation parameters is also shown in orange but with a low flux of evaporation included ($K = 1 \times 10^{-6}$). The additional graphs in each figure use the same segregation parameters as obtained in Chapter 6 but with evaporation included ($K = 1 \times 10^{-6}$), and with the specific segregation parameter under discussion altered to illustrate the effect on the segregation profile.

8.3.1 The pre- exponential factor D_0

The influence of different values of D_0 on a segregation profile with evaporation is shown in figure 8.2.

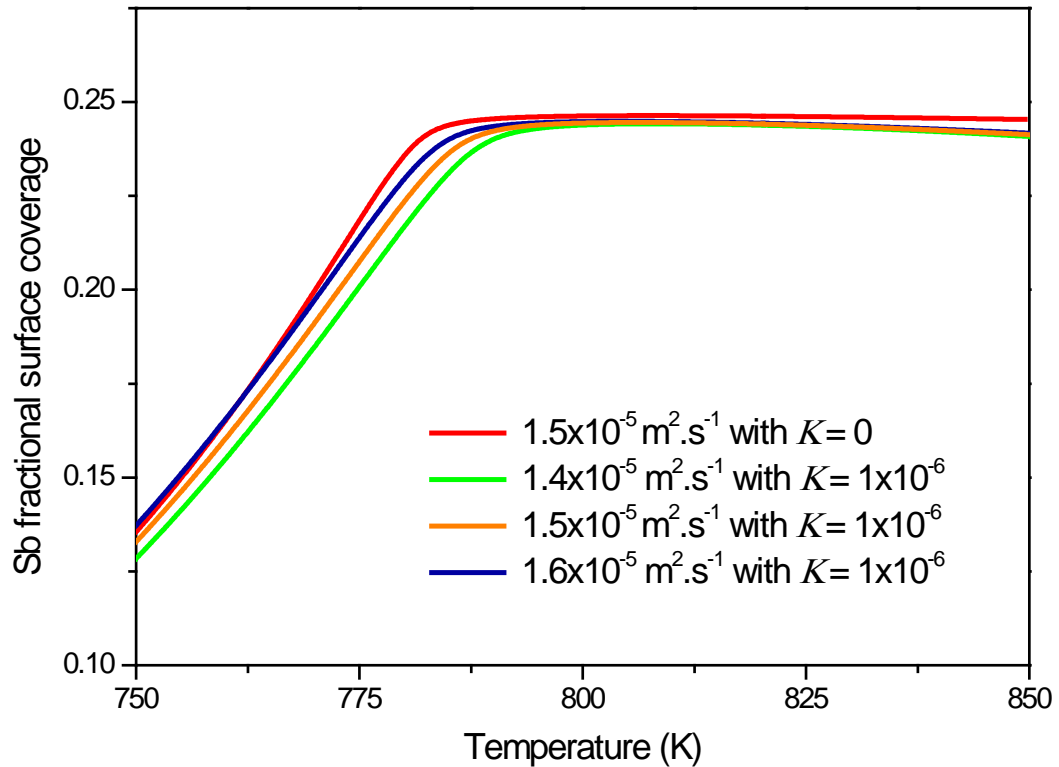


Figure 8.2: The influence of different values of D_0 on a segregation profile with evaporation.

It can be seen in figure 8.2 that in order to shift the segregation profile inclusive of evaporation (orange graph) to fit the original profile (red graph) the pre- exponential factor D_0 must be increased. Therefore not taking evaporation into account could result in a fit that underestimates the value of D_0 . An increase in D_0 will result in an increase of the diffusion coefficient D . Physically this makes sense because removing atoms from the surface layer as in the case of evaporation will lead to a higher diffusion flux from the bulk to compensate for the decline in surface concentration brought on by the evaporation. In terms of diffusion, the pre- exponential factor D_0 is dependent on parameters like the atomic jump distance, the atomic vibrational frequency and terms related to vacancy formation (Elliot, 1998). As these

parameters are related to the bulk characteristics of the matrix in the segregation system, any change in D_0 , in order to shift a segregation fit should be carefully considered, but is possible.

8.3.2 The activation energy E

The influence of different values of E on a segregation profile with evaporation is shown in figure 8.2.

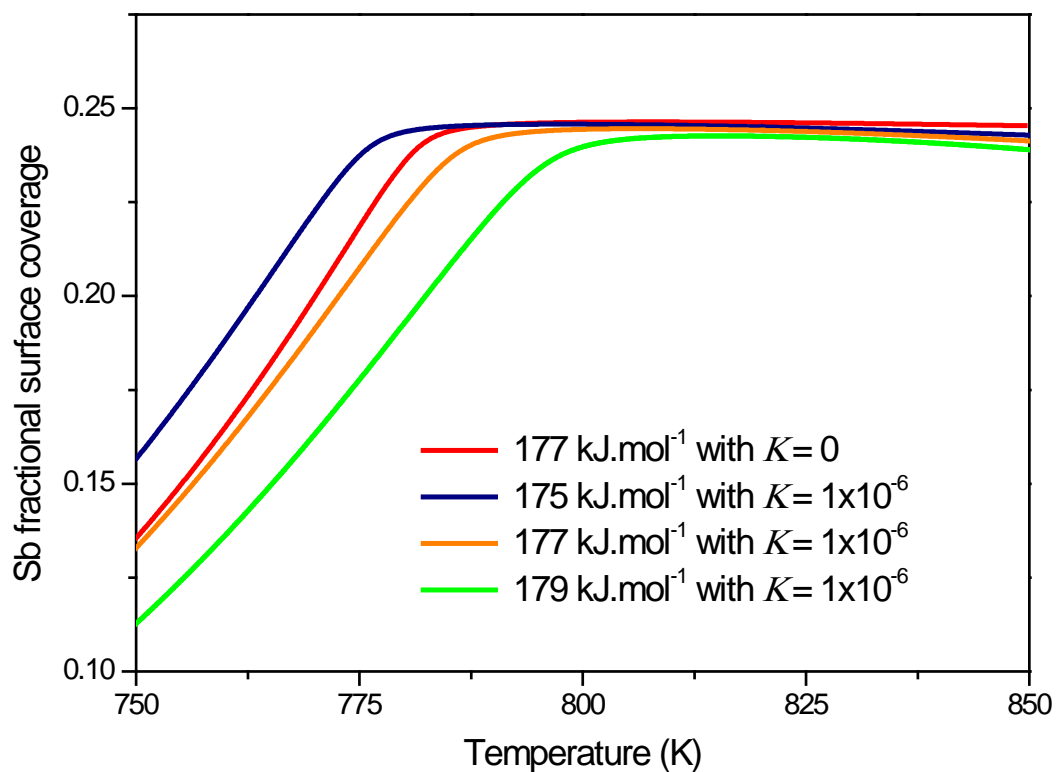


Figure 8.3: The influence of different values of E on a segregation profile.

The situation for E is similar to that for the case of D_0 , because both parameters determine the diffusion coefficient, D . It can be seen in figure 8.3 that in order to shift the segregation profile inclusive of evaporation (orange graph) to fit the original profile (red graph) the activation energy E must be decreased. Therefore not taking evaporation into account could result in a fit that overestimates the value of E . An decrease in E will result in an increase in the diffusion coefficient D . Again this makes sense as removing atoms from the surface layer

as in the case of evaporation will lead to a higher diffusion flux from the bulk to compensate for the lower surface concentration brought on by the evaporation. The activation energy E is given by the sum of defect formation (vacancy) and atom mobility terms (Elliot, 1998) which are characteristically related to the bulk properties of the matrix. Again as in the case of D_0 , drastically altering E in order to shift the segregation fit to compensate for evaporation should be carefully considered, but is possible.

8.3.3 The segregation energy ΔG

The influence of varying magnitudes of ΔG on a segregation profile with evaporation is shown in figure 8.4.

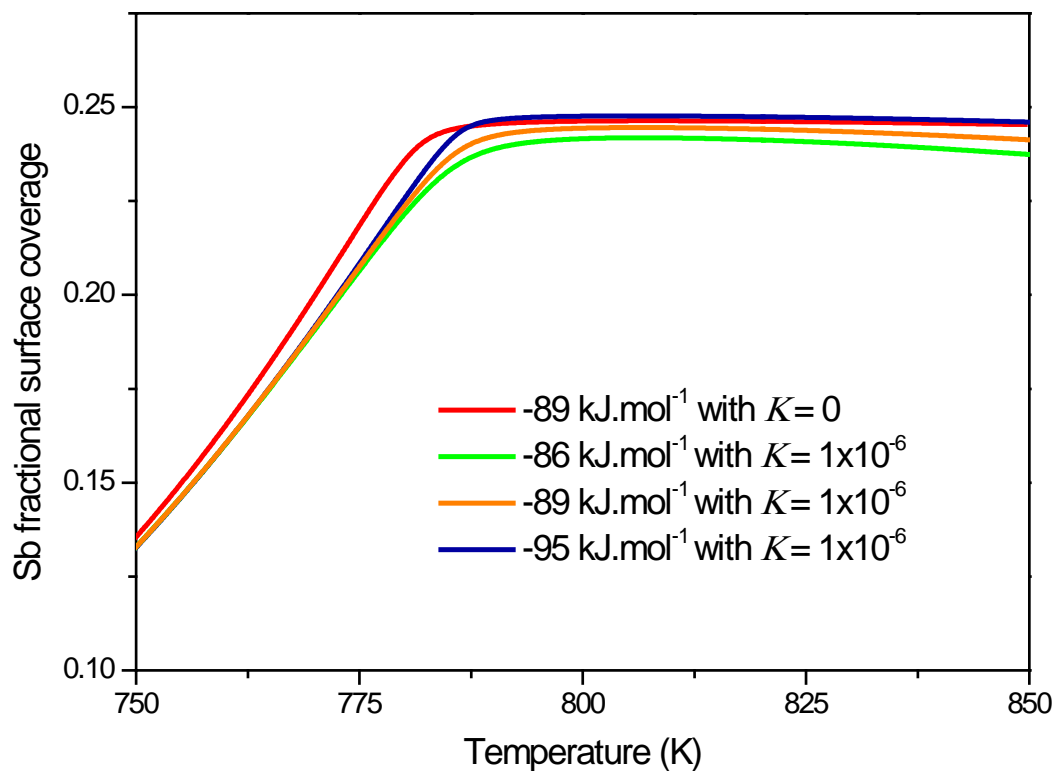


Figure 8.4: The influence of varying magnitudes of ΔG on a segregation profile.

It can be seen in figure 8.4 that in order to shift the segregation profile inclusive of evaporation to fit the original profile the segregation energy ΔG must be made more negative or the absolute value of ΔG has to increase. Therefore not taking evaporation into account

could result in a fit that overestimates the value of ΔG . This implies that the energy barrier for desegregation must be higher to compensate for the higher number of atoms which do segregate to the surface, but which are not measured due to the atoms being lost from the surface because of evaporation.

8.3.4 The interaction parameter Ω

The influence of different values of Ω on a segregation profile with evaporation is shown in figure 8.3.

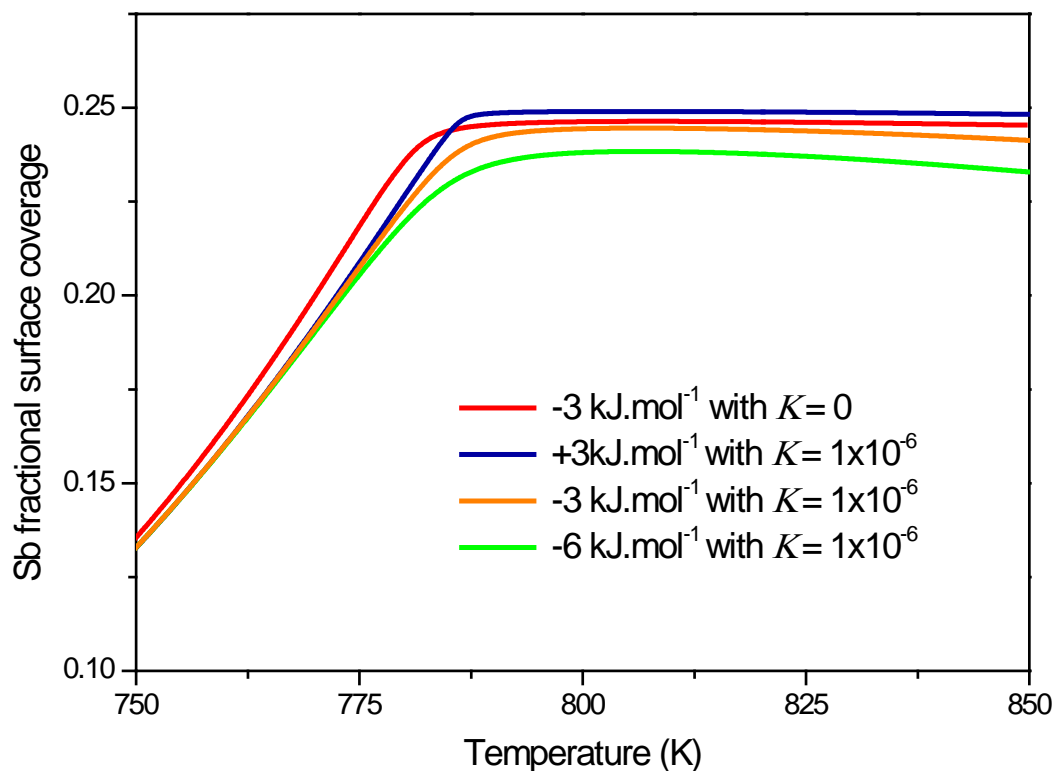


Figure 8.5: The influence of different values of Ω on a segregation profile.

It can be seen in figure 8.5 that in order to shift the segregation profile inclusive of evaporation to fit the original profile the interaction parameter Ω must be more positive. Therefore not taking evaporation into account could result in a fit that underestimates the value of Ω . As the interaction between atoms on the surface is of great importance when

considering whether evaporation will take place or not (in terms of bonding strengths) and to what extent if evaporation does occur, a closer look at this parameter is called for.

The interaction parameter Ω describes the interaction between different atomic species. The interaction parameter is defined for two atomic species I and 2 by

$$\Omega_{12} = Z \left[\varepsilon_{12} - \frac{1}{2}(\varepsilon_{11} + \varepsilon_{22}) \right] \quad (8.2)$$

where ε_{ii} is the interaction energy per mole between the same species and ε_{ij} is the interaction energy per mole between different atom species. The coordination number of an atom in the solid is given by Z which is the number of nearest neighbours for a particular atomic structure of species i and j (Du Plessis, 1990; Wang *et al.*, 1999).

The first important fact to notice is that the $\frac{1}{2}(\varepsilon_{11} + \varepsilon_{22})$ term in equation 8.2 is simply the average interaction energy per mole of species i and j in proximity of the same species. This means that if this average interaction energy of the pure species is equal to ε_{12} , then the interaction coefficient $\Omega_{12} = 0$. Thus $\Omega_{12} = 0$ does not imply that no interaction between the different species exist, as the interaction energy between species 1 and 2 will still be ε_{12} and this value is not zero.

The second point concerns the sign of Ω_{12} . Du Plessis (1990) states that the sign of Ω_{12} may either indicate an attractive or repulsive interaction. This is an over simplification as it has already be shown that $\Omega_{12} = 0$ does not imply that no interaction exists between the dissimilar species. It can subsequently not simply be stated that a negative interaction coefficient Ω_{12} indicates an attractive interaction and that a positive interaction coefficient Ω_{12} indicates a repulsive interaction. If $\varepsilon_{12} = 0$ (i.e. no interaction) then the interaction parameter is $\Omega_{12} = -\frac{Z}{2}(\varepsilon_{11} + \varepsilon_{22})$, and what can be stated is that where there is a strong bonding interaction

between two atomic species the interaction parameter Ω_{12} will be less than this critical value (which is some positive number since ε_{11} and ε_{22} are negative numbers). Therefore there will be some range of positive values for Ω_{12} still corresponding to attraction rather than repulsion.

This can be useful in interpreting segregation parameters. In general contemporary segregation equations do not provide unique solutions for the various segregation parameters. This is illustrated in figure 8.6 where the Modified Darken fit used in Chapter 6 are compared with an alternative but similar fit with different values for Ω and ΔG . In both instances evaporation was not included into the calculations. These values are shown in table 8.1.

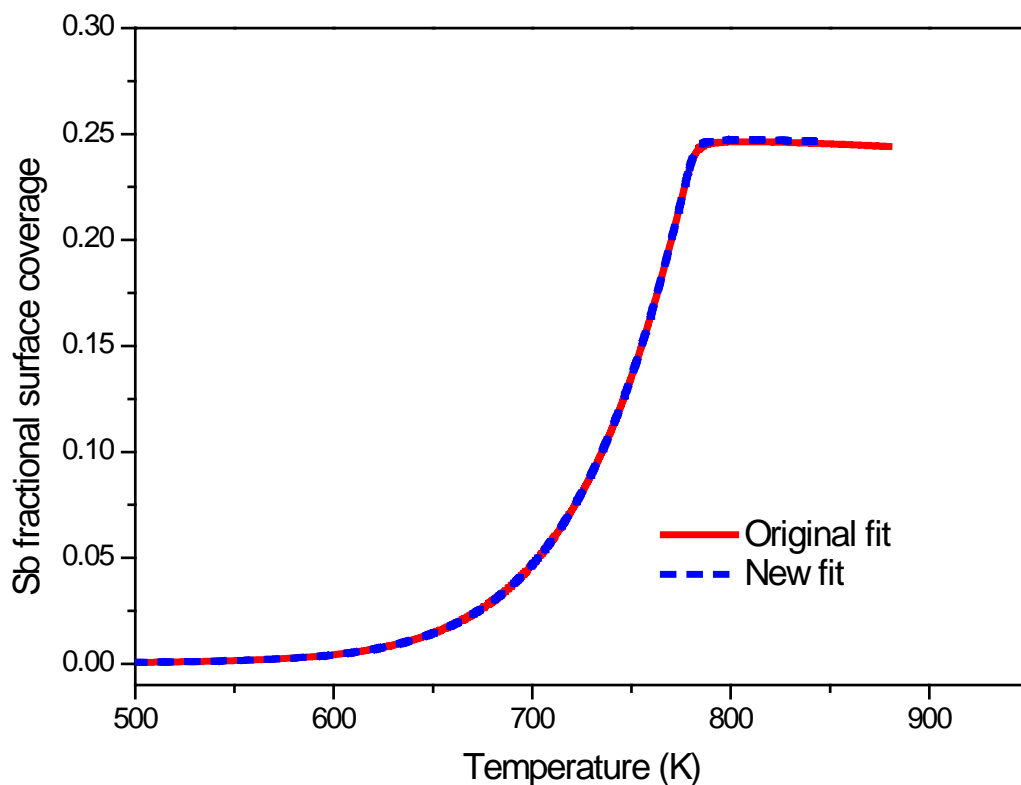


Figure 8.6: Original Modified Darken model fit compared to new alternative fit without evaporation.

Table 8.1: Segregation parameters extracted from the Modified Darken model fits without evaporation.

	Original	Alternative
ΔG (kJ.mol ⁻¹)	-89	-73
Ω (kJ.mol ⁻¹)	-3	6
D_0 (m ² .s ⁻¹)	1.5x10 ⁻⁵	1.5x10 ⁻⁵
E (kJ.mol ⁻¹)	177.0	177.0

Ignoring the effects of additional surface contaminants, the observation that evaporation of Sb from the Cu(100) surface is less than predicted by theory for pure elemental evaporation, indicates a relatively strong chemical bond on the surface between the Sb atom and the nearest Cu neighbours. This suggests a more negative Ω . This can be used to argue that the original set of segregation parameters extracted in Chapter 6 are more appropriate and physically realistic than those extracted from the new alternative fit shown in figure 8.6.

8.4 Summary

This chapter includes simulated segregation results obtained using software developed during this study which updates the Modified Darken model with evaporation taken into account. The effect of the proposed evaporation parameter K is discussed and shows how sensitive the profile is to even very small values of K (below the detection limit of the QCM). Guidelines are given on correcting segregation parameters extracted from Modified Darken model fits for the influence of evaporation. Interpreting segregation parameters in terms of evaporation is also discussed. It is clearly demonstrated that omitting evaporation from the simulations can generate inaccurate segregation parameters.

8.5 References

Du Plessis J. [1990] *Solid State Phenomena, surface segregation (11)*.

Elliot S. [1998] *The Physics and Chemistry of Solids*, John Wiley & Sons.

Jafta C.J. [2010] *Segregation in a Cu bicrystal*, MSc dissertation, University of the Free State.

Terblans J.J. [2001] *Modelling en eksperimentele ondersoek van Sb – oppervlak segregasie in Cu-enkelkristalle*, PhD thesis, University of the Free State.

Chapter 9

Final Conclusions and Remarks

9.1 Introduction

The aim of this project was to investigate surface loss due to evaporation during segregation and create a model for this effect to assess the impact that neglecting such surface loss has on the extracted segregation parameters. Research pertaining to the effects of evaporation on the segregation process not only leads to a better understanding of segregation and of evaporation, but broadens the general knowledge base of the processes which determine the material properties of metals and alloys. Such an increase in knowledge can only have a positive knock-on effect for industry in terms of how metallurgical products are manufactured and their applications.

A topic as complex as evaporation during segregation requires that a number of sub-topics be understood before a complete picture of the physical processes at a fundamental level can be formed. The challenging nature of such a topic might explain the paucity of previous studies on this subject.

Certain aspects like the modifications made to an AES system or the extraction of segregation parameters using the standard contemporary models could be addressed directly, however other aspects as shown in this study, requires and deserve not only further investigation, but a more fundamental approach. While certain direct contributions to science was made during the study, maybe the most important contribution is the fact that this study paves the way forward for further study on the sub-topics which forms the big picture of surface loss during segregation, and segregation as a whole.

9.2 Conclusions regarding segregation measurements

The sample preparation to dope Cu crystals with Sb proved extremely challenging and time consuming. This was especially true for the annealing phase of the sample preparation as a number of samples failed at this stage due to oxidation, despite sealing the samples in Ar filled quartz ampoules. While the deposition of a thin layer of Sb onto a Cu crystal in order to obtain a specific concentration level of dopant proceeded well, it was also demonstrated that the thickness of the deposited layers could be verified by means of mass measurements or direct thickness measurements using a scanning electron microscope. A Sb doped Cu(100) sample was successfully prepared. Refinement of the annealing process of doped samples to ensure a homogeneous distribution of the dopant is however required to reduce the percentage of failed sample preparation attempts.

Segregation experiments were performed using this Sb doped Cu(100) sample. Extra care had to be taken compared to previous studies to sputter clean the entire sample surface since evaporation from the surface was a key issue in this work, which made the measurements technically more challenging and time-consuming. A segregation profile was obtained using an LTR measurement and the Modified Darken model without evaporation being considered was fitted to the quantified data. The segregation parameters were extracted. Despite active research of segregation for Sb doped Cu single crystals in the past, this study is the first announcement of the segregation parameters (D_0 , E , ΔG , Ω) for Sb doped Cu(100) and therefore complements previous work well. The values obtained compare well with previous segregation parameters of Sb doped Cu in the literature for other orientations.

9.3 Conclusions regarding the modifications made to the AES and subsequent evaporation measurements

An Inficon XTC/3s deposition controller was successfully incorporated into an AES system. The quartz crystal sensor was mounted in the AES system in such a way that the specimen mounted on a resistance heater could be repositioned from a position in front of the AES electron gun/analyser to a position underneath the sensor. This was achieved by making use of a manipulator with a flip mechanism. This modification allows the surface of a metal sample used for evaporation studies or even thin layer growth to be sputter cleaned and analysed by means of AES. A mathematical model using the evaporation geometry between the evaporation source or sample in this study and the quartz crystal sensor to predict the fraction of evaporated particle which would be detected was developed and implemented in Matlab based software. This is an important contribution as the derived equations can be applied to other deposition systems used for the growth of thin films. Measurements were made to ascertain the maximum heating of samples near the quartz crystal sensor before spurious readings were created.

The evaporation rate of solid pure Sb as a function of temperature was measured and found to be qualitatively similar to the evaporation rate predicted by the Hertz-Knudsen equation using tabulated vapour pressure data for Sb, although the measured rate of evaporation was substantially less than calculated values. This can be interpreted as a very low evaporation coefficient α for Sb evaporation. In this study however, the quantitative difference was partly attributed to the segregation of S to the Sb surface, although it is clear from the literature that the evaporation of Sb is not a simple process and that different models have been proposed to explain the low evaporation coefficient, e.g. assuming the evaporation of Sb_4 molecules or a mixture of Sb_4 and Sb_2 molecules instead of just Sb_2 molecules as in this study. It was demonstrated that the Inficon XTC/3s monitor is theoretically capable to measure the low evaporation fluxes expected from a CuSb binary system during segregation if the evaporation behaviour follows that of classical theory. It was however shown that the classical theory overestimate the evaporation rate of Sb from a CuSb system. Subsequently the evaporation rate was lower than the detection limit of the equipment used.

9.4 Conclusions regarding the adding of evaporation effects to the Modified Darken model

An existing software program which implemented the Modified Darken model was updated to include the effects of surface evaporation. This was done using a combination of the Hertz-Knudsen equation and Raoult's law. To compensate for a number of physical factors including the different species on the surface an evaporation parameter K was introduced. At this point of time it would be premature to use this updated model to extract segregation parameters until the physical meaning of K is better understood. The updated model can however show what qualitative effect evaporation will have, not only on the segregation profile, but also on the segregation parameters themselves. In addition segregation profiles generated with the updated software suggest that evaporation of Sb does in fact take place from the Cu(100) surface during segregation even though the evaporation rates are below the Inficon XTC/3s detection limits.

Since multiple sets of segregation parameters can yield rather similar segregation profiles for a binary system, the concept of evaporation during segregation in the context of the interaction parameter Ω was used to give guidelines in choosing the most appropriate set of solutions.

9.5 Suggestions for future work

Various possible approaches exist to further this study. The most simplistic would be to use the existing changes made to the AES system and the updated Modified Darken model and apply them to a segregation system which produces higher evaporation fluxes. If evaporation rates could be obtained during a segregation run that is detectable by the QCM the data could be used to refine the physical meaning of the evaporation parameter K . An Mg-Al alloy could

be considered. Alternatively the QCM could be exchanged for more sensitive devices and techniques which would enable the measuring of even lower evaporation rates. Techniques like Mass Spectroscopy and Electron Impact Emission Spectroscopy are two possible options. While the Hertz-Knudsen equation is widely used, other evaporation theories can be investigated for incorporation in the Modified Darken model. These include the continuum approach or statistical rate theory.

The current modified AES system in conjunction with the understanding gained regarding the evaporation geometry involved during this study also allows for numerous fundamental experiments to be performed on sublimation from solid surfaces.

Appendix A

Modified Darken Software with Evaporation

The Modified Darken model has, for a number of years been used at the Physics Department, University of the Free State, to simulate segregation profiles and to extract segregation parameters. It is thus not surprising that software was developed in the department for predicting segregation in binary systems. This software was originally developed by J.J. Terblans, but which did not consider surface evaporation. The software program was modified during this study to include the effects of surface evaporation using the equations discussed in Chapter 4 section 4.4. The mathematical foundations for the original programming code used by J.J. Terblans can be found in Appendix A of Terblans J.J. [2001] *Modellering en eksperimentele ondersoek van Sb – oppervlak segregasie in Cu-enkelkristalle*, PhD thesis, University of the Free State. The new updated user interface is shown in figure A1.

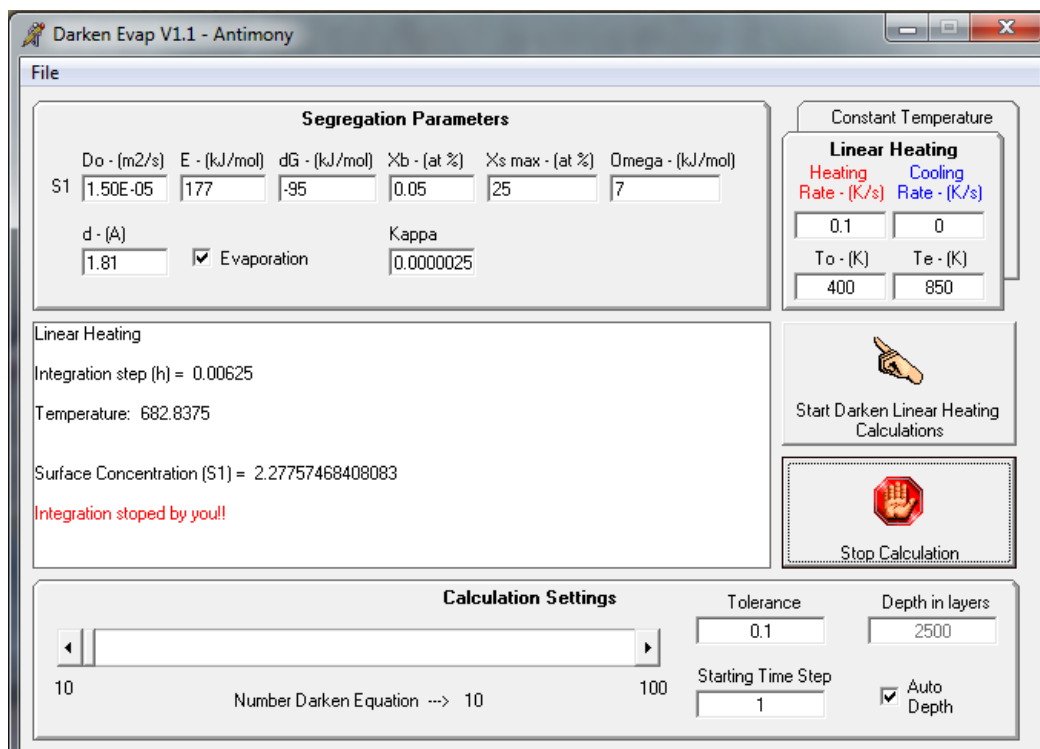


Figure A1: User interface of Modified Darken model software which includes the effects of evaporation.

The updated user interface and software still allows the user to perform simulations without evaporation effects being considered. This is done by simply deselecting the “evaporation” check box as can be seen in figure A1. In this mode any binary system can be used to perform either a linear heating ramp, or constant temperature ramp simulation. At this point of time the software can only simulate segregation profiles for a Sb doped Cu(100) binary system if evaporation is considered. The refining of the software to include other binary systems is planned for a later stage, but only involves updating the interface to change more parameters and is therefore trivial.

The original software includes numerous forms and modules. Only the most important changes in the Euler module made are shown (figure A2) and explained. All coding was performed using Microsoft Visual Basic version 6.0 (SP6).

```

For E_Time = a To b Step h

    Call Darken_dy_dt(i_species, m_species, Temperature, F())

    For l = 1 To N - 1

        If (h * F(l)) / Y(i_species, l) > (Tol) Or (h * F(l)) > Y(i_species, l) / 2 Then
            GoTo Euler_Error
        End If

        (1) If FrmDareken2CA.Chk_Evaporation.Value = 1 And l = 1 Then
            (2) {
                sA = -14.9322
                sB = -13754
                sC = 15.738
                sD = -0.023835
                sE = 0.0000051947
            }
            (3) sP = 10 ^ (sA + sC * (Log(Temperature) / Log(10)) + sB / Temperature + sD * Temperature + sE * Temperature ^ 2)
            (4) sM = 121.75 * 2
            (5) JV = 3.513E+22 * (sP / (sM * Temperature) ^ 0.5)
            (6) sKappa = Val(FrmDareken2CA.Txt_sp(16).Text)
            (7) FV = sKappa * (2 * JV / 1.53E+15) * Y(i_species, l)
            (8) Y(i_species, l) = Y(i_species, l) + h * F(l) - FV * h

        Else
            Y(i_species, l) = Y(i_species, l) + h * F(l)
        End If

        If Y(i_species, l) < 0 Then
            GoTo Euler_Error
        End If

    Next l

Next E_Time

```

Figure A2: Module changed to include surface evaporation showing relevant steps.

Referring to the steps indicated in figure A2:

1. The software confirms that the user wishes to include the effects of surface evaporation in the calculations. The code also confirms that the calculations are done using concentrations in atomic layer 1 which is the surface layer from which evaporation will occur.
2. The constants used in the vapour pressure calculations for Sb are read in.
3. The vapour pressure for the specific temperature is calculated using equation 4.8.
4. It is assumed that the evaporant is the molecule of Sb_2 . The molecular mass for the Sb_2 is calculated.
5. The evaporation flux is calculated for pure Sb_2 using equation 4.15.
6. The value of the evaporation parameter K is read in as specified by the user.
7. The evaporation flux in terms of monolayers is calculated. This is first done by normalizing the flux in step 5 in regards to the molecular form of Sb used, and the amount of atoms possible in a total surface coverage for the crystal orientation of Cu used, in this case for Cu(100). This flux is then multiplied by the fractional surface coverage at that specific temperature and time as calculated by the Modified Darken model.
8. The new surface coverage is calculated by adding the segregation flux in a time interval (step h) and then subtracting the evaporation flux over the same time step h .

Appendix B

Evaporation Geometry Software

The mathematical and physical principles involved in relating the deposition rate measured by the QCM to the evaporation rate from the sample surface is discussed in Chapter 5 section 5.4.3.

If the sample surface from which evaporation can take place has a radius r_e and is separated by a distance h from the gold coated quartz crystal of the QCM sensor, then the fraction of evaporated particles collected by the quartz crystal surface with radius r_s is given by equation 5.22 in Chapter 5, namely

$$\frac{(n+1)h^{n+1}}{\pi r_e^2} \int_{l=0}^{r_s} \int_{\alpha=0}^{2\pi} \int_{s=0}^{r_e} \frac{sl}{[h^2 + (l - s \cos \alpha)^2 + (s \sin \alpha)^2]^{\frac{(n+3)}{2}}} ds d\alpha dl$$

where n relates to the shape of the vapour cloud of evaporating particles.

A Matlab R2008a routine was used to perform this integration numerically. Two modules are used, and are relatively self explanatory. In the first module (“intergrnd.m”) shown in figure B1 the term which is to be integrated inside the triple integral, namely

$$\frac{sl}{[h^2 + (l - s \cos \alpha)^2 + (s \sin \alpha)^2]^{\frac{(n+3)}{2}}}$$

is defined. This term is then imported into the second module (“SC.m”) shown in figure B2, where it is evaluated in terms of the triple integral by the built-in Matlab function “triplequad” which requires the term to be integrated and the various integral limits as input

Appendix C

Conference Contributions and Publications

- 1) South African Institute of Physics annual conference 2009
The effect of surface evaporation on contemporary segregation models
S. Cronjé, R.E. Kroon, W.D. Roos

- 2) South African Institute of Physics annual conference 2011
Measuring the effect of surface evaporation on the segregation process
S. Cronjé, W.D. Roos, R.E. Kroon, J.K.O. Asante

The first prize in the category Doctorate Poster for the best poster presentation in the field of Condensed Matter Physics and Materials Sciences was awarded for this contribution.

- 3) Die Suid-Afrikaanse Akademie vir Wetenskap en Kuns studentesimposium 2011
Die invloed van verdamping op die segregasieproses
S. Cronje, W.D. Roos, R.E. Kroon, J.K.O. Asante

The third prize in the category Chemical Sciences was awarded for this oral contribution.

- 4) S. Cronjé, W.D. Roos, R.E. Kroon and J.K.O. Asante. “*Measuring the effect of surface evaporation on the segregation process*”, Proceedings of SAIP2011, 68, 2011.
- 5) S. Cronje, W.D. Roos, R.E. Kroon en J.K.O. Asante. “*Die invloed van verdamping op die segregasieproses*”. Suid Afrikaanse Tydskrif vir Natuurwetenskap en Tegnologie 32(1), 2013, Art #407.